



UNIVERSITY OF NAPLES FEDERICO II

DEPARTMENT OF INDUSTRIAL ENGINEERING

- MECHANIC AND ENERGETIC SECTION -

PH.D. SCHOOL IN INDUSTRIAL ENGINEERING – XXX CYCLE

A MULTI-VARIABLE MULTI-OBJECTIVE METHODOLOGY APPLIED TO ENERGY CONVERSION SYSTEMS

Doctoral Thesis

Ph.D. School Coordinator

prof. Michele Grassi

Tutor

prof. Alfredo Gimelli

Ph.D. Candidate

Raniero Sannino

Contents

| | |
|---|-----|
| List of figures | iii |
| List of tables | vi |
| Abbreviation and nomenclature | vii |
| Abstract | 1 |
| 1. World energy critical issues and Introduction | 2 |
| 2. General multi-variable multi-objective methodology applied to energy conversion systems..... | 7 |
| 2.1. Design of Experiments | 9 |
| 2.2. Genetic algorithm MOGA-II..... | 9 |
| 2.3. Energy conversion systems models: descriptions and goals..... | 11 |
| 3. Case design study: Combined Heat and Power systems..... | 13 |
| 3.1. Users schematization..... | 14 |
| 3.2. Energy conversion system schematization..... | 19 |
| 3.3. System design results | 24 |
| 3.4. A methodology improvement: robust analysis..... | 28 |
| 3.4.1. System design results: robust analysis on CHP rated power..... | 33 |
| 3.4.2. System design results: robust analysis on reference scenario | 37 |
| 3.5. Discussion | 40 |
| 4. Case design study: Manufacturing production..... | 41 |
| 4.1. User schematization | 42 |
| 4.2. Energy conversion system schematization..... | 46 |
| 4.3. System design results | 50 |
| 4.4. Discussion | 50 |
| 5. Case experimental validation study: micro gas turbine systems..... | 52 |
| 5.1. Micro gas turbine thermodynamic analysis | 53 |
| 5.1.1. Experimental validation: Capstone C30 | 59 |
| 5.1.2. Experimental validation: Turbec T100..... | 64 |
| 5.1.3. Discussion..... | 67 |
| 5.2. Micro gas turbine one-dimensional analysis..... | 69 |
| 5.2.1. Pipes | 71 |

| | |
|--|----|
| 5.2.2. Turbomachinery | 71 |
| 5.2.3. Recuperator..... | 72 |
| 5.2.4. Experimental validation: Capstone C30 | 75 |
| 5.2.5. Discussion..... | 84 |
| 6. Case experimental validation study: Pyro-gasification system..... | 85 |
| 6.1. RM-09 system model | 86 |
| 6.2. Experimental validation results | 90 |
| 6.3. Discussion | 94 |
| 7. Conclusions and outlook..... | 95 |
| References..... | 98 |

List of figures

| | |
|---|----|
| Figure 1: World primary energy demand | 2 |
| Figure 2: Global GDP, energy demand and energy-related CO ₂ [3] | 3 |
| Figure 3: Primary Energy Savings vs Electric CHP efficiency | 5 |
| Figure 4: Methodology flowchart..... | 8 |
| Figure 5: Annual electric demand for Ospedale San Paolo..... | 15 |
| Figure 6: Annual thermal demand for Ospedale San Paolo | 16 |
| Figure 7: Annual electric demand for the CROB | 17 |
| Figure 8: Annual thermal demand for the CROB..... | 18 |
| Figure 9: Plant and user scheme | 19 |
| Figure 10: Thermal and electrical nominal efficiencies and specific investment cost as a function of the CHP gas engine size..... | 20 |
| Figure 11: Methodology application to hospital facilities | 23 |
| Figure 12: Bubble chart representing gas engine size and number for Ospedale San Paolo and the MPESM strategy. | 24 |
| Figure 13: Comparative analysis between MPESM and MPM management strategy for Ospedale S. Paolo | 25 |
| Figure 14: Comparative analysis: TPES as a function of TI_{thr} for S. Paolo Hospital | 26 |
| Figure 15: Bubble chart representing gas engine size and number for the CROB and MPESM strategy..... | 27 |
| Figure 16: Comparative analysis between MPESM and MPM management strategies for the CROB..... | 27 |
| Figure 17: Comparative analysis: TPES as a function of TI_{thr} for the CROB. | 28 |
| Figure 18: Methodology application to hospital facilities (robust analysis on CHP rated power)..... | 31 |
| Figure 19: Methodology application to hospital facilities (robust analysis on reference scenario) | 32 |
| Figure 20: Pareto optimal solutions from the multi-objective robust design analysis for Ospedale S. Paolo . | 34 |
| Figure 21: Pareto optimal solutions from the multi-objective robust design analysis for the CROB | 35 |
| Figure 22: Comparison between deterministic and stochastic approaches to multi-objective optimization for Ospedale S. Paolo..... | 36 |
| Figure 23: Comparison between deterministic and stochastic approaches to multi-objective optimization for the CROB | 36 |
| Figure 24: Pareto optimal solutions from the multi-objective robust design analysis for Ospedale S. Paolo . | 38 |
| Figure 25: Pareto optimal solutions from the multi-objective robust design analysis for the CROB. | 39 |
| Figure 26: Manufacturing user electric demand..... | 43 |
| Figure 27: Manufacturing user thermal demand (annealing oven) | 44 |
| Figure 28: Manufacturing user electric demand without annealing oven | 45 |
| Figure 29: Micro gas turbine efficiency (thermodynamic cycle without regeneration) | 47 |
| Figure 30: Energy conversion system schematization..... | 47 |

| | |
|--|----|
| Figure 31: Methodology application on manufacturing industry user | 49 |
| Figure 32: SPB vs TPES for CHP plants supplying taping manufacturing process..... | 50 |
| Figure 33: Micro gas turbine layout | 53 |
| Figure 34: Radial turbomachinery efficiency [67] | 55 |
| Figure 35: Methodology application on Capstone C30 thermodynamic analysis model | 57 |
| Figure 36: Methodology application on Turbec T100 thermodynamic analysis model..... | 58 |
| Figure 37: Capstone C30 thermodynamic analysis, multi-variable multi-objective results (η_G, P)..... | 60 |
| Figure 38: Capstone C30 thermodynamic analysis multi-variable multi-objective results ($m_{fuel} \cdot HHV, P$).. | 61 |
| Figure 39: Capstone C30 thermodynamic analysis multi-variable multi-objective results ($\eta_G, m_{fuel} \cdot HHV$) | 61 |
| Figure 40: Capstone C30 thermodynamic analysis, multi-variable multi-objective results (T_3, P and T_3, η_G). | 62 |
| Figure 41: Capstone C30 compressor (left) and turbine (right) performance maps..... | 63 |
| Figure 42: Turbec T100 thermodynamic analysis, multi-variable multi-objective results (η_G, P)..... | 65 |
| Figure 43: Turbec T100 thermodynamic analysis, multi-variable multi-objective results (T_3, P) | 65 |
| Figure 44: Turbec T100 thermodynamic analysis, multi-variable multi-objective results (T_4, P) | 66 |
| Figure 45: Turbec T100 thermodynamic analysis, multi-variable multi-objective results (p_{CC}, P) | 66 |
| Figure 46: 1D Capstone C30 micro gas turbine model schematization | 69 |
| Figure 47: Capstone C30 1D model, electric generator | 70 |
| Figure 48: Capstone C30 annular recuperator model..... | 73 |
| Figure 49: Pressure drops in recuperator..... | 73 |
| Figure 50: Methodology application on Capstone C30 1D thermodynamic model | 74 |
| Figure 51: Capstone C30 1D analysis, multi-variable multi-objective results (P_C, P) | 76 |
| Figure 52: Capstone C30 1D analysis, multi-variable multi-objective results (P_T, P) | 77 |
| Figure 53: Capstone C30 1D analysis, multi-variable multi-objective results (P_C, P_T)..... | 77 |
| Figure 54: Capstone C30 1D analysis, multi-variable multi-objective results (shaft speed, mass air flow)... | 78 |
| Figure 55: Capstone C30 1D analysis, multi-variable multi-objective results ($\Delta p_{loss,air}, \Delta p_{loss,gas}$) | 79 |
| Figure 56: Capstone C30 1D analysis, multi-variable multi-objective results (T_3, T_{stk}) | 79 |
| Figure 57: Capstone C30 1D analysis, multi-variable multi-objective results (T_2, T_{2R}) | 80 |
| Figure 58: Capstone C30 1D analysis, multi-variable multi-objective results (T_2, T_{stk}) | 80 |
| Figure 59: Capstone C30 1D analysis, multi-variable multi-objective results (T_3, T_4)..... | 81 |
| Figure 60: Capstone C30 1D analysis, multi-variable multi-objective results (T_3, T_{2R}) | 81 |
| Figure 61: Capstone C30 1D analysis, multi-variable multi-objective results (T_4, T_{2R}) | 82 |
| Figure 62: Pyro-gasification plant schematization | 87 |
| Figure 63: Methodology application on RM-09 pyro-gasifier | 89 |
| Figure 64: RM-09 thermochemical analysis, multi-variable multi-objective results (syngas volume concentration of CO, CO_2 , and CH_4, N_2)..... | 91 |
| Figure 65: RM-09 thermochemical analysis, multi-variable multi-objective results (syngas volume concentration of C_3H_6, C_3H_8 and SO_2, H_2)..... | 91 |

Figure 66: RM-09 thermochemical analysis, multi-variable multi-objective results (syngas volume concentration of CO, O₂ and CH₄, C₃H₈) 92

Figure 67: RM-09 thermochemical analysis, multi-variable multi-objective results (air/fuel ratio vs CH₄ in syngas)..... 93

List of tables

| | |
|--|----|
| Table 1: Constants parameters used in design application of the methodology | 22 |
| Table 2: Main characteristics of the most stable solution for S. Paolo Hospital | 34 |
| Table 3: Main characteristics of the most stable solution for the CROB | 35 |
| Table 4: Stochastic decision variables used in robust design optimization..... | 37 |
| Table 5: Main characteristics of the most stable energetic and economic solution for Ospedale S. Paolo | 38 |
| Table 6: Main characteristics of the most stable energetic and economic solution for the CROB | 39 |
| Table 7: Fuel composition [66] | 54 |
| Table 8: Capstone C30 reference data | 59 |
| Table 9: Methodology setting for Capstone C30 thermodynamic analysis..... | 59 |
| Table 10: Capstone C30 preferred design | 62 |
| Table 11: Turbec T100 reference data [75]..... | 64 |
| Table 12: Methodology setting for Turbec T100 thermodynamic analysis..... | 64 |
| Table 13: Turbec T100 preferred design | 67 |
| Table 14: Methodology application overview | 68 |
| Table 15: Capstone C30 1D model, pipes features [mm]..... | 71 |
| Table 16: Capstone C30 1D analysis, recuperator features | 72 |
| Table 17: Methodology setting for Capstone C30 one-dimensional analysis | 75 |
| Table 18: Capstone C30 preferred design (1D analysis) | 83 |
| Table 19: Pulp paper feedstock composition..... | 88 |
| Table 20: Methodology setting for RM-09 thermochemical analysis | 90 |
| Table 21: RM-09 preferred design | 93 |

Abbreviation and nomenclature

| | |
|--------------------|--|
| A | Heat exchanger surface [m ²] |
| A _{cross} | Cross sectional flow area [m ²] |
| A _s | Heat transfer surface [m ²] |
| CHP | Combined Heat and Power |
| c | Flow speed [m/s] |
| C _F | Fanning factor |
| c _p | Specific heat at constant pressure [J/kg·K] |
| D _{eq} | Flow hydraulic diameter [m] |
| ECS | Energy conversion system |
| g | Gravitational acceleration [m/s ²] |
| GDP | Gross Domestic Product [\$] |
| H _{is} | Isentropic head |
| HHV | Higher heating value [kJ/kg] |
| L | Characteristic linear dimension [m] |
| LHV | Lower Heating Value [kJ/kg] |
| m | Polytropic exponent |
| \dot{m} | Mass flow rate [kg/s] |
| MGT | Micro gas turbine |
| N _s | Specific speed |
| Nu | Nusselt number |
| P _E | Net electric power [kW] |
| P _C | Mechanical power of compression [kW] |
| p _{CC} | Combustion chamber pressure |
| p _{loss} | Pressure drop [bar] |
| P _M | Net mechanical power [kW] |
| P _T | Mechanical power of expansion [kW] |
| P _{TH} | Thermal power [kW] |
| Pr | Prandtl number |
| Q _{HX} | Heat transfer rate [W] |
| R | Gas constant [J/kg·K] |

| | |
|-------------------|--|
| Re | Reynolds number |
| SPB | Simple Pay Back period [years] |
| T ₁ | Ambient air temperature / Compressor inlet temperature [K] |
| T ₂ | Compressor outlet temperature [K] |
| T ₃ | Turbine inlet temperature [°C] , [K] |
| T ₄ | Turbine outlet temperature [°C] , [K] |
| TI | Thermal Index |
| TI _{thr} | Thermal Index threshold |
| T _{ML} | Logarithmic mean temperature difference [K] |
| T _{STK} | Temperature at stack outlet [K] |
| U | Overall heat transfer coefficient [W/m ² ·K] |
| V | Volume [m ³] |
| \dot{V} | Volume flow rate [m ³ /s] |

Greek symbols

| | |
|-----------------|---|
| α | Thermal diffusivity [m ² /s] |
| β | Pressure ratio |
| $\eta_{E,CHP}$ | Electric rated efficiency of CHP plant |
| $\eta_{E,ref}$ | Electric average efficiency of the national generation system |
| $\eta_{TH,CHP}$ | Thermal rated efficiency of CHP plant |
| $\eta_{TH,ref}$ | Reference thermal efficiency |
| η_G | Overall efficiency |
| $\eta_{IS,T}$ | Isentropic expansion efficiency |
| $\eta_{P,C}$ | Polytropic compression efficiency |
| $\eta_{P,T}$ | Polytropic expansion efficiency |
| λ | Air index |
| μ | Dynamic viscosity [kg/m·s] |
| ν | Kinematic viscosity [m ² /s] |
| ρ | Density [kg/m ³] |
| ω | Angular velocity [1/s] |

Subscripts

| | |
|--------|---------------------------|
| air | Air properties |
| calc | Calculated value |
| exp | Experimental value |
| f | Free stream conditions |
| fuel | Fuel properties |
| gas | Exhaust gas properties |
| nom | Nominal conditions |
| stoich | Stoichiometric conditions |
| w | Wall conditions |

Abstract

World climate change and global warming increase are two urgent and strategic issues that national and international governments have to face, and different scenarios aimed to estimate the world energy demand were realized by several research centers: each scenario distinguishes itself by energy policies over the years, and the desirable one requires many efforts to keep the temperature increase below 2°C above pre-industrial level. These efforts imply challenging targets on both primary and final energy employment, and this thesis is focused on two of them: improvement of renewable energy exploitation and reduction of final energy consumption, and energy conversion systems able to efficiently achieve these targets are cogenerated distributed plants, in particular the small scale. Nevertheless, in order to achieve significant primary energy saving, combined heat and power plants need to be designed with a substantial thermal power exploitation, as well as the design need reliable and congruent system models to evaluate the plant performances. The methodology carried out in this doctorate course was focused on the analysis of these topics and it was made by two main elements, an energy conversion system model, which describes the peculiar studied case, and a multi-variable multi-objective optimization algorithm, which depends on the specific application. In particular, two different applications of the methodology were realized, one aimed at designing the more efficient energy interaction between energy system and user and one aimed at validate thermodynamic models and experimental data congruence; the first application concerned combined heat and power plants based on internal combustion engine and gas turbine, while the second application was performed on micro gas turbines and pyro-gasification biomass plant. The methodology showed to be a potentially powerful tool about conversion energy systems analysis, due to the relevant primary energy saving related to designed cogenerated power plant and to the analysis of reliability performed on mathematical models of energy conversion systems.

1. World energy critical issues and Introduction

Nowadays, holding the increase in the global average temperature below 2 °C above pre-industrial levels [1] is one of the most relevant world challenge. Figure 1 shows primary energy demand by fuel and scenario, based on data reported in [2]: the first column represents the 2011 world total primary energy supply; the second one shows the foreseeable future primary energy supply in 2050 if the world energy politics don't change; the third column depicts the desired so-called 450 Scenario, which was named in this way in World Energy Outlook 2008, because it involved an energy scenario where greenhouse gases in the atmosphere were limited to 450 parts per million of CO₂ equivalent. Today, this scenario is expressed as realizing a 50% chance of limiting warming to a 2 °C temperature rise in 2050, that is a consistent target with the previous concentration-based definition.

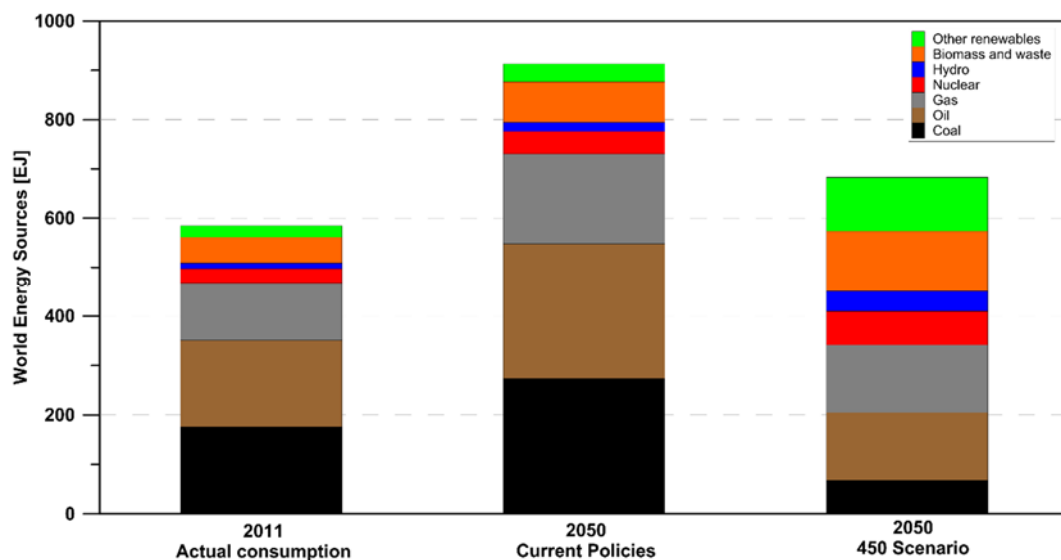


Figure 1: World primary energy demand

These assessments take in account both world population growth and energy intensity, that is an indicator of the link between gross domestic product (GDP) and energy demand: in Figure 2, population growth, primary energy demand and energy-related CO₂ emissions are shown for three scenarios: Current Policies, 450 and New Policies. The New Policies Scenario is based on a detailed review of policy announcements and plans already made by countries governments, and takes in account energy sectors strategies over the coming years [3].

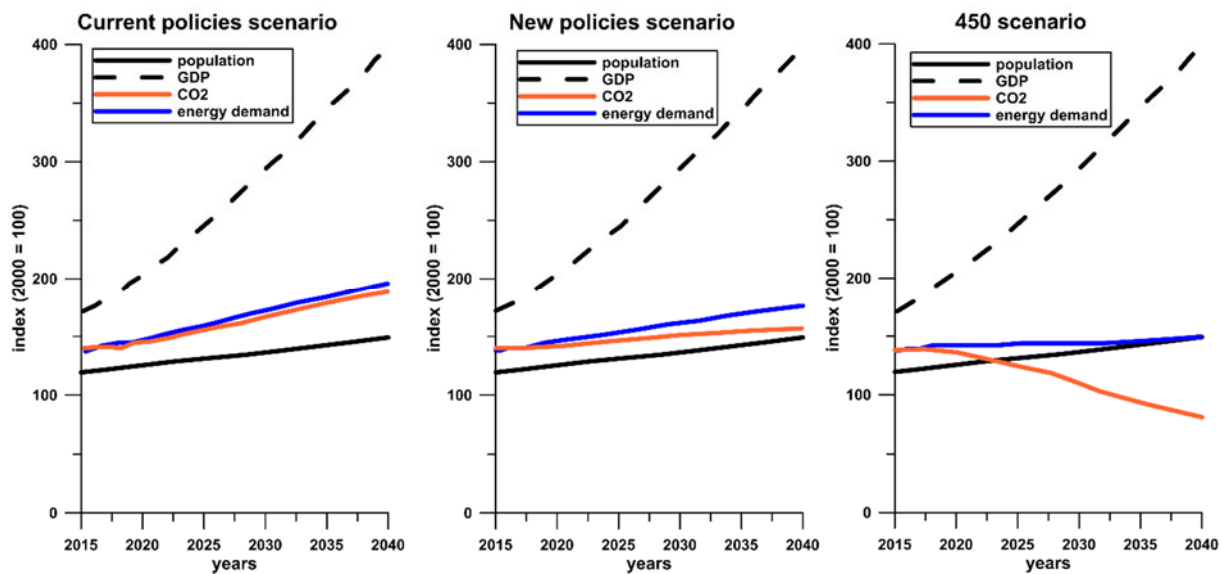


Figure 2: Global GDP, energy demand and energy-related CO2 [3]

Concerning the energy renewable sources, as stated in [3], any solid and plausible pathway to reach climate objectives must be based on renewables; the growth noticed in recent years was driven by wind and solar photovoltaic plants, but it must be underlined that bioenergy and hydropower are the largest source of supply (Figure 1). In particular, bioenergy is employed in traditional and modern way, where traditional refers to the use of solid biomass for cooking or heating, while modern implies the use of recent technology to obtain processed biomass, liquid and gaseous biofuels. Nevertheless, bioenergy entails a sustainability issue, since there are relevant aspects such as deforestation, loss of biodiversity and land use changes: from this viewpoint, the use of residues and waste represents an advantageous exception to these aspects. The concept of “waste” illustrated in [4] is meaningful, “because it applies to any biomass-derived by-product for which supply greatly exceeds demand.” restating the abundance of bioenergy potential, which is many times greater than world demand. Two processes commonly used to obtain biofuels are gasification and pyrolysis: in general, gasification consists in the oxidation of a substance to produce gaseous fuel, using air, oxygen as oxidizing agents. Pyrolysis, in turn, is a thermochemical process of decomposition of organic matter between the temperatures of 400 and 800 °C [5].

To reach the above mentioned targets, namely renewable energy sources improvement and energy demand reduction, and the challenging goal of 2 °C limit, the most effective solutions are the adoption of the distributed generation with small scale power plants with the use of the combined heat and power (CHP) technics. International Energy Agency, in turn, highlights in [3] the key role of decarbonization and energy efficiency improvement to face the greenhouse gas emission reductions,

underlining the importance of the five-year review mechanism outlined during COP21¹. This mechanism helps countries to observe and control, during the years, the achieving of their climate pledges. Moreover, the main topics to reach emissions reductions in power sector are a boosted deployment of renewables, a thrust for larger electrification and an expansion in clean energy research and development effort by governments and companies. One of most promising technics for primary energy saving continues to be the cogeneration [6]: combined heat and power (CHP) systems are widely studied [7]-[14] and their widespread application can lead to a significant reduction of energy demand and greenhouse gas emission [15]-[17] and can enhance power reliability [18]. In addition to these positive aspects, the growth of distributed power generation systems can provide technical and economic benefits, like reduction of energy losses and operating costs of transmission and distribution [19]-[20]. The most used technologies for distributed generation are cogeneration plants (based on micro gas turbines or internal combustion engines), wind turbines, photovoltaic plants, and mini hydro plants; the renewable sources, even if they distinguish themselves for environmental performances, have the disadvantage of uncertain availability. In fact, a hydro plant needs a reservoir, that is not always feasible, while solar radiation and wind speed anyhow depend on climate factors, even using advanced modeling approaches [21]. On the other hand, CHP systems powered by fossil fuels can ensure steady operating conditions, high efficiency, electric and thermal power supply. In order to exploit the renewable energies, in particular biomass and solar heating in CSP, that have small energy density, and to obtain the energy demand reduction it is necessary to adopt small scale distributed power plants with the adoption of the cogeneration technology. Small scale distributed power plants mean electric rated power in the interval from 0.5 kW to 3 MW. The small scale distributed generation systems modeled in cases studies are usually power plants supplied by conventional primary fossil fuels and by renewables (solid waste and solar), with combined heat and power layout.

However, some critical issues are related to the adoption of distributed generation with small scale power plants and the use of cogeneration: first, electric efficiency in most of energy systems increases along with rated power, and small distributed generation plants, ranging between 0.5 kW and 3 MW, have generally efficiency lower than 0.40. Due to this limitation, the study of the exploitation of recovered heat is a fundamental issue to identify solutions that achieve useful energy saving. In Figure 3, there are shown different curves related to different thermal power usage, on a plane with electric

¹ 21st Conference of the Parties since the adoption of the UN Framework on Climate Change (UNFCCC), held in Paris in 2015.

efficiency of generic energy conversion system on x-axis and Primary Energy Saving (PES) on y-axis; PES is defined as:

$$\text{PES} = \left(1 - \frac{1}{\frac{\eta_{E,ECS}}{\eta_{E,ref}} + \frac{\eta_{TH,ECS}}{\eta_{TH,ref}}} \right) \quad (1.1)$$

and $\eta_{TH,ref}=0.90$, $\eta_{E,ref}=0.46$ [22].

As stated in chart legend, each curve performs the PES trend for a specific ratio of thermal power actually used on available nominal thermal power. Based on Figure 3, it must be highlighted that it is necessary to design ECS with a high value of electric efficiency, but it is mandatory to achieve high thermal power exploitation. As stated in [23], this can be accomplished through a deep analysis of user demand and ECS-user energetic interaction.

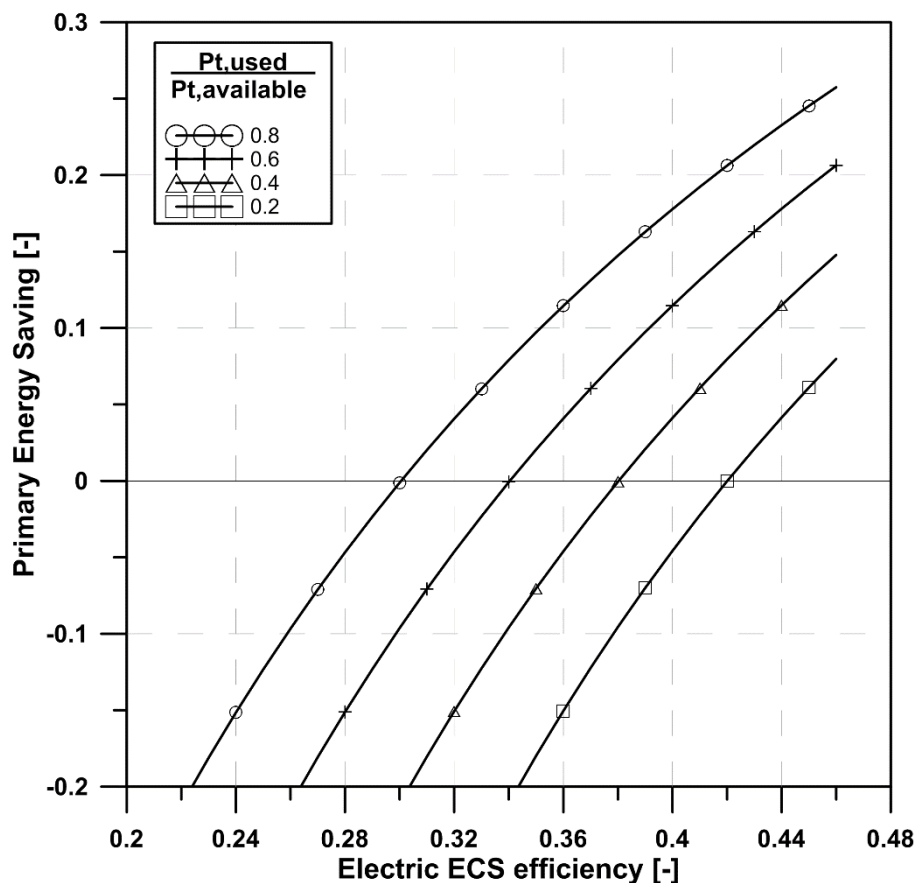


Figure 3: Primary Energy Savings vs Electric CHP efficiency

Besides this aspect, there are also other critical issues of distributed energy systems, such as energetic and economic objectives, that are often conflicting: to face this topic, optimal plant layout and management are fundamental to achieve relevant energetic and economic results; moreover, in

order to avoid an overestimation of the expected results, is useful to analyze the stability of the adopted solutions to possible changes, according to various energetic and/or economic scenarios during the plant life.

Thus, the challenging aim to face the issues related to small scale distributed power plant and CHP technology was pursued in this doctorate activities. Based on this sophisticated energy scenario, the work was focused on the development of a multi-variable multi-objective methodology applied to energy conversion systems. The methodology is substantially broken down in two main coupled elements: a model for the energy conversion system and a multi-variable multi-objective algorithm; within the algorithm, input variables and objective functions must be set, depending on the particular application. The methodology leads the calculation to find out the optimized solutions which take account of the whole objectives and constraints.

The proposed methodology was performed on two kind of applications: one aimed to achieve the more efficient plant layout designs, and one aimed to validate thermodynamic models reliability. The study shows that this methodology is a useful tool to analyze, examine and figure out the most efficient solutions in terms of total primary energy saving, suggesting power plants configurations in order to achieve the advantageous values on the PES index, as shown in Figure 3. In addition, this methodology can be used to verify consistency and reliability of the thermodynamic model and the experimental data, making it a relevant tool in designing energy systems that are capable of satisfying user demand reducing energy consumption.

The methodology and all the operating elements are described in chapter 2; chapters 3 and 4 concern two applications of the methodology on CHP plant designing coupled with two different users, hospitals (chapter 3) and manufacturing industry (chapter 4). Chapter 5 illustrates the validation application of the methodology onto two micro gas turbine plants, to verify the effectiveness of the thermodynamic model and the consistency of experimental data input and output. The last case study is in chapter 6, where an energy conversion system that combines both pyrolysis and gasification is analyzed through the proposed methodology to find the most efficient plant layout. Finally, conclusions and outlook are reported in chapter 7.

2. General multi-variable multi-objective methodology applied to energy conversion systems

Evolutionary multi-objective optimization, in a survey announced during the 2006 World Congress on Computational Intelligence (WCCI), is considered one of the three fastest growing fields of research and application among all computational intelligence topics. A generic evolutionary optimization algorithm uses “a population based approach, where more than one solution participates in an iteration and evolves a new population of solutions in each iteration” [24]. These algorithms became popular due to several reasons, such as lack of any derivative information requirement, quite easy implementation and high flexibility that allows these methods to be applied to vast variety of fields. Inherent to any multi-objective optimization problem, there is the concept of Pareto-optimal solutions: they are a set of non-dominated solutions which need a decision making process to define a single preferred solution. This Pareto set (also called Pareto front) is very important because two or more objective functions set in the optimization can lead the calculation to a trade-off, since most optimization problems are characterized by several objectives, which are usually conflicting real functions to be maximized or minimized, and the awareness of non-dominated solutions addresses the choice of the preferred solution. A clear and accurate definition of a multi-objective optimization problem can be found in [25], as the problem of finding “a vector of decision variables which satisfies constraints and optimizes a vector function whose elements represent the objective functions. These functions form a mathematical description of performance criteria which are usually in conflict with each other. Hence, the term “optimize” means finding such a solution which would give the values of all the objective functions acceptable to the decision maker.”

The proposed methodology flowchart is reported in Figure 4 and follows these steps: the calculation starts in Design of Experiments (DoE), where several sets of input variables combinations are made using mathematical methods, such as Sobol technique [26] and an augmenting algorithm [27]; these DoE sets are the first to be used as input in the energy conversion system model. The model evaluates every DoE set, generating a results vector for each input set; these results are conveniently managed by objective functions, and are ranked by the evolutionary algorithm. Based on the specific methodology application, the objectives must be maximized or minimized and, after all the DoE sets were evaluated, new input sets were generated by a genetic algorithm called MOGA-II ([24],[28],[29]), in order to find solutions aimed to achieve the specified objective functions.

The author and his tutor’s team have already adopted this multi-objective approach ([23],[30]-[32]), demonstrating the importance of a predictive investigation conducted on a wide number of possible plant configurations to achieve optimized energetic and economic results. Similar optimization methods have been used by other authors in [33]-[35].

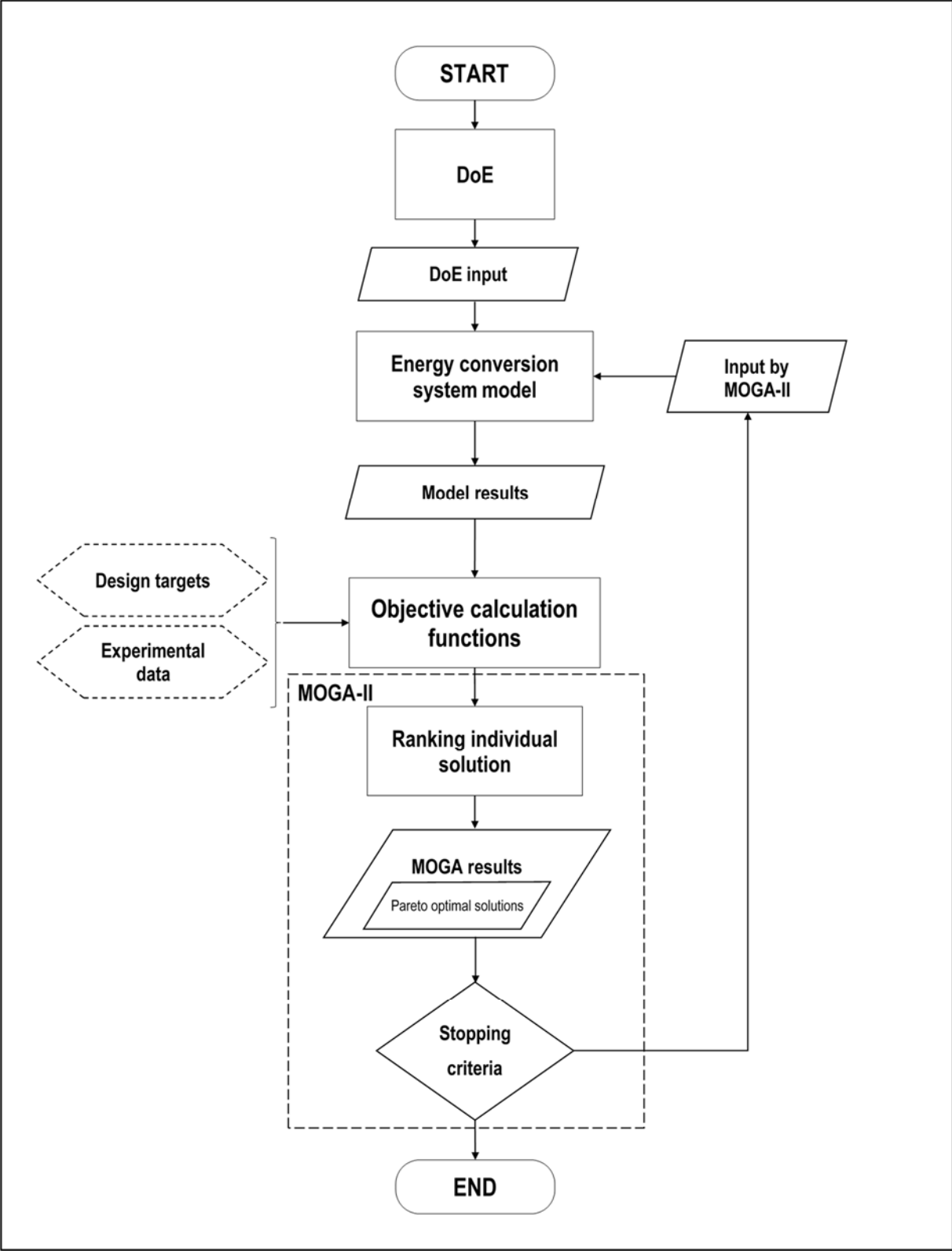


Figure 4: Methodology flowchart

2.1. Design of Experiments

Design of experiments is a methodology used for guiding the choice of experiments to be performed in an efficient way [26]; DoE techniques allow one to extract as much information as possible from a limited number of test runs, and, in the cases illustrated in this thesis, DoE also provides an initial population of designs to the optimization algorithms.

Two of the DoE methodologies adopted are Sobol [26] and an augmenting algorithm: Sobol is a deterministic algorithm aimed at performing a uniform sampling of the design space. Experiments in this type of sequence are maximally avoiding of each other, filling the design space in a uniform manner; furthermore, a Sobol sequence is more resistant to high-dimensional degradation. After the first designs are generated by using the Sobol methodology, the augmenting algorithm is then used to generate a uniform distribution of points in the input space using the maximin criterion [27]. It starts from the existing points in the database and adds new points sequentially, where the minimum distance from the existing points is maximized, to fill the space in a uniform way.

2.2. Genetic algorithm MOGA-II

The evolutionary technique adopted in the methodology is MOGA-II [24],[28], an efficient multi-objective genetic algorithm (MOGA, [29]) that uses a smart multi-search elitism, aimed at preserving some excellent solutions without bringing premature convergence to local-optimal frontiers [24]. The algorithm attempts to perform a total number of evaluations that is equal to the number of points in the Design of Experiments (the initial population) multiplied by the number of generations. With reference to Figure 4, the vectors used to perform the calculation are the following:

X is a vector made by *decision variables*,

$$X = \begin{bmatrix} x_1 \\ \dots \\ x_i \\ \dots \\ x_n \end{bmatrix} \quad (2.1)$$

f is the function that operates on the input variables to obtain the vector Y as a result, namely the *energy conversion system model*,

$$Y = f(X) = \begin{bmatrix} y_1 \\ \dots \\ y_j \\ \dots \\ y_m \end{bmatrix} \quad (2.2)$$

Z is *experimental data* vector that is used in model validation cases,

$$Z = \begin{bmatrix} z_1 \\ \dots \\ z_j \\ \dots \\ z_m \end{bmatrix} \quad (2.3)$$

more details about Z vector are in section 2.3.

In the case of multiple objectives, it is recommended to examine the concept of Pareto optimality and the correlated idea of dominance. By definition, Pareto solutions are considered optimal because there are no other designs that are superior in all objectives. Formally, the definitions are as follows:

Pareto Optimal: for the purpose of maximizing all functions f_i , a decision vector $X_p \in S$ is Pareto optimal if there does not exist another decision vector $X \in S$ such that

$$f_i(X) \geq f_i(X_p)$$

for all $i = 1, \dots, k$, and

$$f_j(X) > f_j(X_p)$$

for at least one index j , where S is the definition domain of the function f and k is the number of objectives that we want to maximize.

Dominance: A decision vector X_d dominates another decision vector X if

$$f_i(X_d) \geq f_i(X)$$

for all $i = 1, \dots, k$, and

$$f_j(X_d) > f_j(X)$$

for at least one index j .

MOGA-II efficiency is controlled by its operators (classical crossover, directional crossover, mutation and selection) and by the use of elitism [24], which plays a crucial role in multi-objective optimization because it helps preserve the individuals that are closest to the Pareto front and the ones that have the best dispersion. At each step of the reproduction process, MOGA-II chooses one of its four operators with regard to the predefined operator probabilities.

In multi-objective optimization, each point located on the Pareto front is an optimum solution, and there is not just one best solution because no decision vector exists that can optimize all the objectives at the same time. In practice, only one of these solutions is to be chosen and, compared to single-objective optimization problems, in multi-objective ones, there is another important task beyond the optimization: decision-making for choosing a single most preferred solution [24]. While in design application of the methodology in was chosen a halfway solution as a preferred one, concerning the model validation application, it was identified the lowest Euclidean norm as a decision-making process: this criteria is formulated in (2.4),

$$\begin{cases} X_p \\ Y_p = f(X_p) \end{cases} : \min \left[\sum_{j=1}^m \left(\frac{Y_j - Z_j}{Z_j} \right)^2 \right] \quad (2.4)$$

and it evaluate each objective as a minimization objective, and the preferred solution is the one identified by the value closer to zero. In other words, in the objectives space, the optimal solution is the one with the minimum distance from the ideal solution, which corresponds to the origin of the space.

2.3. Energy conversion systems models: descriptions and goals

As stated in the above sections, the methodology carried out in this thesis has been applied with two different goals: designing a more efficient ECS layout and validating an ECS model. Models and objective functions differentiate the two approaches. Design applications discussed in chapters 3 and 4, consider mathematical models of both ECS and users, since this kind of methodology employment focuses on evaluating the energetic and economic performances of ECS and, as shown in Figure 3 it is mandatory to match the energy supplied by power plant with user demand. Concerning the objective functions for these cases, they contemplate the *design targets* of Figure 4 and lead the optimization algorithm to find the best non-dominant solutions in term of maximizing total primary energy saving (TPES) and minimizing simple pay back (SPB). The validation applications discussed in other chapters, on the other hand, are based on thermodynamic (chap. 5) and thermochemical (chap. 6) models: in these cases, the objective functions aim to minimize the variation between calculation results and *experimental data* (as well as shown in Figure 4). For each calculation cycle, the resulting components of the vector Y are compared to the corresponding components of the experimental data vector Z to minimize the difference (2.5):

$$\min |f_j(X) - z_j| = \min |y_j - z_j| \quad \forall j \in [1, m] \quad (2.5)$$

Equations (2.5) represent the *objective calculation functions* as reported in the logical flowchart (Figure 4), in case of model and experimental data validation. The Pareto optimal set comprises the decision vectors X_p that satisfy the following conditions:

$$|f_j(X) - z_j| \leq |f_j(X_p) - z_j| \quad (2.6)$$

for each $j \in [1, m]$, and

$$|f_k(X) - z_k| < |f_k(X_p) - z_k| \quad (2.7)$$

for at least one index $k \in [1, m]$.

However, for each examined case, there are a detailed description of model, decision variables and objective functions.

3. Case design study: Combined Heat and Power systems

The strategic role of combined heat and power (CHP) generation [7] has led many research centers to study and develop micro-CHP systems based on internal combustion reciprocating engines [36],[37]. However, in addition to the energetic performance optimization of the specific cogeneration system, equally important is the study of an effective utilization of the recovered heat. This is fundamental to identify a set of CHP solutions that maximize the relevant energetic and economic objectives (e.g., primary energy saving and simple payback period) through a suitable use of the recovered thermal power and generated electricity.

To face this challenging task, several simulations and optimization tools have been adopted in recent years [38]-[41]. The most comprehensive approaches consider fluctuating energy prices, variable energy demands, part-load efficiency integration, carbon price and the possibility of selling electricity fed into the grid, as reported in [42]. A specific calculation algorithm has also been developed by the author tutor's group [23] to conduct several analyses based on the loads of given energy users through the study of the CHP system-user interaction. In particular, to find optimum solutions (engine size and number, plant configuration and management logic) that approach the best energetic results while ensuring a reasonable profit, a multi-objective approach has been used. The developed algorithm considers several complex elements including the different pricing periods during the day (Italian time of use three tier tariff), the Italian regulatory framework, thermal and electrical nominal efficiencies (which vary depending on the CHP engine size, according to the related nominal values of some CHP reciprocating gas engines currently on the market), the specific investment costs, the possibility of selling surplus electricity to the grid at different prices according to the time band, etc.

The developed methodology was applied, in this case study, to perform a comparative analysis based on the load profiles of two specific Italian hospital facilities, thus allowing more general considerations about the potential of cogeneration within the Italian hospital sector. The case highlights how the specific load profiles of different users (even if they belong to the same sector) and the plant management strategy affect the distribution of the Pareto optimal solutions.

However, designing a CHP plant for a specific energetic, economic, regulatory or market scenario does not guarantee good performance when these scenarios change. In [43], for example, the authors said that many studies ignore uncertainties that could alter the outcome of the optimizations. For example, most of the researches considered fixed energy prices, electricity tariffs, grid carbon intensity, etc., while these quantities can vary through the plant life. Moreover, as also stated in [42], most of the proposed models do not provide real-life solutions because CHP unit sizes obtained from the numerical solution of the optimization problem could not be available in the market. Therefore,

to account for some economic and technical uncertainty, sensitivity analyses were then performed adopting multi-objective robust design optimization techniques to identify the most stable plant solutions, ensuring the highest robustness of the calculated results (section 3.4). The growing importance of robust design can be noticed especially within some specific engineering fields: for example, in [44], the robust design of structures has been formulated and solved, and the computational structural robust design problem is formulated as a multi-objective optimization problem. In [45], the authors presented specific application examples including a truss structure and an automotive inner body panel. Paper [46] addresses the robust design of a vibration absorber with mass and stiffness uncertainty in the main system. A robust optimal design method is also proposed in [47] to conduct the unit sizing of energy supply systems under uncertain energy demands, while the robust optimization of tri-generation systems is addressed in [48]. Nevertheless, while the use of robust design methods for studying energy systems is still uncommon, this analysis proposes an unconventional and effective approach to energy systems, providing two application examples. In particular, the proposed methodology, based on the multi-objective robust design approach, has been used to analyze two likely key issues: the sensitivity of the expected results to an eventual mismatch between the CHP gas engine size currently available in the market and that suggested by the numerical solution and the sensitivity of the results to certain possible changes in the reference energetic scenario and electricity market.

3.1. Users schematization

The methodology described in chapter 2 has been applied to two Italian hospital facilities, Ospedale San Paolo and Centro di Riferimento Oncologico della Basilicata (CROB). With regard to the energy consumption of Ospedale San Paolo, a detailed description of the procedure used for estimating the reference load profiles can be found in [23]: Figure 5 shows hospital's annual electric demand while Figure 6 shows the thermal load. The electric load was also characterized on the basis of the time band of purchase, according to a three-tier pricing system to properly take into account the costs of plant operation.

The second user analyzed is the CROB, located in southern Italy. Starting from the energy consumption invoiced during the whole year of 2012 but lacking detailed monitored data, the load profiles for the CROB were estimated by properly scaling the corresponding curves obtained for Ospedale San Paolo according to the ratio between the annual thermal and electrical energy required by the two studied hospital facilities. The estimated curves obtained for the CROB are shown in Figure 7 and Figure 8.

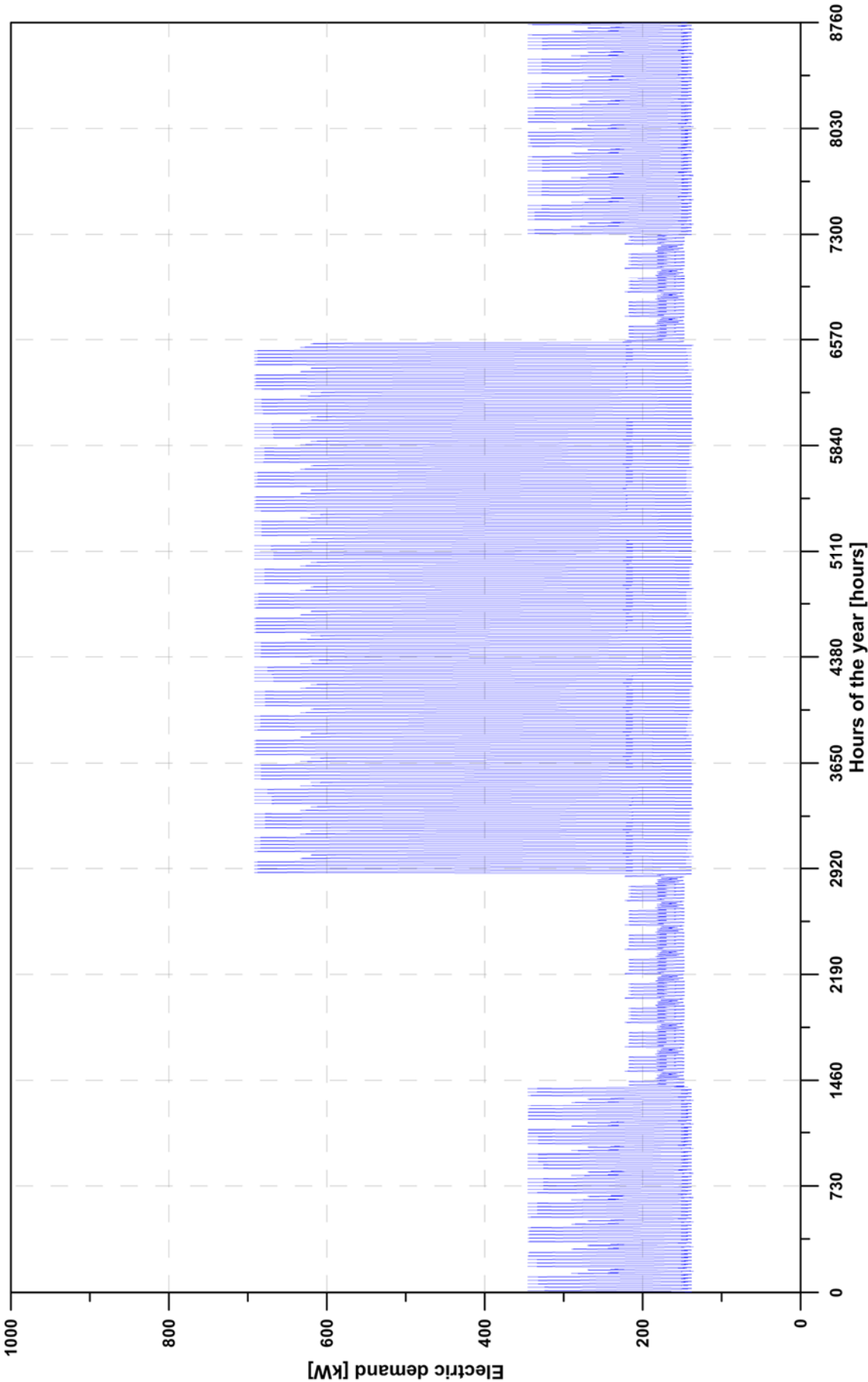


Figure 5: Annual electric demand for Ospedale San Paolo

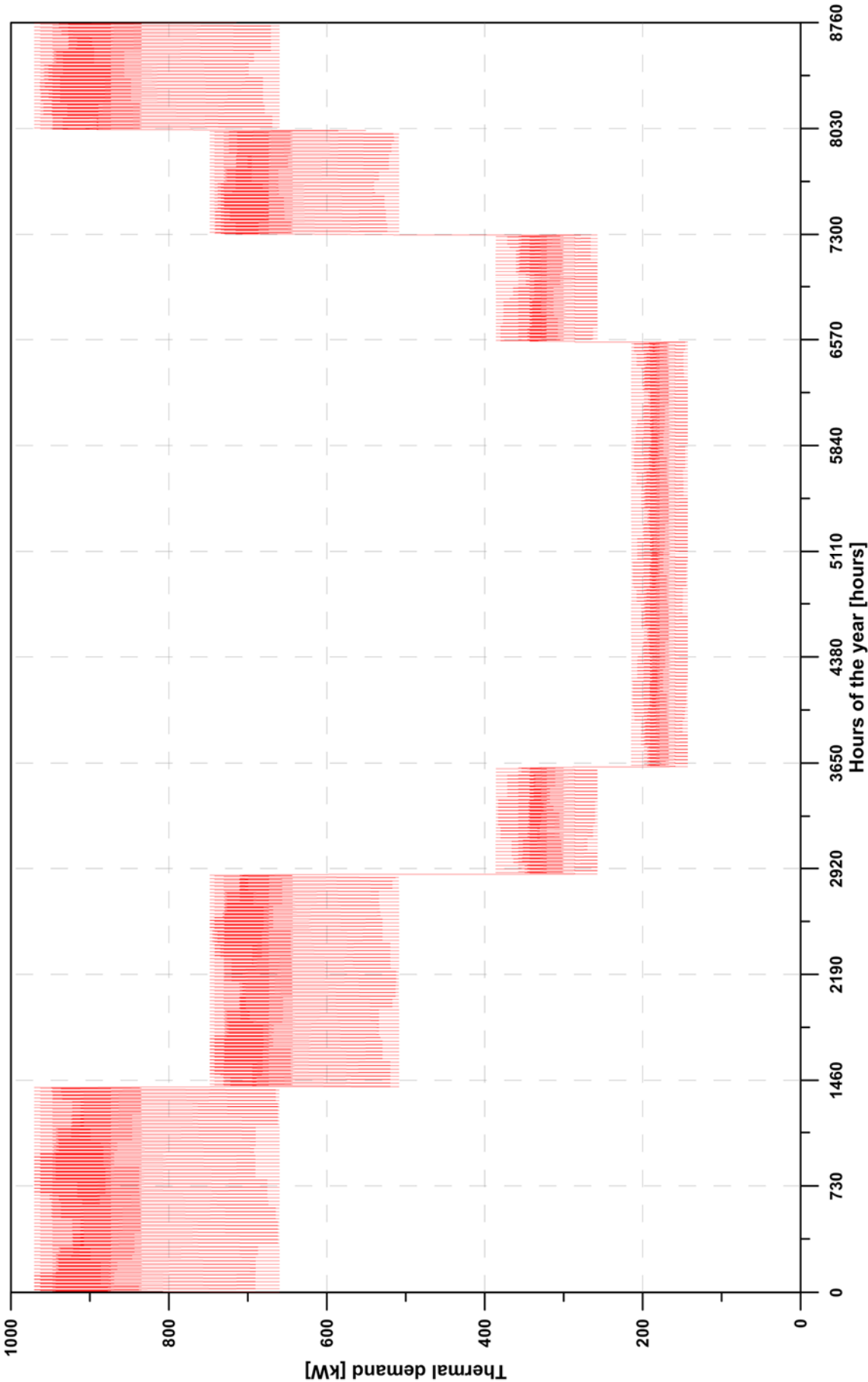


Figure 6: Annual thermal demand for Ospedale San Paolo

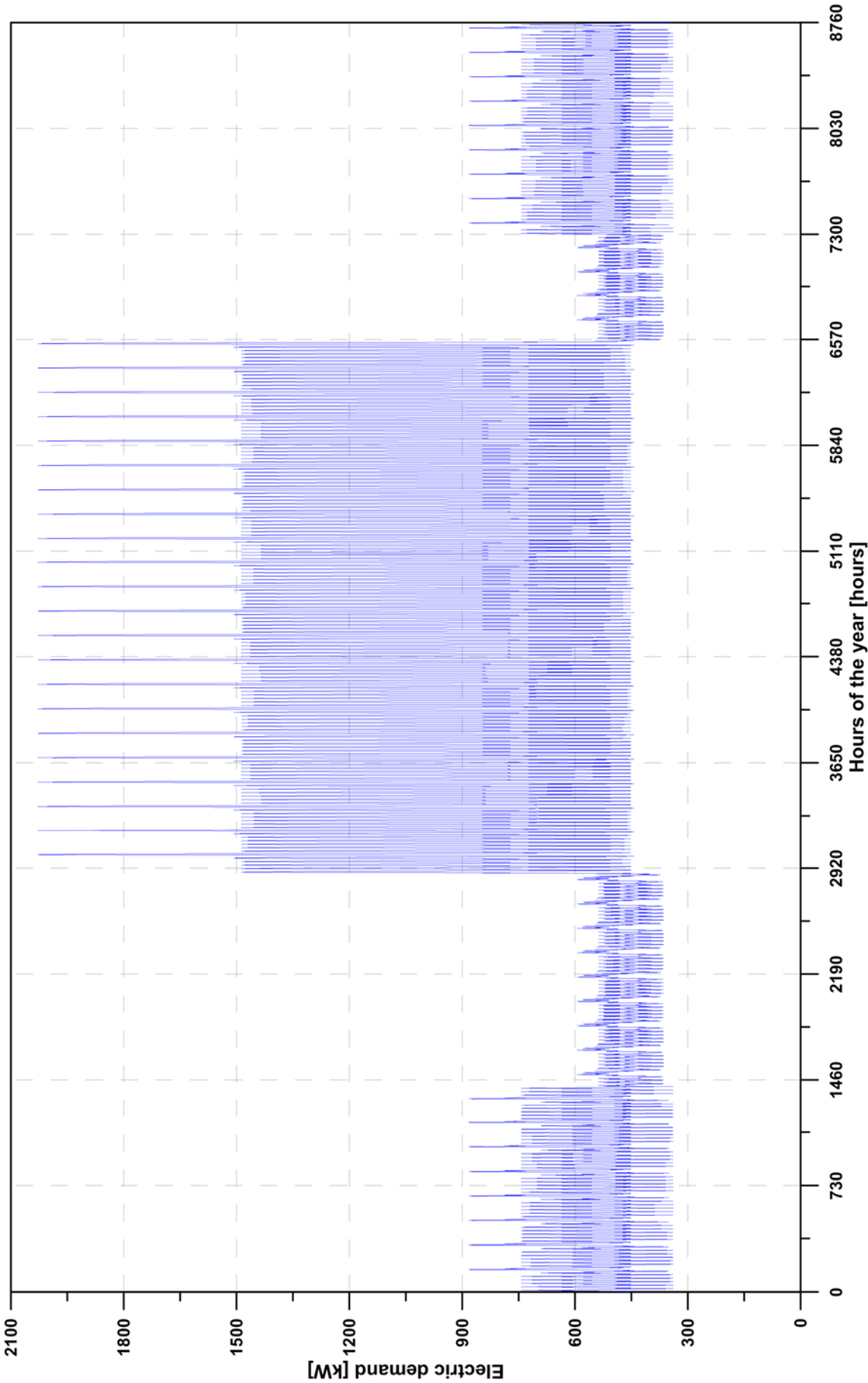


Figure 7: Annual electric demand for the CROB

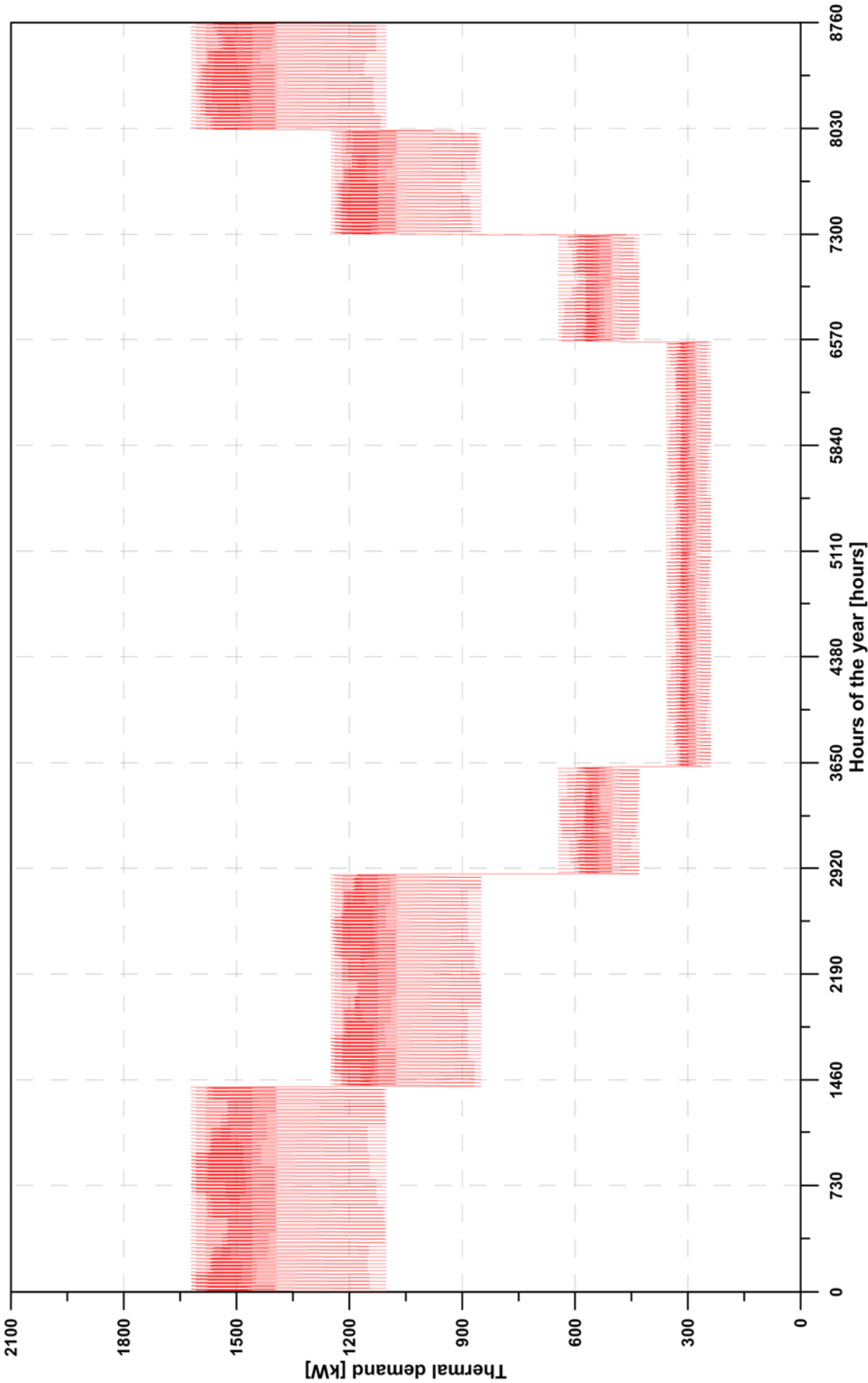


Figure 8: Annual thermal demand for the CROB

3.2. Energy conversion system schematization

The CHP systems studied are based on reciprocating internal combustion engines fueled by natural gas, due to the dominance of this technology in small scale CHP plants applications. Starting from the load profiles of the two users (hospital facilities) described in the previous subsection, one of the goals of the current methodology application was the calculation of the potential energetic and economic benefits achievable through the whole service life of the CHP plant, which is estimated to be 10 years long. For this reason, with the goal of optimizing specific target quantities, some constrained optimization problems were solved to find optimal plant configurations (i.e., CHP engine size and number). An effective solution of these problems requires complex methods.

The energy interaction between CHP plant and user is shown in Figure 9: the plant has two energy stream, one electric and one thermal, which supply the user needs. The electric demand is easy to model and compute, unlike the thermal needs, that require a more detailed characterization because specifying the thermal power just quantitatively is not enough to define the best supplying energy system. The thermal demand has been modeled firstly by fixing the maximum and minimum required temperature; secondly, by matching this thermal quality characterization with the whole amount of needed thermal power, in order to obtain an overall thermal depiction of user needs, hour-by-hour.

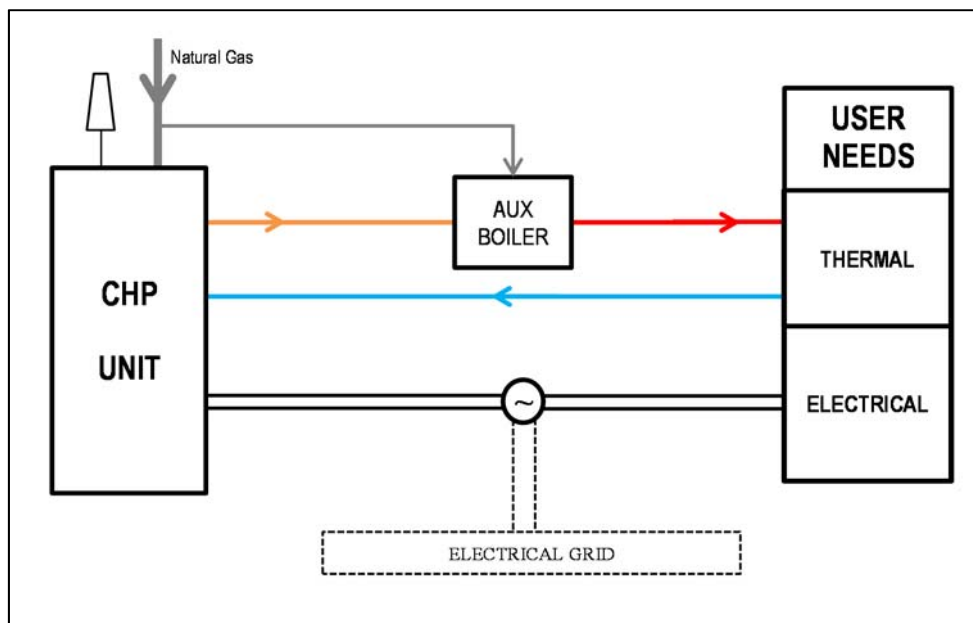


Figure 9: Plant and user scheme

An ON/OFF operation has been imposed on each CHP system, with the engines ON or OFF depending on their profitability or energetic advantage, as described below. Defining the thermal efficiency as in (3.1), variations in the rated electric and thermal efficiency with the engine size have

been properly defined (Figure 10), while the thermal power really cogenerated ($P_{TH,CHP}$) is calculated on the basis of the temperature level required by the users for the carrier fluid.

$$\eta_{TH} = \frac{P_{TH,CHP}}{\dot{m}_{fuel} \cdot LHV} \quad (3.1)$$

The efficiency curves in Figure 10 are based on the related nominal values of some CHP reciprocating gas engines currently on the market ([49],[50]) and cover the electric power range between 150 and 1000 kW. Assuming an ON/OFF management of the CHP gas engine in design conditions, the electric power output of the plant only depends on the engine size. Figure 10 also shows the linear regression curve used to define the specific investment cost of a single CHP unit as function of its size. To estimate the plant operating costs, the electric load profile is characterized according to the time band of purchase from the grid.

Analyses are based on the hourly average cogenerated thermal power ($P_{TH,CHP}$), as calculated from thermodynamic considerations. This calculation is essential in defining the operating range of the CHP plant whether one seeks to maximize the energetic or the economic results (the total primary energy savings, TPES, as defined in equation (3.2), and SPB, or other significant quantities, respectively).

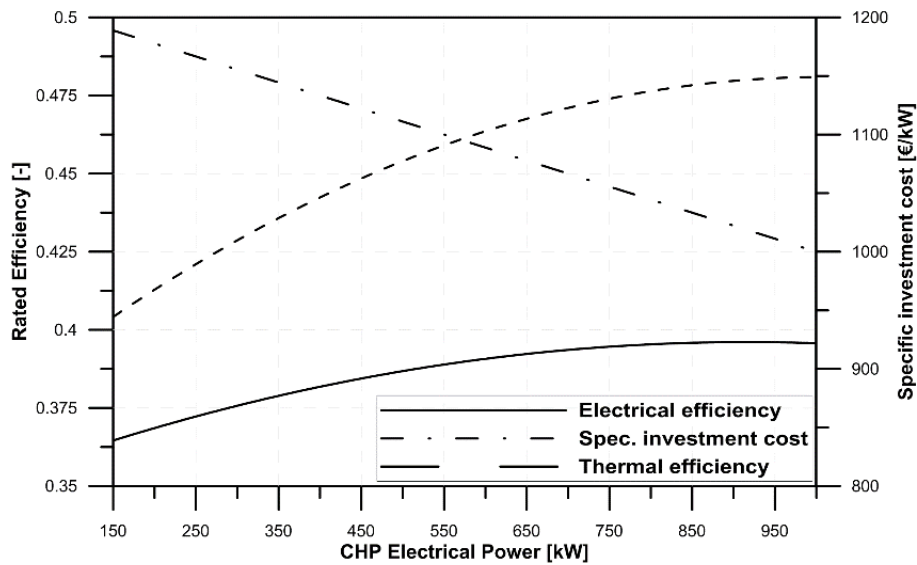


Figure 10: Thermal and electrical nominal efficiencies and specific investment cost as a function of the CHP gas engine size

$$TPES = \left(1 - \frac{E_{P,CHP} + \frac{E_{E,int}}{\eta_{E,ref} \cdot p_{grid}} + \frac{E_{TH,int}}{\eta_{TH,ref}}}{\frac{E_E}{\eta_{E,ref} \cdot p_{grid}} + \frac{E_{TH}}{\eta_{TH,ref}} + \frac{E_{E,exc}}{\eta_{E,ref} \cdot p_{grid}}} \right) \quad (3.2)$$

The TPES in equation (3.2) is the overall primary energy saving index, which accounts of all the energy fluxes between user, CHP plant and the grid. In particular, the TPES compares the primary

energy consumption that characterize the interaction between reference user, CHP plant, auxiliary boilers and the grid in the proposed energy system to the primary energy consumption related to the separate production of the same amount of energy. This implies that possible energy integrations from the grid and auxiliary boilers are also considered. Moreover, the TPES also considers the electric energy generated by the CHP plant that exceeds the user demand, being accounted, in the separate production, with the average efficiency of thermoelectric power generation ($\eta_{E,ref}=0.46$ for the Italian power generation [22]).

In Figure 11, the optimization problem formulation is summarized: the decision variables are the nominal electric power of the CHP engine and a non-dimensional parameter called threshold thermal index (TI_{thr}): this index is defined as the hourly ratio between the user's thermal demand and the nominal thermal power delivered by a single CHP engine under investigation ($TI=P_{TH}/P_{TH,nom}$), and it is adopted within the developed code to quickly guide the search toward more efficient plant configurations (specifically, the number of CHP engines). It represents a threshold value imposed to the TI and has values in the range from 1 to 2. For a given CHP engine size, it is used to estimate, hour by hour, the number of CHP engines, between 1 and 9, that best meets the user's energy demand. This variable is used within the code as follows: if a value of 1.3 is fixed for TI_{thr} , the plant should conveniently use two CHP engines at the i -th hour of the year only if the thermal demand required by the user exceeds the maximum thermal power delivered by the first engine of over 30% (specifically, if $TI=P_{TH}/P_{TH,nom}>1.3$ and $TI<1.3+1$); similar considerations apply for every additional CHP engine and for every hour of the year. Thus, the obtained plant configuration (CHP engine size and number) could be conveniently oriented toward modular plant solutions characterized by an adequate exploitation of the thermal power delivered by each CHP unit, if an optimal value is set for TI_{thr} , ensuring that clearly inefficient plant configurations should not be considered anyway.

Most of the main quantities of interest are described through their respective hourly average values within the developed algorithm, offering the possibility to simulate, during a reference year, the hourly operation of the entire plant; advantages and disadvantages of this assumption are described in [23]. Others significant input constants to the algorithm and their values are shown in Table 1.

Table 1: Constants parameters used in design application of the methodology

| CONSTANTS PARAMETERS FOR CHP DESIGN | | |
|--|--------|---------------------|
| | VALUE | UNITS |
| Natural gas tariff | 0.39 | €/Nm ³ |
| Average national Electric efficiency | 0.46 | - |
| Average boiler efficiency | 0.90 | - |
| Natural gas taxation | 0.0187 | €/Nm ³ |
| CHP plant maintenance cost | 0.015 | €/kWh |
| Electricity selling price (band F1) | 0.120 | €/kWh |
| Electricity selling price (band F2) | 0.096 | €/kWh |
| Electricity selling price (band F3) | 0.065 | €/kWh |
| Fuel lower heating value | 9.58 | kWh/Nm ³ |
| Electricity cost (band F1) | 0.160 | €/kWh |
| Electricity cost (band F2) | 0.117 | €/kWh |
| Electricity cost (band F3) | 0.088 | €/kWh |

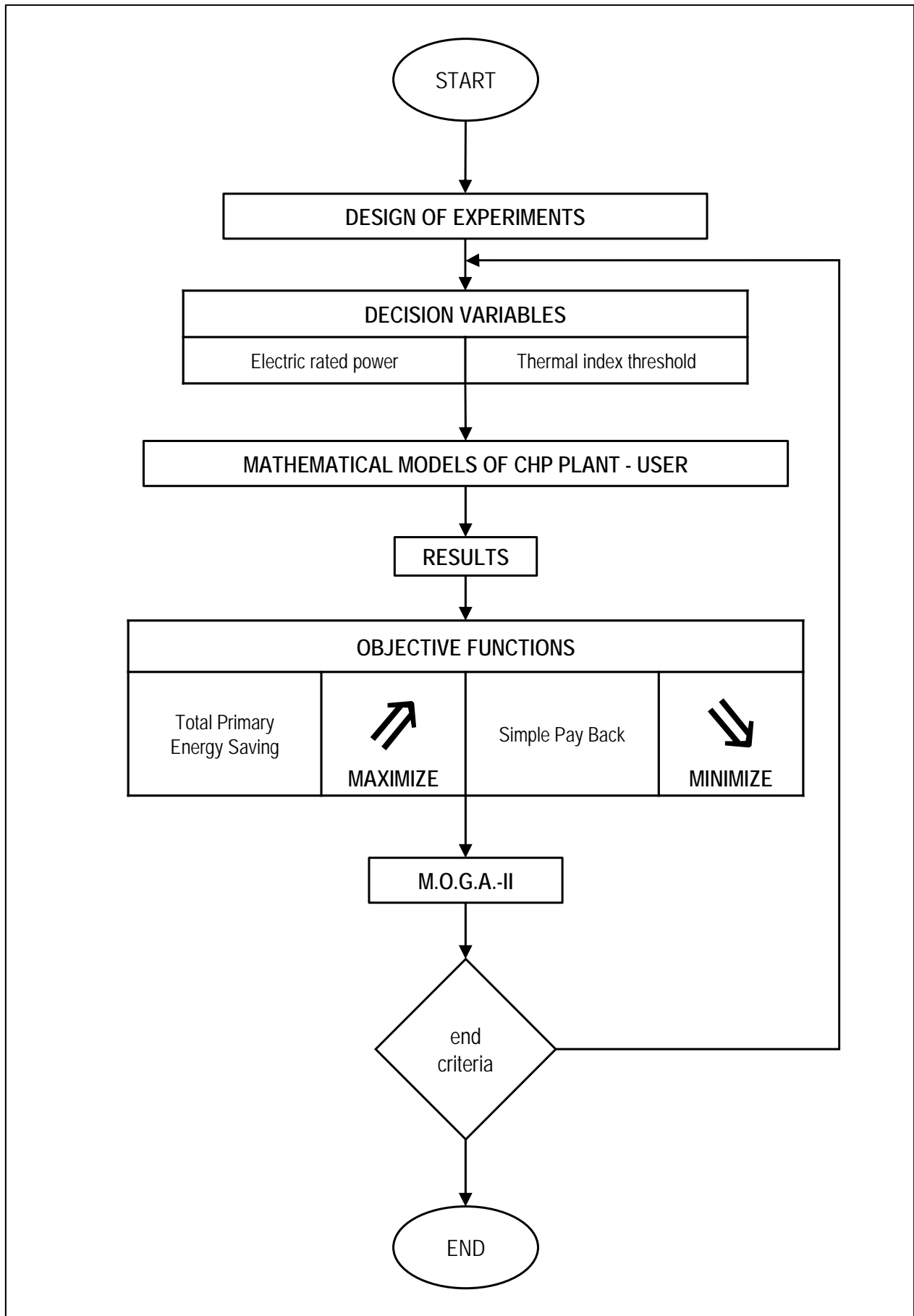


Figure 11: Methodology application to hospital facilities

3.3. System design results

In order to find optimized plant configurations able to maximize energetic and economic results, the multi-objective optimization problem was solved considering both the hospital facilities and two optimized management strategies: Maximum Primary Energy Saving Management (MPESM) and Maximum Profitability Management (MPM). In MPESM strategy the CHP gas engines are ON if TPES is positive in the considered hour, while in MPM strategy the CHP gas engines are ON if there is economic profit in the considered hour. All the solutions were obtained by properly constraining the decision variable space constituted by the electric size of the single CHP unit, which varied from 150 to 1000 kW, and the number of CHP units, which can vary within the range of 1-9. With reference to the two objective functions, Total Primary Energy Saving (to be maximized) and Simple Payback Period (to be minimized), the proposed approach identified over 2600 plant configurations along with the achievable energetic and economic results. Figure 12 shows the bubble chart of the distribution of the calculated solutions with reference to the two objective functions and the two decision variables: the number of engines and their nominal power output. The results refer to Ospedale San Paolo and the MPESM management strategy.

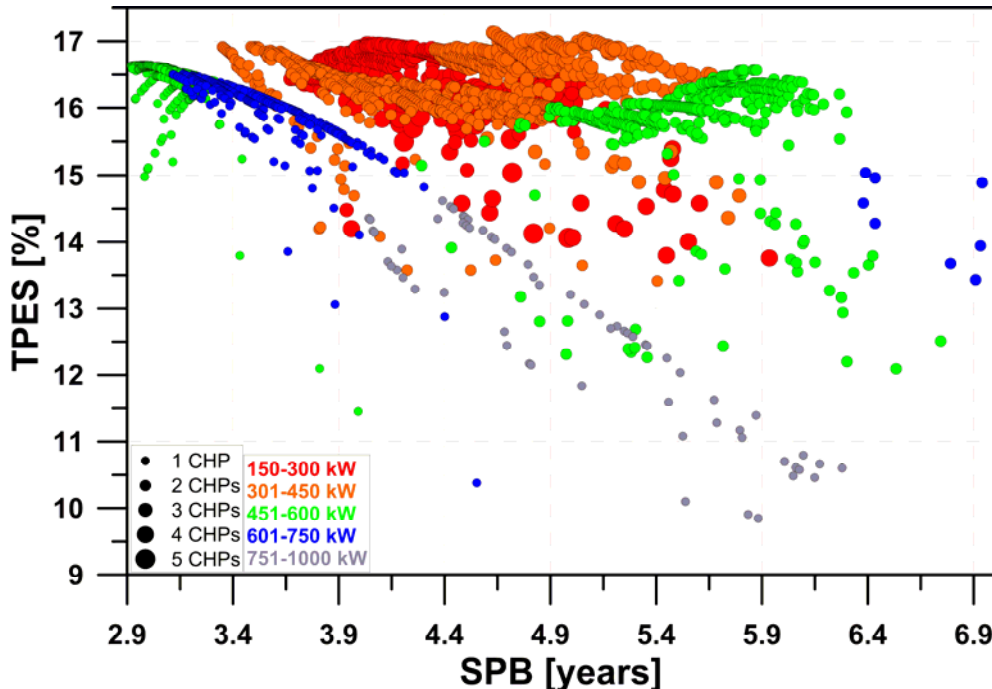


Figure 12: Bubble chart representing gas engine size and number for Ospedale San Paolo and the MPESM strategy.

Solutions from the Pareto optimal front demonstrate that plant configurations which maximize the overall energy savings increase the payback period, in agreement with results reported in literature [51],[52]. In particular, small TPES enhancements are associated with significantly worsening SPB

in this specific case. Moreover, the slope of this front, representing the trade-off between TPES and SPB, is highly affected by the regression curves of Figure 10.

As already discussed in paragraph 3.2, the number of CHP gas engines for each solution is only indirectly obtained using the threshold thermal index as a decision variable for the optimization algorithm, ensuring that clearly inefficient plant configurations should not be analyzed, even among the initialization set of points belonging to the DoE. However, the analyses demonstrate that the range of expected economic and energetic results could be wide, varying in the range of 2.9–8 years for the SPB and 6.5–17.2 for the TPES, highlighting the complex mutual interaction between economic, energetic and legal aspects.

Figure 12 also shows how multiple CHP units solutions characterized by two or three gas engines provide a good compromise between energetic and economic results. In particular, solutions in Pareto front are concentrated around values of energy savings greater than 16.5%, SPB periods of 2.9–4.6 years, 1–3 engines and rated electric power ranging from 260 to 570 kW for each engine. Moreover, among the Pareto optimal front, the minimum SPB solution consists of a single CHP engine with an electric power output of 554 kW.

To evaluate the effects of the plant management strategy on the expected results, a further multi-objective optimization using the MPM logic was performed. Figure 13 shows how the adopted strategy affects the global results, with values of the TPES that decrease by approximately 1.5% if the MPM logic is used. The Pareto optimal front ultimately collapses into a single optimal solution.

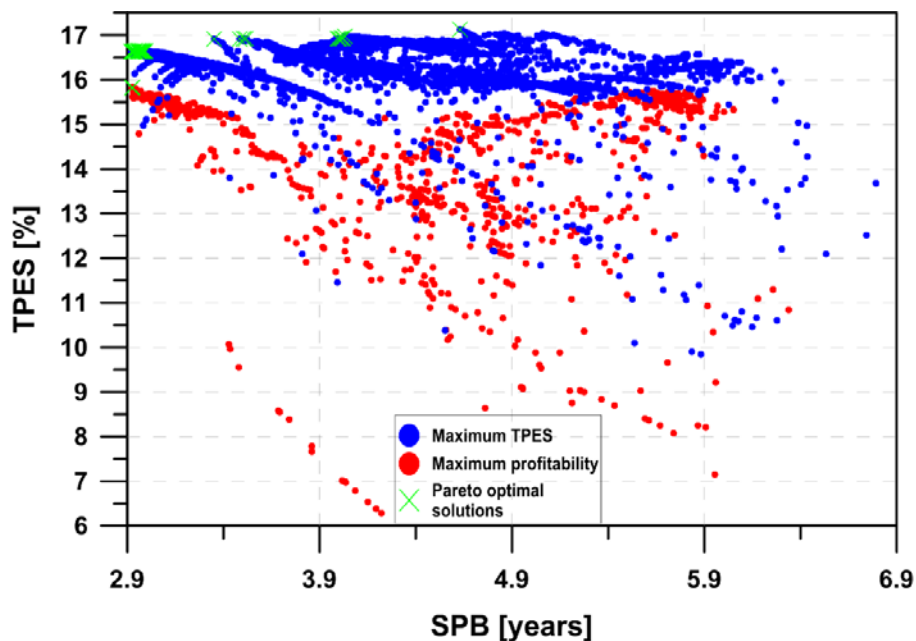


Figure 13: Comparative analysis between MPESM and MPM management strategy for Ospedale S. Paolo

This is characterized by the use of a single 540 kW CHP engine providing values of TPES of approximately 15.8% along with an SPB of less than three years. Thus, Figure 13 demonstrates how a change in the management logic could significantly decrease the degrees of freedom available to design an optimized plant configuration.

Figure 14 shows the TPES as a function of the threshold thermal index used to define the number of CHP engines. The results clearly demonstrate that the Pareto optimal solutions are characterized by values of TI_{thr} in the range of 1.4–1.55 for both management logics. As confirmed by the results from the CROB, this range is expected to change according to the load profile of the user, as the TPES is affected by the simultaneous demand for thermal and electric power once the energetic performance of the CHP system is fixed.

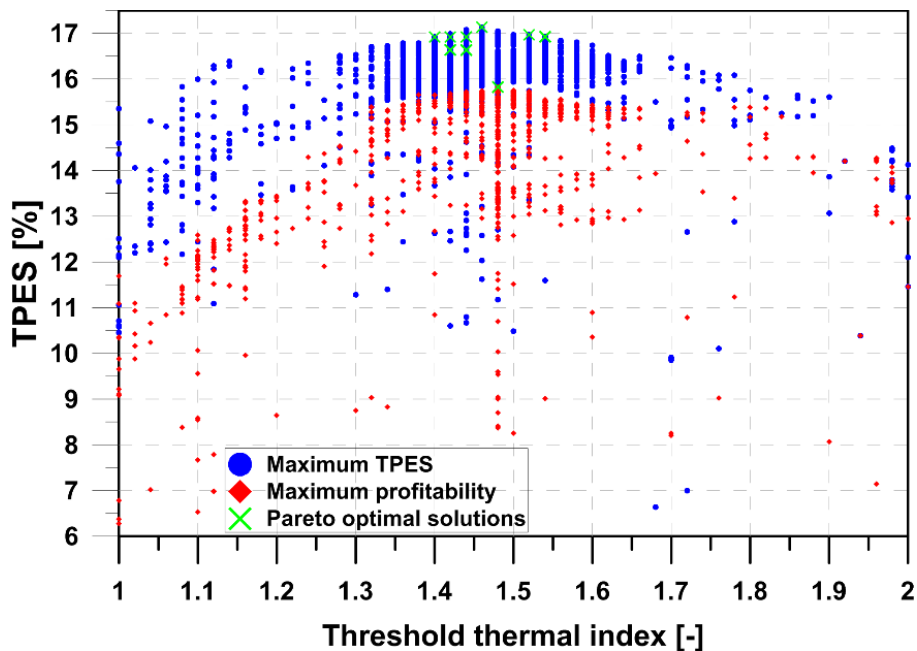


Figure 14: Comparative analysis: TPES as a function of TI_{thr} for S. Paolo Hospital

Figure 15 shows the optimal CHP plant configurations obtained for the CROB Hospital. The Pareto optimal front shows a higher slope compared to the results in Figure 12. Therefore, it is possible to achieve the highest TPES results while accepting a reasonable worsening of the payback period. The overall energy savings reaches 18.2% (approximately 1% higher than for Ospedale S. Paolo), achieving an SPB of just over three years using three CHP engines of approximately 440 kW.

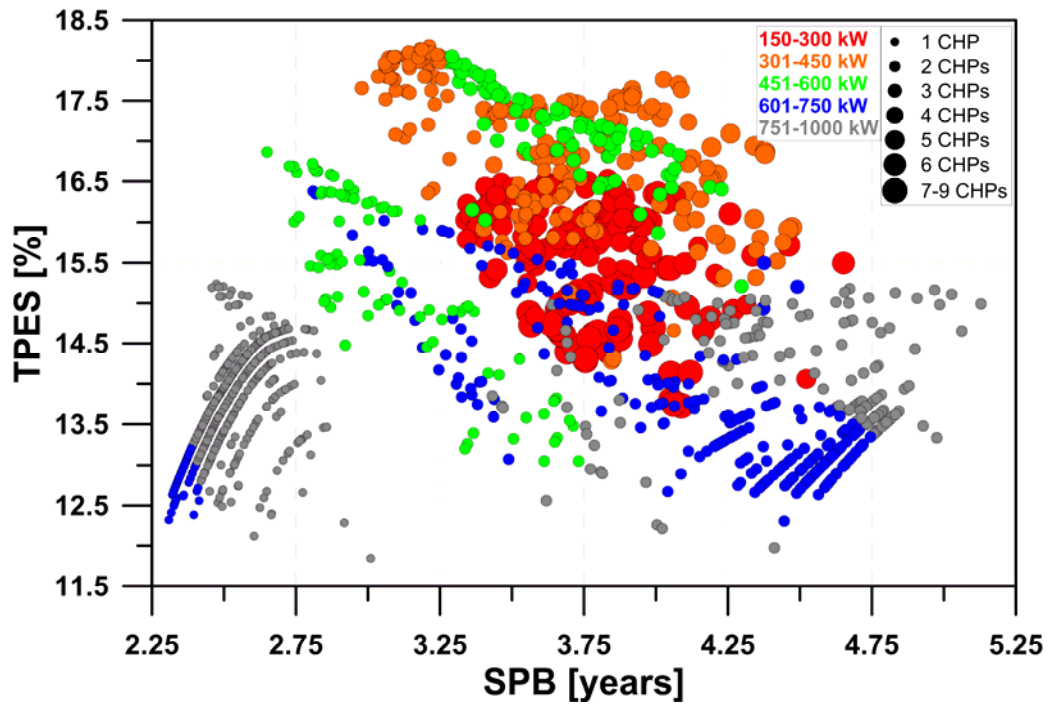


Figure 15: Bubble chart representing gas engine size and number for the CROB and MPESM strategy

Figure 16 shows how the management strategy adopted for the CHP plant influences the global results for the CROB. In particular, the values of the TPES decrease by approximately 0.5% if the MPM strategy is used, while the Pareto optimal front just shifts downwards, mostly maintaining the same trend already shown in Figure 15. However, the maximum TPES value is provided in both cases by the same plant configuration: three CHP gas engines with 440 kW of electric power output each.

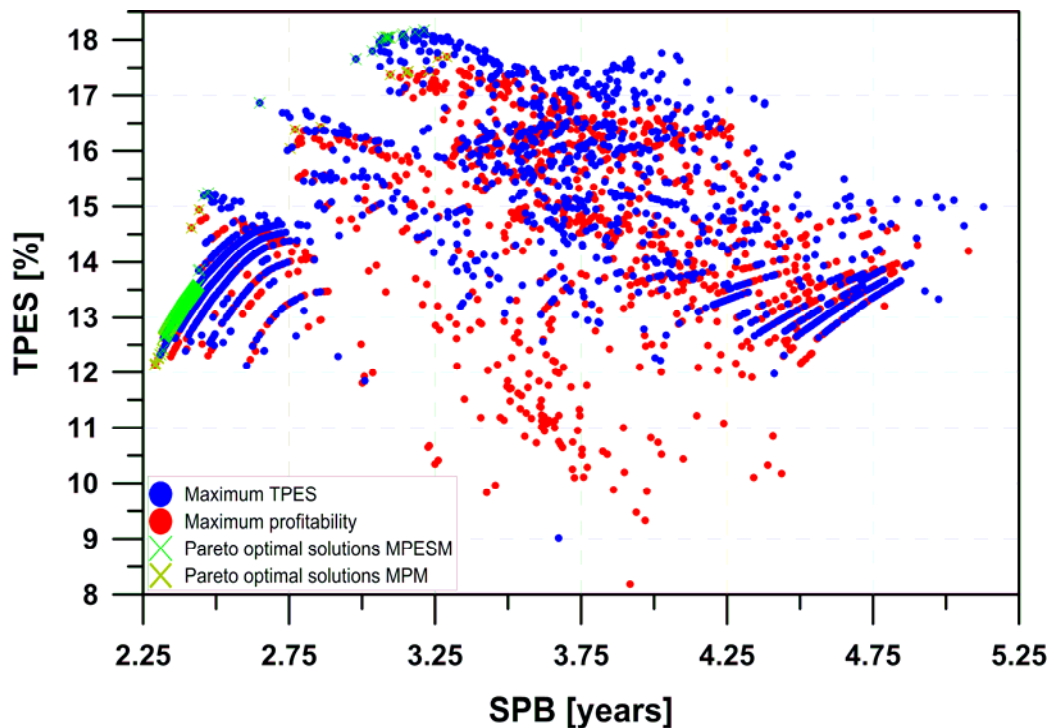


Figure 16: Comparative analysis between MPESM and MPM management strategies for the CROB

Figure 17 shows the TPES as a function of the threshold thermal index, TI_{thr} . The results of the optimization process show that the Pareto optimal solutions have values of TI_{thr} in the range of 1.4–2 for both of the considered management logics. This range has changed compared with Ospedale S. Paolo to match the peculiar energetic characteristics of the CHP system to the load profiles of the user under investigation. In fact, the CROB is characterized by lower hourly values of the ratio between thermal and electrical loads. The higher values of TI_{thr} for most of the dominant solutions suggest that the rated thermal power delivered by each CHP engine must be almost completely exploited to ensure a positive contribution to the TPES together with a reasonable profit.

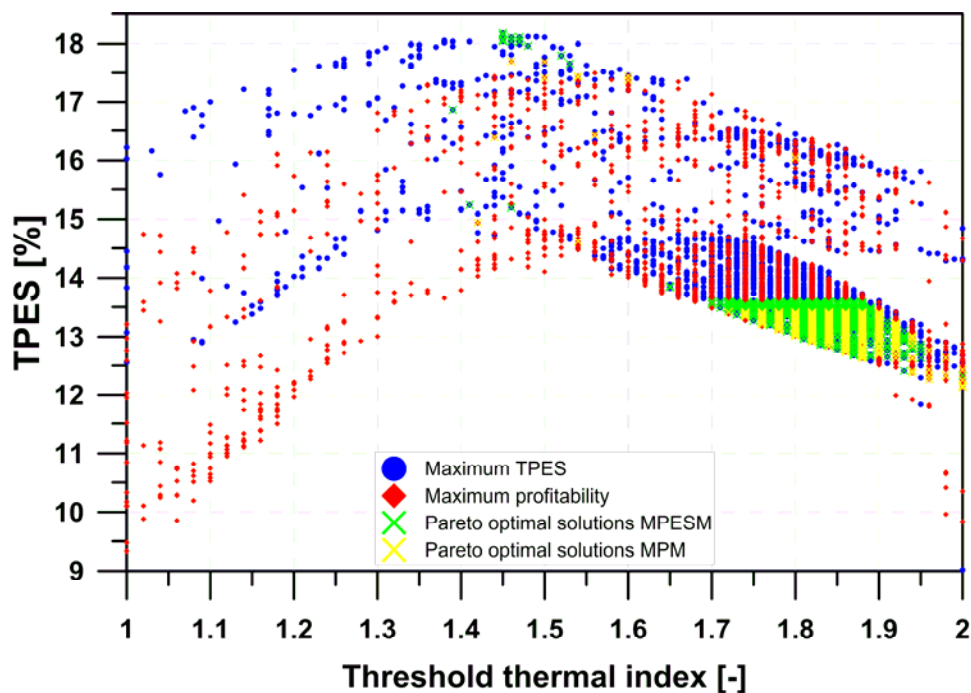


Figure 17: Comparative analysis: TPES as a function of TI_{thr} for the CROB.

3.4. A methodology improvement: robust analysis

As in many engineering design problems, some input quantities may only be known to some tolerance or may change during the plant life. For this reason, optimizing a CHP plant for a specific energetic, economic or market scenario does not guarantee good performance when these scenarios change. Moreover, a calculated technical solution (i.e., CHP gas engine rated power and related nominal energetic performances) may not be matched by a corresponding product in the market. Ultimately, dominant solutions such as those calculated by solving the optimization problem expressed in chapter 2 may not include the most stable solution or may overestimate their performances. Therefore, two specific methodology application were carried out, one to estimate the

sensitivity of the results to a probable mismatch between numerical and marketed solutions, and one to consider eventual changes in the reference energetic and economic scenarios.

A robust design approach was adopted to evaluate the robustness of the calculated results by solving the problem described in 3.2-3.6. In particular, some key decision variables or economic and energetic parameters of the developed calculation algorithm were redefined using a probability distribution before the related multi-objective optimization problems were solved. A probabilistic characterization was assigned to the decision variable X_n . When a robust design optimization is performed, the investigation for the most stable region is performed by defining two different objectives for each function to optimize: both the mean value and the variance of each function are involved in the optimization process. Obviously, using probabilistic models for the input variables, the objective functions obtained as outputs of the optimization problem will also become stochastic.

The mathematical formulation of the robust design optimization problem, considering a discrete formulation for the mean value and variance as usually occurs in the engineering field, can be generally formalized as follows:

$$\min F(x, \sigma) \quad (3.3)$$

$$p(x_j): P(x_j) = \sum_{j=1}^j p(x_j) \in [0,1] \quad (3.4)$$

$$\max F_{mean} = \bar{F} = \sum_{j=1}^q \frac{F_j}{q} \quad (3.5)$$

$$\min \sigma_F^2 = \sum_{j=1}^q \frac{(F_j - F_{mean})^2}{q - 1} \quad (3.6)$$

where:

$$x_j \in R, \quad F: R \rightarrow R$$

σ is the fluctuation of the variable x ,

$p(x_j)$ is the probability density function

$P(x_j)$ is the cumulative distribution function.

When the random variable x is not continuous, it is possible to define the mean and the variance starting from a series of q data using the following formula:

$$\bar{x} = \sum_{j=1}^q \frac{x_j}{q} \quad (3.7)$$

$$\sigma^2 = \sum_{j=1}^q \frac{(x_j - \bar{x})^2}{q - 1} \quad (3.8)$$

Two probability density functions were used in this study: the uniform distribution and the normal distribution. The uniform distribution is a continuous probability density function that can be written as:

$$p(x) = \frac{1}{(b - a)} \quad (3.9)$$

where $x \in [a, b]$

The mean and the variance can be easily evaluated as follows:

$$\bar{x} = \frac{(a + b)}{2} \quad (3.10)$$

$$\sigma^2 = \frac{(b - a)^2}{12} \quad (3.11)$$

This probability density function is suitable to describe a situation where the probability that x occurs inside a given interval is proportional to the interval width.

The normal distribution, also known as Gaussian distribution, has a symmetric bell shape function with respect to its mean value and two flex points located at $\bar{x} \pm \sigma$. It is used to describe how the random errors of independent measurements are statistically distributed and can be written as:

$$p(x) = \frac{1}{\sqrt{2\pi\sigma^2}} e^{-\frac{(x-\bar{x})^2}{2\sigma^2}} \quad (3.12)$$

where

$$x, \bar{x} \in R, \quad \sigma \in R^+$$

\bar{x} and σ are the mean value and the standard deviation of the normal distribution, respectively.

Figure 18 depicts the robust approach of the methodology related to the sensitivity analysis of CHP rated power fluctuation, while Figure 19 concerns the study of the reference scenario variation; in next analyses, the MPESM management strategy was definitively adopted because of the better results provided compared to the MPM logic.

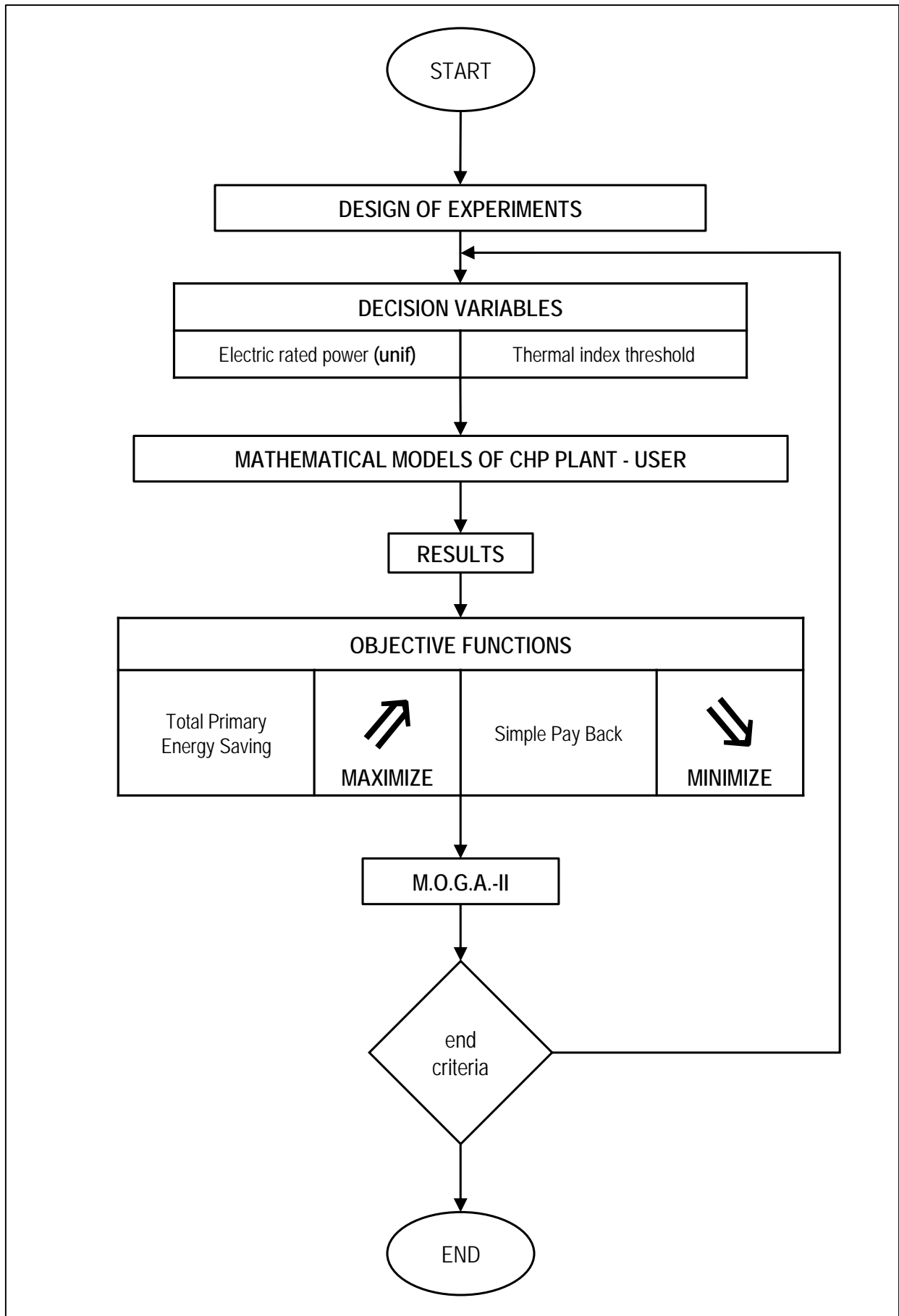


Figure 18: Methodology application to hospital facilities (robust analysis on CHP rated power)

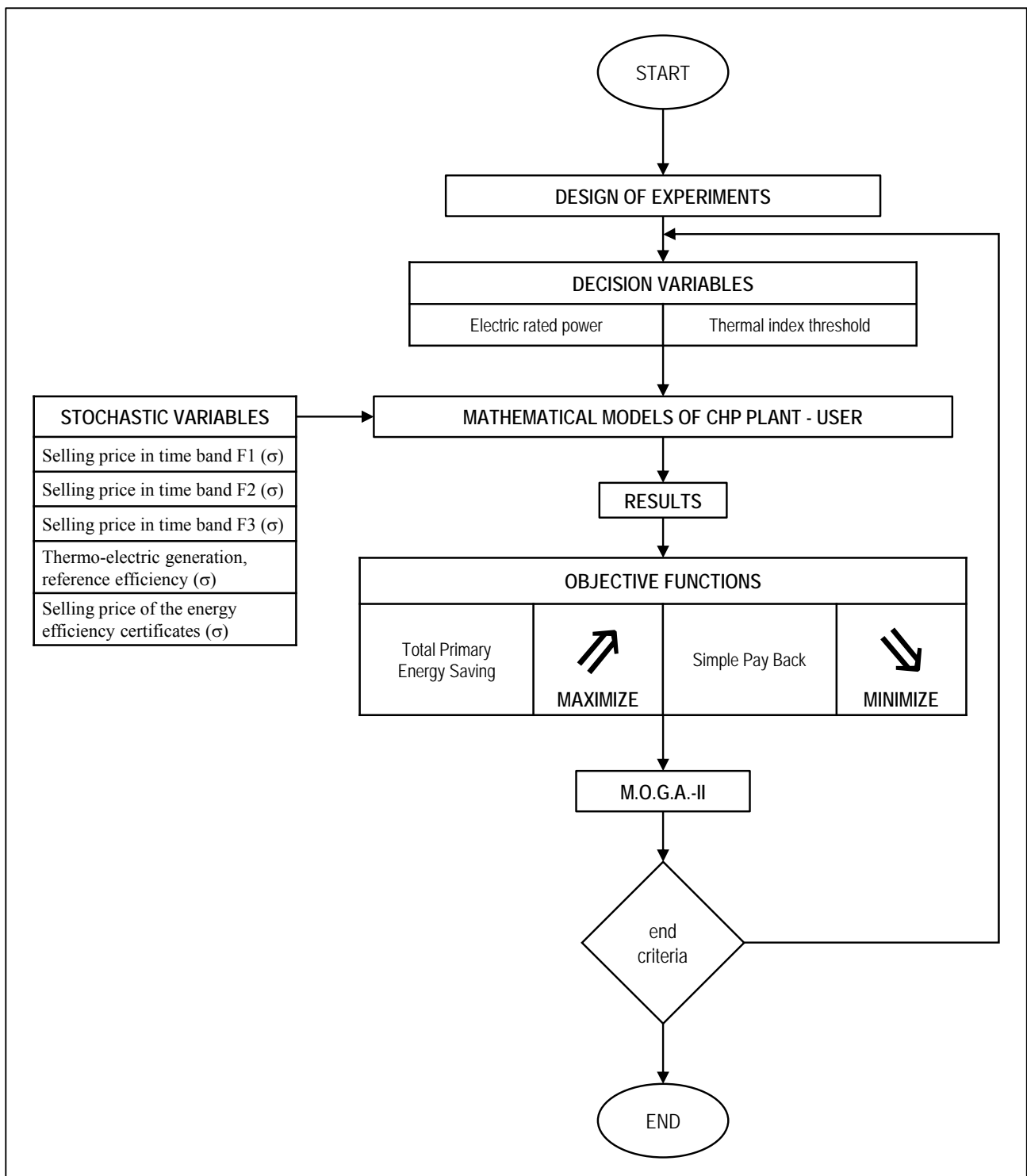


Figure 19: Methodology application to hospital facilities (robust analysis on reference scenario)

3.4.1. System design results: robust analysis on CHP rated power

As shown in previous section, a multi-variable multi-objective robust design optimization process has been carried out in order to investigate for stable economic and energetic solutions. The goal of the robust analysis was to minimize the mean values of the SPB and maximize the mean values of the TPES while obtaining low standard deviation values (referred to as *std-dev* in the following charts) for these quantities. The solutions that minimize the ratio σ_F/\bar{F} (*std-dev/mean-value*) for both the TPES and SPB are recognized as most robust energetic and economic results: the ratio (σ_F/\bar{F}) accounts for the relative weight of the standard deviation of the considered objective functions over their mean value.

Referencing the objective functions TPES and SPB, a multi-objective optimization problem was solved to estimate the sensitivity of the expected results to possible difficulties in finding commercially available CHP gas engines with rated power reasonably close to the optimal numerical solutions. To pursue this aim, the CHP engine size was turned into a statistical decision variable of the optimization problem and described through a uniform distribution (see equations 3.9-3.11). In particular, CHP engine size was defined through a set of 25 sample designs distributed over a range of 60 kW and centered on the mean value currently analyzed by the genetic algorithm MOGA II.

Figure 20 shows, in the σ_F/\bar{F} (SPB) – σ_F/\bar{F} (TPES) plane, the Pareto optimal solutions obtained from the multi-objective robust design optimization for Ospedale S. Paolo. For the single objective functions, Figure 20 highlights a higher energetic stability for most of the optimal solutions because of the imposed management strategy (MPESM logic), whereas the SPB is highly affected by variations in the engine size actually available. In fact, given a value of the threshold thermal index, TI_{thr} , a change in the available gas engine rated power could even induce variations in the number of engines adopted and the related investment costs as a consequence of the changes in the hourly values of the ratio $P_{TH}/P_{TH,nom}$. For this reason, the results indicates that the economic sensitivity is often higher than the energetic sensitivity, with standard deviation accounting up to 7% of its mean value for the SPB, whereas the ratio of σ_F/\bar{F} for the TPES is always under 3%. This representation also enables ranking these solutions according to the equal-stability curves, depicted by dashed lines in Figure 20. Consistently with the notion of multi-objective analysis, these curves are defined as arcs of circumference in the reference plane. The most stable plant design is shown in red, and its main features are summarized in Table 2.

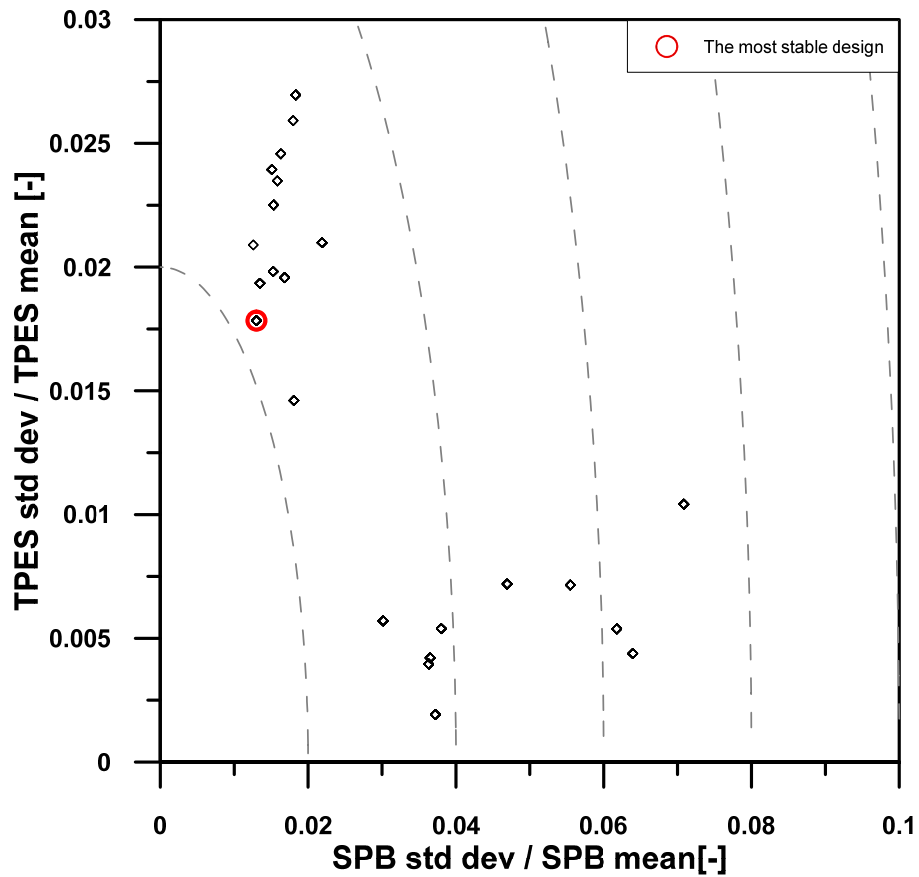


Figure 20: Pareto optimal solutions from the multi-objective robust design analysis for Ospedale S. Paolo

Table 2: Main characteristics of the most stable solution for S. Paolo Hospital

| S. PAOLO HOSPITAL: THE MOST STABLE PLANT DESIGN | | |
|--|--------|-------|
| | VALUE | UNITS |
| CHP units | 1 | - |
| Electric power (mean value) | 482.19 | kW |
| TPES min | 14.32 | % |
| TPES mean | 14.87 | % |
| TPES max | 15.23 | % |
| SPB min | 2.91 | years |
| SPB mean | 2.98 | years |
| SPB max | 3.05 | years |

The Pareto optimal solutions obtained for the CROB are shown in Figure 21, with most of the optimal solutions characterized by even higher energetic stability if compared to the S. Paolo Hospital (the ratio of σ_F/\bar{F} for the TPES is mostly under 2%). The most stable plant design for the CROB is shown in red, and its main characteristics are summarized in Table 3.

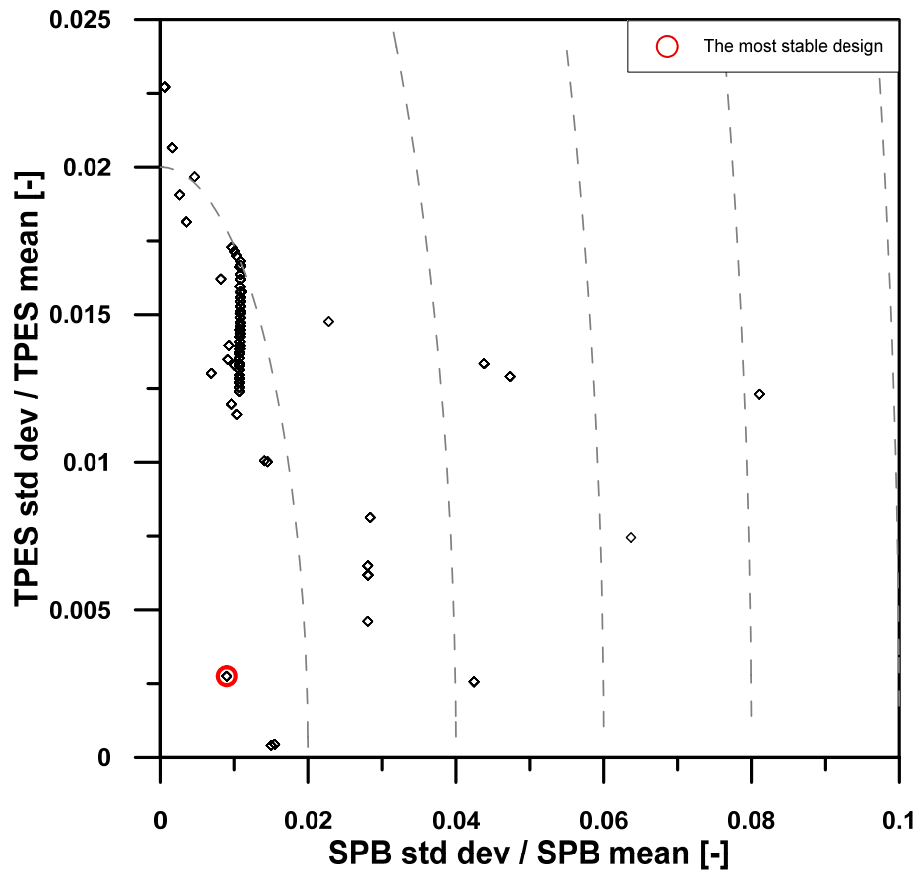


Figure 21: Pareto optimal solutions from the multi-objective robust design analysis for the CROB

Table 3: Main characteristics of the most stable solution for the CROB

| CROB: THE MOST STABLE PLANT DESIGN | | |
|---|-------|-------|
| | VALUE | UNITS |
| CHP units | 1 | - |
| Electric power (mean value) | 969.7 | kW |
| TPES min | 15.14 | % |
| TPES mean | 15.22 | % |
| TPES max | 15.27 | % |
| SPB min | 2.45 | years |
| SPB mean | 2.49 | years |
| SPB max | 2.54 | years |

Figure 22 and Figure 23 show how the expected results obtained through a deterministic definition of the input decision variables within the multi-objective optimization can overestimate the objective functions compared to the robust design approach. Specifically, the red circles represent the maximum TPES solutions obtained in section 3.3 for the two studied hospital facilities. The blue crosses represent the 25 sample designs belonging to the same robust design solution and therefore

to the same statistical distribution for the engine size. In particular, the mean value of this distribution is equal to the engine size of the red solution. Figure 22 shows that SPB can range from 4.3 to 5.3 years and that the TPES can range from 16.7 to 17.1 if the robust design approach is used, according to the actual commercial availability of the target engine size. Figure 23 shows similar energetic and economic variations for the objective functions and the CROB. The significantly higher value of the SPB for the solution on the right hand of Figure 23 is due to having one CHP engine more than the other solutions, according to the current values of the threshold thermal index and CHP engine size.

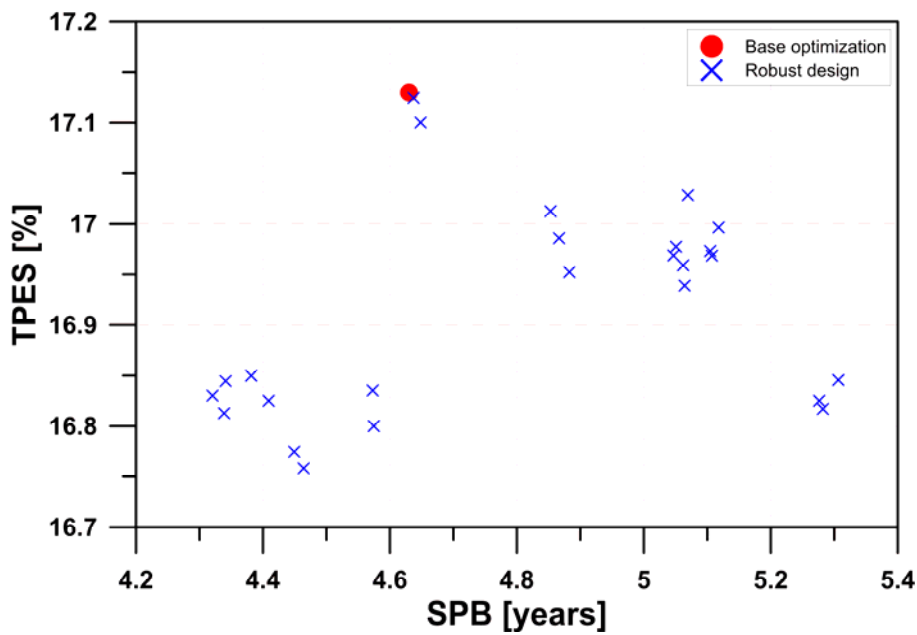


Figure 22: Comparison between deterministic and stochastic approaches to multi-objective optimization for Ospedale S. Paolo

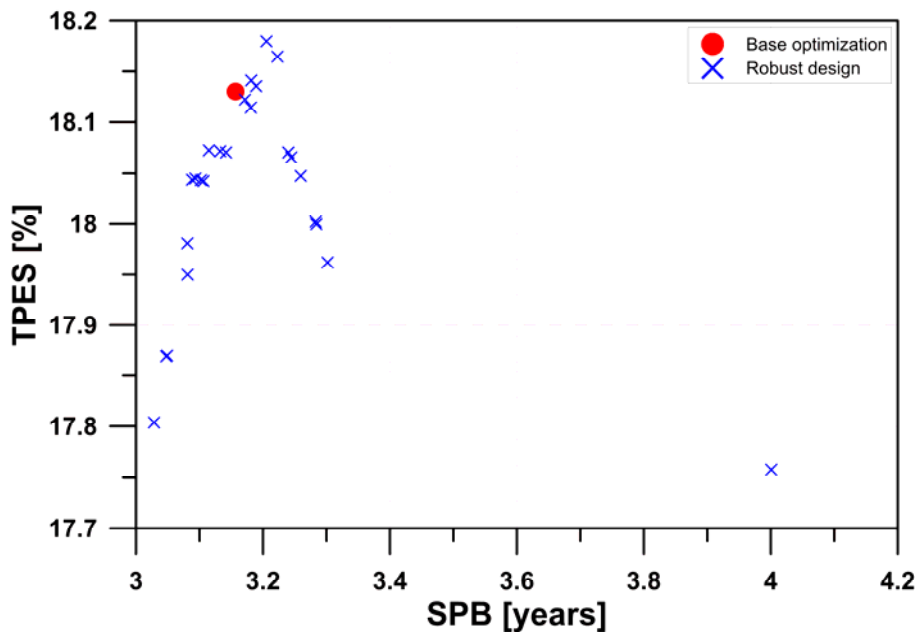


Figure 23: Comparison between deterministic and stochastic approaches to multi-objective optimization for the CROB

3.4.2. System design results: robust analysis on reference scenario

To estimate the fluctuations induced in the expected results due to possible changes in the reference energetic and economic scenarios, a second multi-objective robust design optimization was performed with reference to the TPES and SPB objective functions. In particular, the selling price of the electricity in different time bands, the reference efficiency of the Italian thermoelectric generation and the selling price of the energy efficiency certificates recognized by the Italian legislation to cogeneration plants were set as stochastic variables and were described by normal probability distributions (Table 4). The threshold thermal index and the gas engine size were the two decision variables. Figure 24 summarizes, in the $\sigma_{F/\bar{F}}(SPB) - \sigma_{F/\bar{F}}(TPES)$ plane, the energetic and economic stability of the Pareto optimal solutions for Ospedale S. Paolo. In particular, the standard deviation for the SPB is always under 3.5% of its mean value. This percentage, which gives an estimation of the fluctuations of the objective functions within the plant life cycle, reaches 7% for the TPES. The most stable plant design is shown in red, and its characteristics are reported in Table 5.

Table 4: Stochastic decision variables used in robust design optimization

| ROBUST DESIGN OPTIMIZATION: STOCHASTIC VARIABLES | | | | |
|---|-------------|---------|----------|-----------|
| INPUT DECISION VARIABLE | RANGE | UNIT | DISTRIB. | STD. DEV. |
| Selling price in time band F1 | 0.10–0.14 | €/kWh | Normal | 0.003 |
| Selling price in time band F2 | 0.076–0.116 | €/kWh | Normal | 0.003 |
| Selling price in time band F3 | 0.045–0.085 | €/kWh | Normal | 0.003 |
| Electric average national efficiency | 43.5–48.5 | % | Normal | 1 |
| Selling price of the energy efficiency certificates | 90–110 | €/cert. | Normal | 3 |

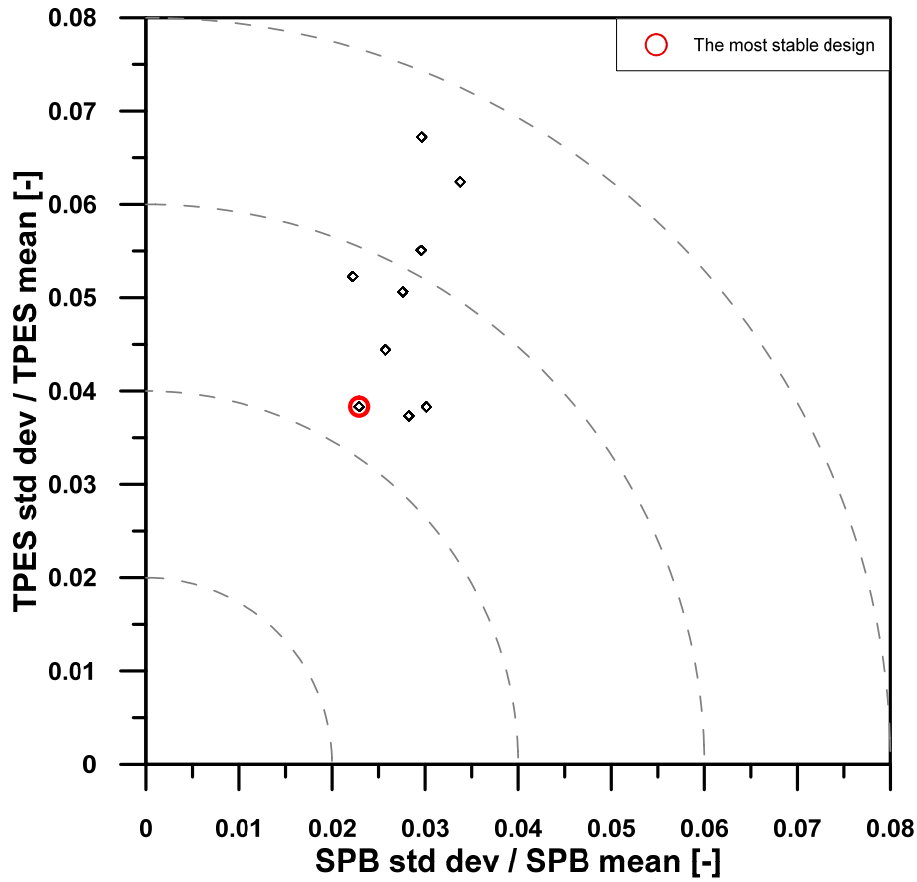


Figure 24: Pareto optimal solutions from the multi-objective robust design analysis for Ospedale S. Paolo

Table 5: Main characteristics of the most stable energetic and economic solution for Ospedale S. Paolo

| OSPEDALE SAN PAOLO: THE MOST STABLE PLANT DESIGN | | |
|---|-------|-------|
| | VALUE | UNITS |
| CHP units | 3 | - |
| Electric power | 331 | kW |
| TPES min | 17.12 | % |
| TPES mean | 17.69 | % |
| TPES max | 19.25 | % |
| SPB min | 4.45 | years |
| SPB mean | 4.58 | years |
| SPB max | 4.79 | years |

The same multi-objective robust design analysis was conducted for the CROB. The energetic and economic stability of the dominant solutions for the CROB is shown in Figure 25 in the σ_F/\bar{F} (SPB) – σ_F/\bar{F} (TPES) plane. The standard deviation for the SPB is always under 2.5% of its mean value. This percentage increases to 6% for the TPES. The most stable plant design is shown in red, and its characteristics are reported in Table 6.

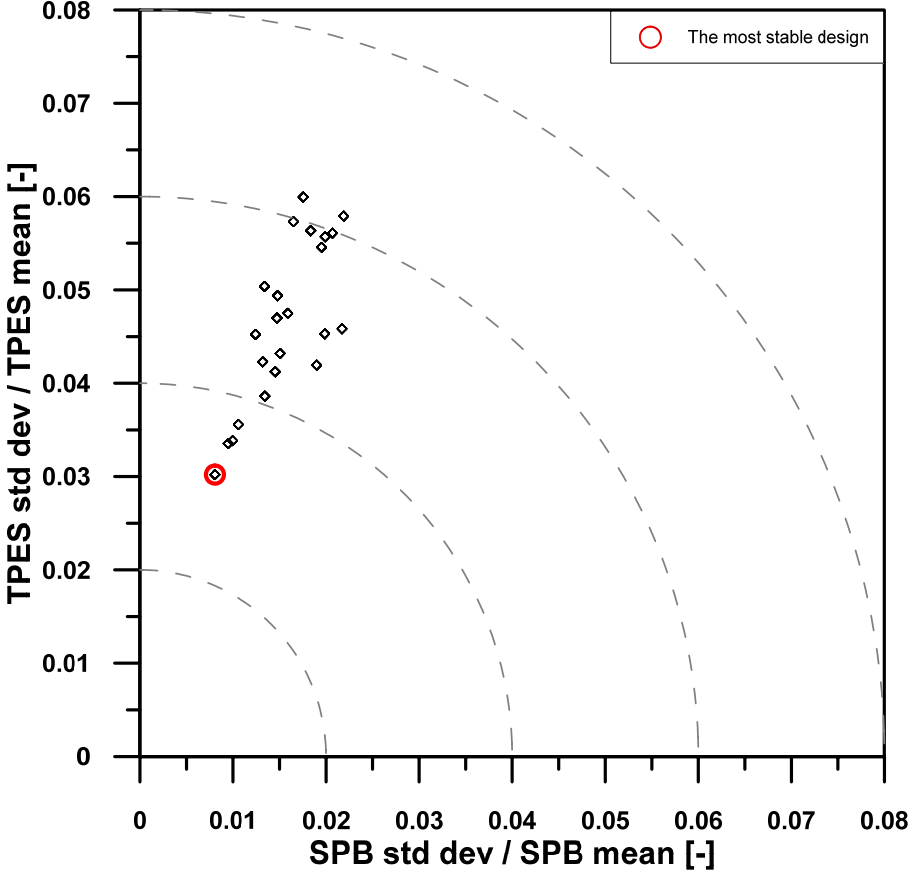


Figure 25: Pareto optimal solutions from the multi-objective robust design analysis for the CROB.

Table 6: Main characteristics of the most stable energetic and economic solution for the CROB

| CROB: THE MOST STABLE PLANT DESIGN | | |
|---|-------|-------|
| | VALUE | UNITS |
| CHP units | 1 | - |
| Electric power | 682 | kW |
| TPES min | 11.93 | % |
| TPES mean | 12.37 | % |
| TPES max | 13.22 | % |
| SPB min | 2.26 | years |
| SPB mean | 2.31 | years |
| SPB max | 2.33 | years |

3.5. Discussion

The application of the studied methodology to design an efficient energy conversion system forecasting the CHP system-user interaction, led to determine optimized plant configurations with primary energy savings of over 17%, along with SPBs under 4.6 years. In particular, the Pareto dominant solutions for Ospedale S. Paolo are concentrated around energy savings greater than 16.5%, SPBs in the range of 2.9 to 4.6 years, 1–3 engines and electric rated power ranging between 260 and 570 kW for each unit. For the CROB, the overall energy saving reaches the maximum value of 18.2% when the SPB is just over three years for a plant configuration consisting of three CHP gas engines with 440 kW of electric rated power output each; the same plant solutions that maximize the TPES provide a reduction of carbon dioxide emissions ranging from 20 to 22% [30].

Furthermore, a multi-objective robust design optimization has been carried out to find most stable economic and energetic solutions, based on minimizing the ratio σ_F/\bar{F} (standard-deviation/mean-value) for both the TPES and SPB. This ratio (σ_F/\bar{F}), accounts for the relative weight of the standard deviation of the considered objective functions over their mean value. A first multi-objective optimization problem was solved to estimate the sensitivity of the expected results to possible difficulties in finding commercially available CHP gas engines with sizes reasonably close to the optimal numerical solutions. The results indicate, for Ospedale S. Paolo, that the economic sensitivity is often higher than the energetic sensitivity for most of the optimal solutions, with standard deviation accounting up to 7% of its mean value for the SPB, whereas the ratio of σ_F/\bar{F} for the TPES is always under 3%. Similar considerations can be conducted for the CROB. The case study also highlights how the expected results obtained through a deterministic definition of the input decision variables within the multi-objective optimization could be overestimated compared to the robust design approach. A second multi-objective robust design optimization has been performed to estimate the fluctuations of the expected results due to possible changes in the reference energetic and economic scenarios. In particular, the selling price of the electricity in different time bands, the reference efficiency of the Italian thermo-electric generation and the selling price of the energy efficiency certificates recognized by the Italian legislation to cogeneration plants have been set as stochastic decision variables. The research highlights how Pareto optimal solutions for the S. Paolo Hospital indicate that the standard deviation for the SPB is always less than 3.5% of its mean value, while this percentage reaches 7% for the TPES. Pareto optimal solutions for the CROB are characterized by standard deviation for the SPB that is always less than 2.5% of its mean value. This percentage increases to 6% for the TPES.

4. Case design study: Manufacturing production

Industrial energy consumption for 2015 was 29% of world total primary energy supply [53], meaning that almost one third of the whole primary energy used on that year was addressed to manufacturing sector. Despite the further development of renewable sources can leads to lower greenhouse gas emission, it can not help to cut down that 29%, and the only way to decrease industrial final consumption is to improve energy efficiency in supply and production chain. Moreover, a more efficient use of energy sources is an effective countermeasure to face the unsecured energy framework and the rising of energy demand [54]: the indicator named industrial energy intensity, ratio between final energy consumption and gross value added (GVA), is a useful tool to control energy demand trend over the years. The indicator must diminish every year and, in last fifteen years, it globally decreased by 30%, while in basic metal manufacturing, which the studied industrial user belongs, it decreased by 15% [55]. In [55] is also highlighted the large number of factors that affects the competitiveness of industries, underlining the importance of energy efficiency for energy-intensive subsectors, due to economic advantages, like a reduction of the impact of volatile energy prices. To prove these statements, two industrial users are compared, and the relevance of energy efficiency towards the depreciation of goods and services came out of analyzed cases data. Dwelling on economic aspect, in [3] there is shown an interesting evaluation about the industrial sector alone: it is stated that, in the 450 Scenario, supplementary investment of around \$300 billion in efficiency can lead to an overall reduction of electricity demand by about 5% in 2040, avoiding to invest about \$450 billion in power generation. Moreover, in [56] the relationship between energy efficiency and financial profits were carried out, showing that a cost reduction in energy supply can lead to a growth in annual profits from 2.2% to 13.8% for each year, depending on industrial subsector. This reduction is induced by energetic improvements in technology and processes, and most of them do not require capital investments: even if capital costs must to be discounted from savings in energy costs, the percent gain is still positive, ranging between 1.7% and 9.6%.

To reaching this energy saving goal, a system-wide approach that goes further than electric motors and motor-driven devices substitution is required, implying also several other measures to enhance the efficiency of the system as a whole, such as predictive maintenance and a more efficient conversion of primary energy supplied. The proposed methodology was applied on a manufacturing plant, in order to find the energy conversion system that achieves the larger primary energy saving. The energy systems investigation involved Combined Heat and Power plants and it is described in section 4.2. The manufacturing process is an innovative wire taping line where an aluminum metallic conductor is taped with kapton®, an insulating polymer that is able to provide a consistent electric and thermal resistance with smaller thickness than other insulating films. A challenging technologic

issue faced during conceptual design of the ECS was that, in order to stick together kapton® and metallic conductor, the wire must be heated from the inside up to 330 °C.

4.1. User schematization

The advanced taping line includes the following main components:

- a pay-off system, that unwind the wire from the spools;
- a concentric taping machine, that put the insulating tape on the conductor wire;
- an induction heating system, where the tape adhesion is ensured by temperature rise on conductor outer surface;
- a liquid cooling system, with re-circulated water;
- a take-up system, that wrap the completed insulated conductor.

In Figure 26, the energy demand of the manufacturing company is shown: all the components described above, are supplied by electric energy, and there is not any thermal need. The only heat required by the cycle is delivered by the induction heating system, but the thermal exchange, in this case, implies a great issue: the heating direction. As stated above, in this manufacturing cycle an induction system is used, because of the need to heat the wire from the inside: the eddy currents involve a Joule effect on outer surface of the metallic conductor, namely in the contact area between wire and tape. The thermal power recoverable from a gas turbine, instead, is available as a radiating source, since the exhaust gases flow through metallic pipes; furthermore, the kapton® tape is a thermal insulating as well as an electric one. In other words, exploiting thermal power from gas turbine exhaust entails a heating of insulated cable from the outside, while it needs to warm up from the inside, and the heat radiated by pipes on the cable is reduced before achieving the interested zone by the thermal insulating property of the kapton® film.

However, after an accurate monitoring of the energetic consumption, a real possibility to supply another component in the manufacturing plant was found out in the annealing oven: this component is adopted for treating metals for all the manufacturing processes in the whole plant and not only for the described one. The electric power peaks in Figure 26 are related to this component, which can be supplied by a thermal source, meaning the exhaust gases from a gas turbine cogenerating plant, instead of conventional electric source. This thermal demand is reported on Figure 27, while Figure 28 shows the electric demand without the annealing oven-related part.

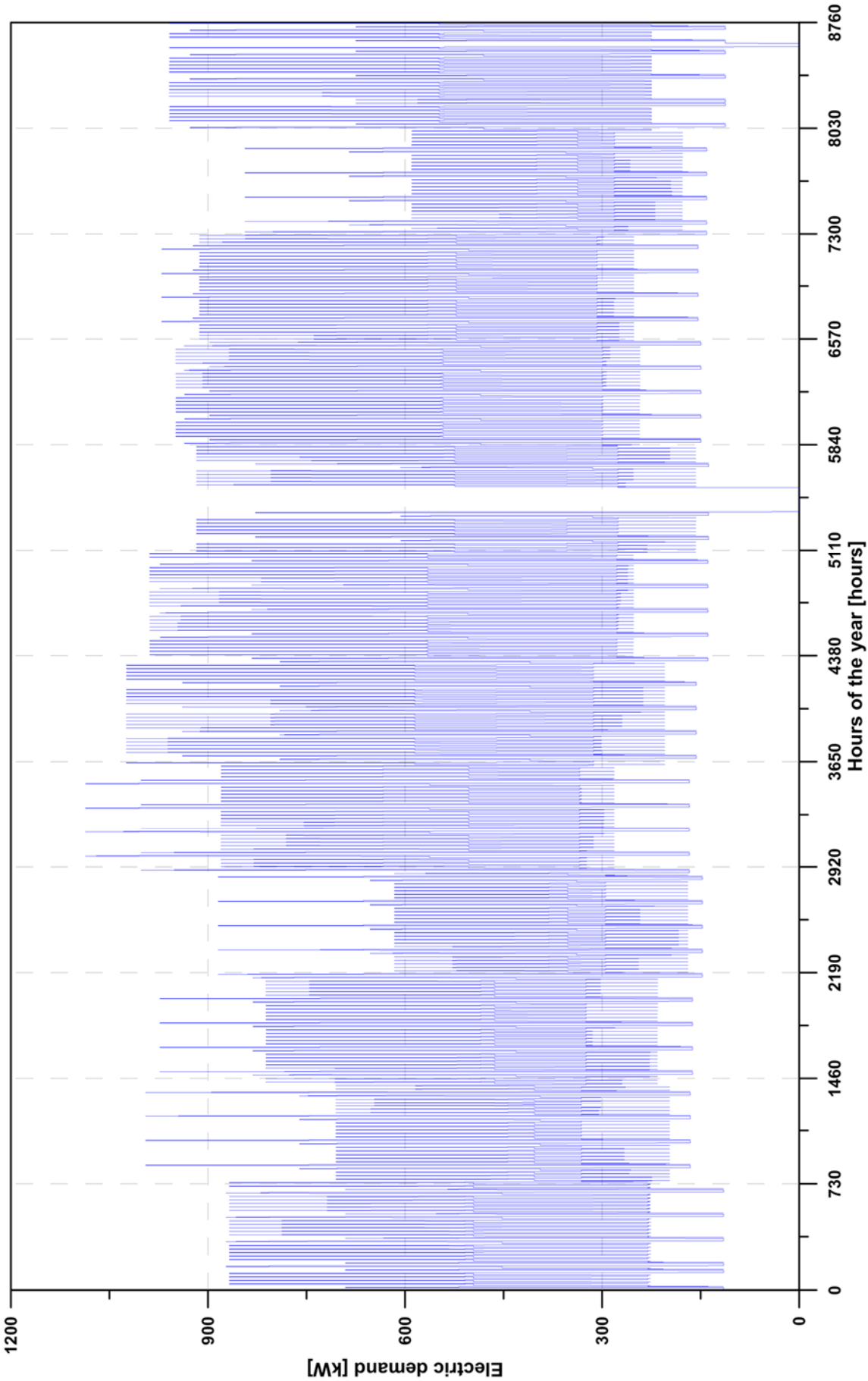


Figure 26: Manufacturing user electric demand

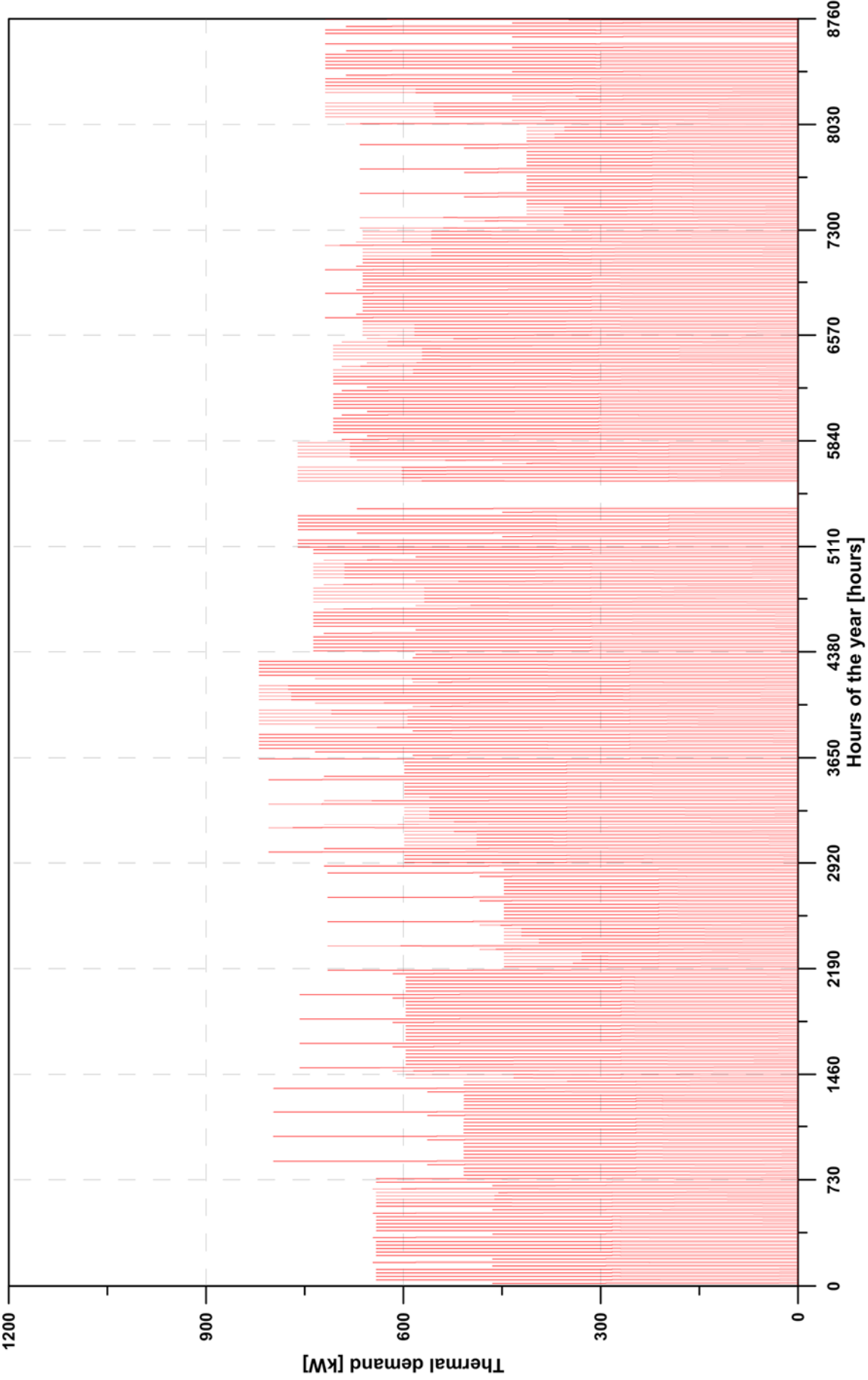


Figure 27: Manufacturing user thermal demand (annealing oven)

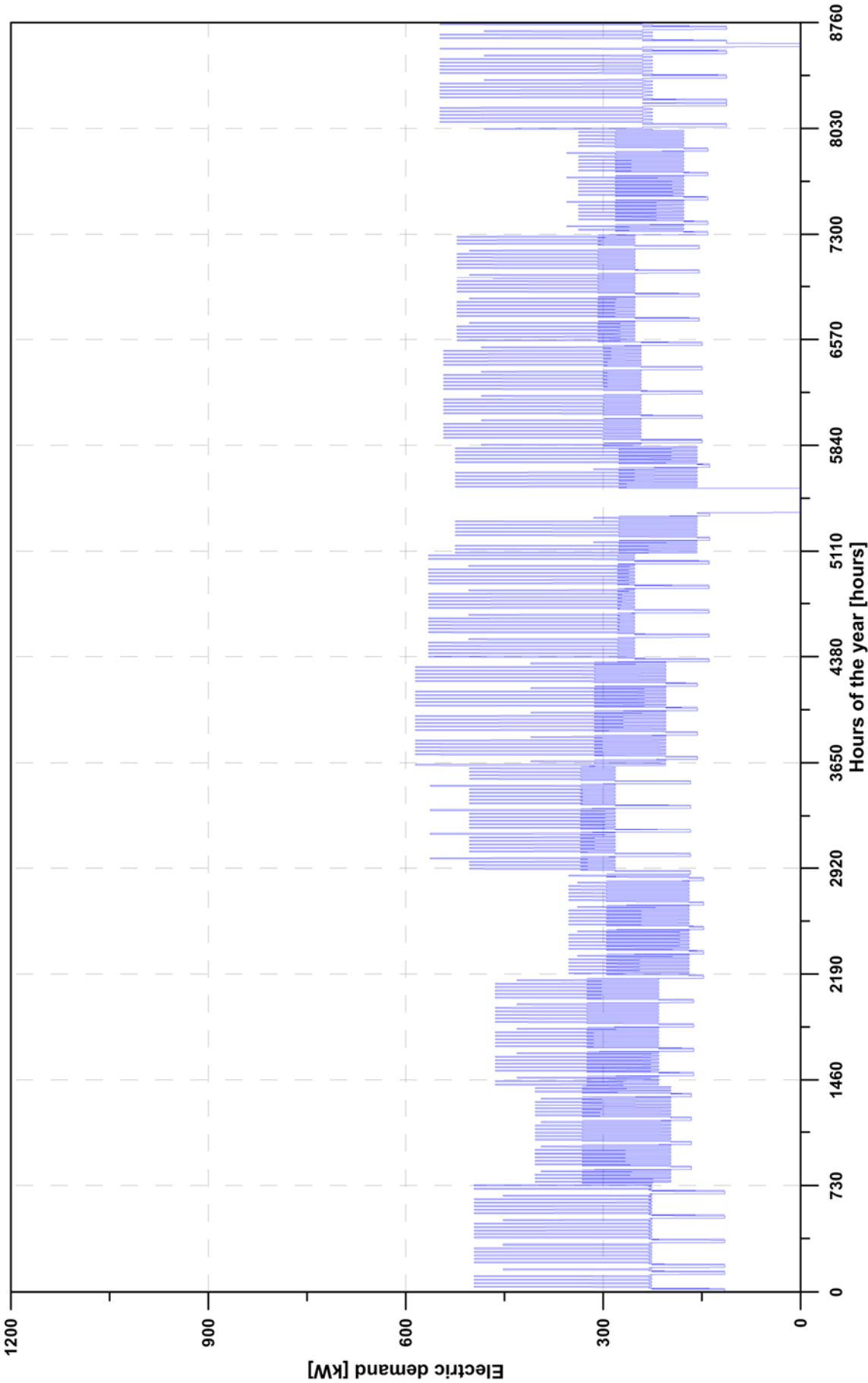


Figure 28: Manufacturing user electric demand without annealing oven

4.2. Energy conversion system schematization

Commonly, the prime mover used in cogeneration plants are reciprocating internal combustion engine (ICE) and gas turbine (GT). Both of them are used since long time in CHP plants, and each of them has peculiar pros and cons that don't allow to define *a priori* which one is the best prime mover for a specific user. "Best" means, in this case, more efficient in term of energy saving, reduction of greenhouse gas emissions and economic investment payback.

After a preliminary investigation, the reciprocating internal combustion engine was dismissed as prime mover because of lower quality of thermal power recovered, since that recoverable power comes from exhaust gas, refrigeration (water) and lubrication (oil) circuits: the thermal power from liquids is at low temperature (100-120 °C) and it isn't suitable for the studied industrial user. In fact, as stated above, the manufacturing cycle requires thermal power at high temperature. Hence, the study was oriented on gas turbine based CHP plant. According to the state of art, most of gas turbine have regenerated cycle in order to achieve higher overall efficiency; however, this plant layout, even if improves significantly the efficiency, entails a penalty in term of thermal power recovery. In fact, exhaust gases of regenerative cycle range their temperature around 260-280 °C, while for ordinary cycle gases this temperature is up to 500 °C. Since the temperature required by the studied manufacturing user is around 330 °C, the adoption of regenerative gas turbine plant would be not adequate to satisfy the thermal need. Thus, two scenarios could be speculated: partial heating of products with regenerative cycle and full heating with standard gas turbine cycle. Despite the first scenario might achieve theoretically higher energy saving, it entails several complex changes in the oven structure that make this component less reliable. Consequently, the second scenario was investigated: the lower overall efficiency related to cycle without regeneration and used in mathematical model is shown in Figure 29. This gas turbine layout involves a higher amount of thermal power against a lower electric generation: in other words, the attainable electricity decreases for a certain amount of primary energy supplied, while the theoretically available thermal power increases.

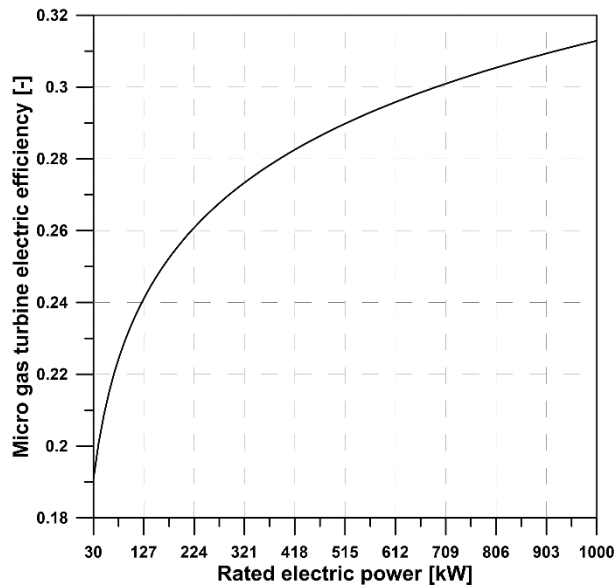


Figure 29: Micro gas turbine efficiency (thermodynamic cycle without regeneration)

This gas turbine, based on this layout, represents the “CHP UNIT” depicted in Figure 30: the exhaust gases are discharged in atmosphere through stack at almost 320 °C: this is a huge destruction of exergy and a waste of primary energy, and it disagrees with the focus point of this research. Therefore, in order to exploit this great quantity of thermal energy, it was added a bottomed Organic Rankine Cycle plant, which, using up most of wasted heat, generates additional electric power: this power must be summed to the one generated by gas turbine, making higher the primary fuel utilization.

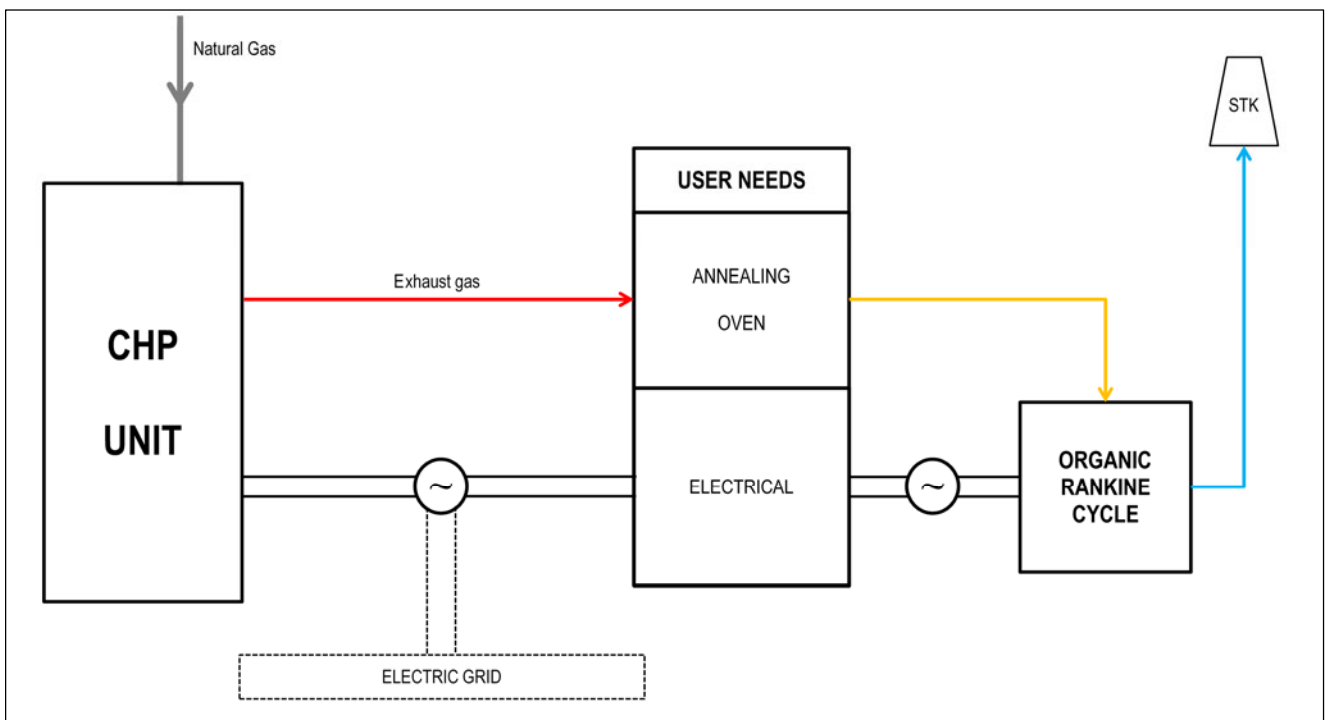


Figure 30: Energy conversion system schematization

In Figure 31 the studied methodology applied to manufacturing user is outlined: the decision variables are, also in this case, nominal electric power of the CHP engine, based on micro gas turbine, and a non-dimensional parameter called threshold thermal index. The mathematical model of the CHP unit comprises the gas turbine and the ORC plant, whose electric power is determined by the amount of wasted heat recoverable from the turbine exhaust; moreover, the same constants listed in Table 1 are used. User energy needs is modeled graphically shown as in Figure 27, concerning thermal demand, and Figure 28, concerning electric demand. Finally, the total primary energy saving and the simple pay back are the objective functions to maximize and minimize, respectively.

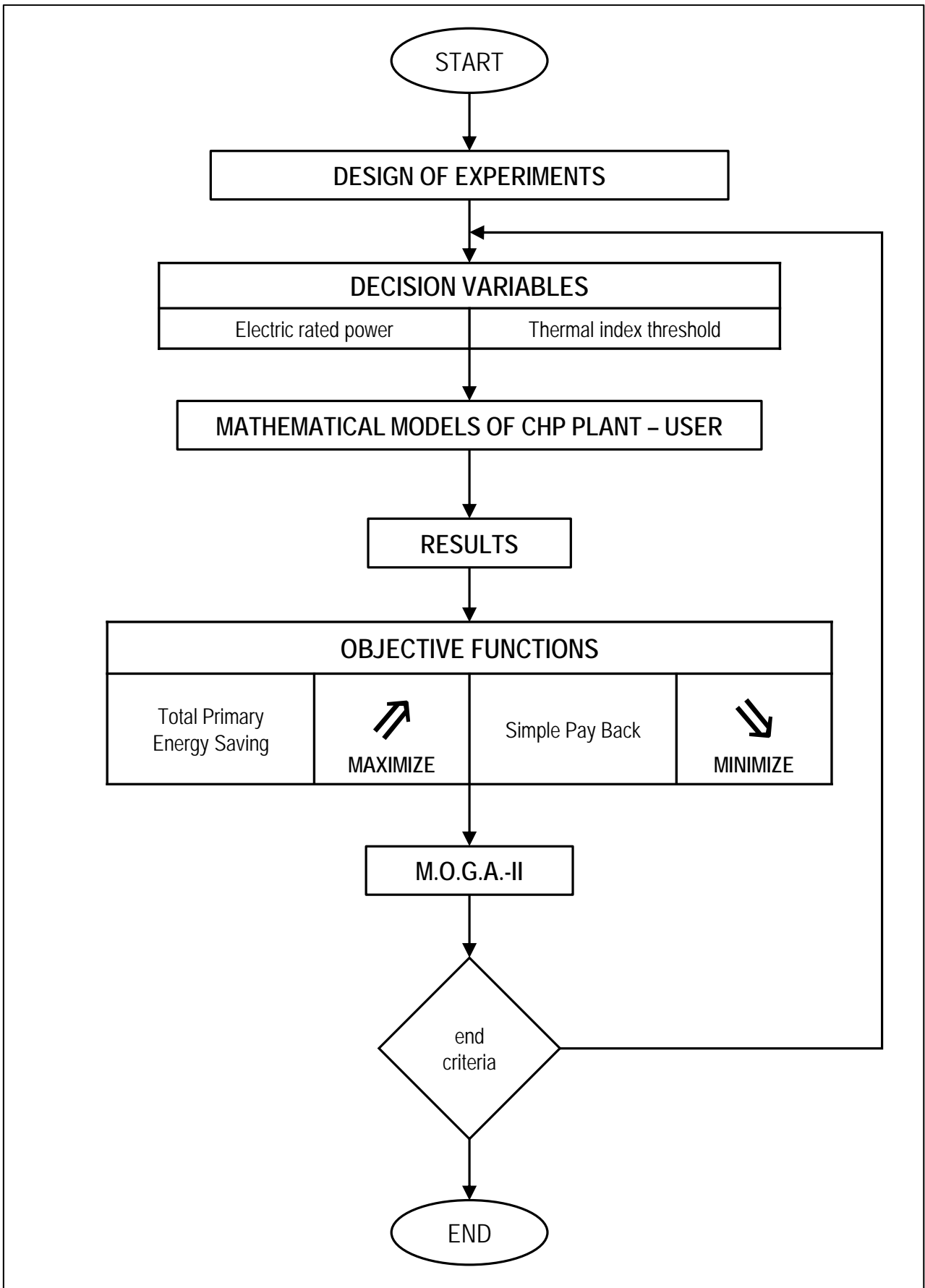


Figure 31: Methodology application on manufacturing industry user

4.3. System design results

Figure 32 shows the results of proposed methodology. On the left chart, all designs are reported in the objective functions plane (SPB, TPES): among these, red crossed ones are the Pareto front for this design optimization. Compared to previous chapter results, in this case the energy saving are undeniably lower because of two main factors: first, the irregular thermal demand allows the CHP plant usage only for the heat-needing hours, that represent almost one third of the whole year, and the primary energy saving is not assured within these hours. Moreover, as described in the introduction, electric efficiency of an energy conversion system is strictly linked to rated power and, as shown on right chart of Figure 32, the highest electric power is 150 kW, which correspond to an overall efficiency of 0.247 (Figure 29).

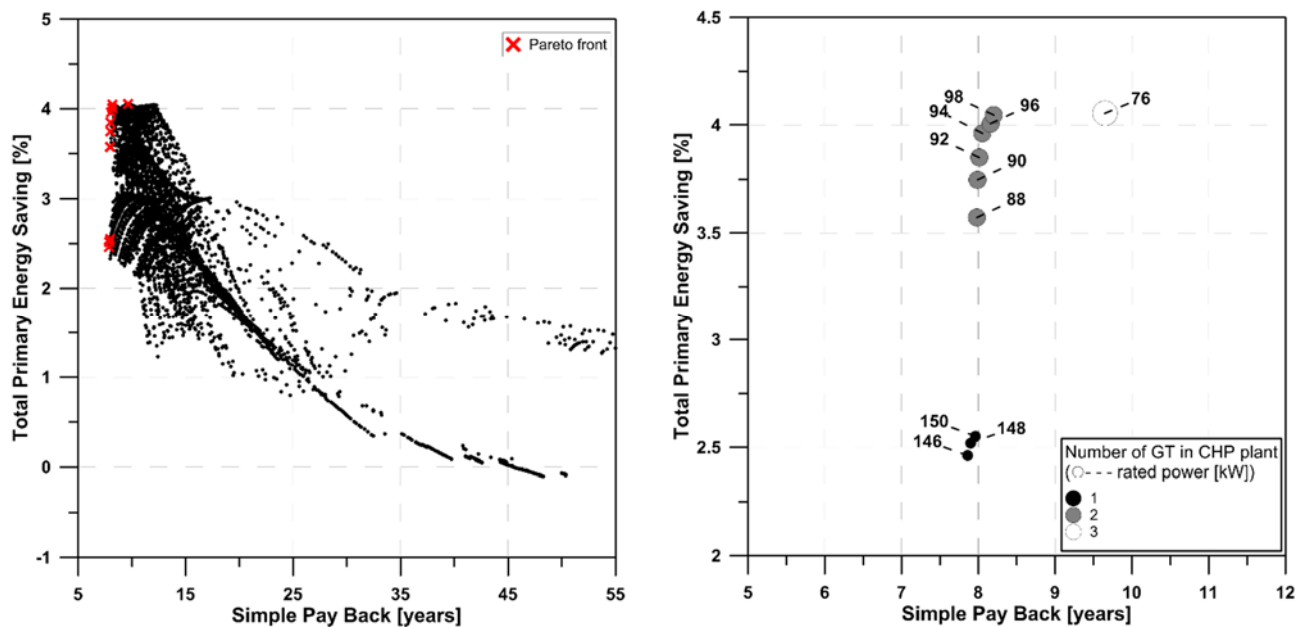


Figure 32: SPB vs TPES for CHP plants supplying tapping manufacturing process

Even if the adopted overall efficiency values are basically prudent, the need of research and development in small scale energy conversion systems arises from the results: improving electric efficiency of these systems and heat exploitation by users can give a relevant contribution to energy saving target.

4.4. Discussion

Irregular and discontinuous energy demand, such the thermal one (Figure 27) of studied industrial user, makes difficult to figure out and design an efficient plant layout, but the methodology was able

to determine a set of optimal solutions, which range between 76 and 150 kW and from 1 to 3 CHP units: this feature highlights the suitability and effectiveness of the methodology to resolve sophisticated energy demands through different and assorted energy conversion system layouts. Compared to previous chapter, the plant was enhanced with an ORC plant, that was able to improve the primary energy employment: these systems are quite recent, and they need to be studied more in detail concerning both machines and working fluids. Moreover, the adoption of energy efficiency strategies within the manufacturing process provide considerable benefits, like energy costs reduction and consequent financial profit increase.

Thus, the improvement in energy exploitation in small scale plants becomes more important in industrial sector because of its large energy saving potential: many cases are already studied, but there still is much work to perform in order to achieve desirable targets of energy efficiency.

5. Case experimental validation study: micro gas turbine systems

In this chapter, the developed methodology was applied with a different purpose than previously reported studies: relating to Figure 4, the energy conversion system model is represented by a thermodynamic model of a micro gas turbine. This application is aimed to achieve two goals at the same time: verify the experimental data reliability and validate the thermodynamic model. In other words, the purpose of current application of the methodology is to improve the thermodynamic model reliability through the minimization of numerical difference between experimental data and calculated values for each thermodynamic parameter involved in the optimization. In fact, the study and design of energy systems which efficiently exploit renewable sources need both the analysis of system-user interaction and the employment of predictive validated models: experimental data are mandatory to perform model validation, but they have intrinsic uncertainties linked to measurement process and elaborate experimental activity carried out on thermal engines system. The extremely unpredictable boundary conditions affect the tests performed on engines by conditioning the unsteady operating state, even for turbomachinery.

The methodology has been applied to two micro gas turbine plants to verify the effectiveness of the thermodynamic model and the consistency of input and output experimental data. Micro gas turbine (MGT) development had a boost in the middle of the twentieth century, owing to their application in automotive and energy markets [57]; the most significant advantages of these small scale power plants are their compact size, low maintenance requirements, low NO_x emissions, and fuel flexibility [57]-[58]. Nowadays, they are also suitable for household use [59]-[60] for power generation and for cogeneration application, due to their low noise and vibration production [61].

Next sections show how much useful was to perform a cross validation among model and experimental data, in order to estimate measurements uncertainty: in fact, a thermodynamic model must be carefully calibrated to represent an acceptable and validated model of the physical system [62],[63]; calibration, in turn, needs a wide experimental campaign to define the model parameters and constraints, because of the uncertain and indeterminable measurement errors [64]. Hence, to validate thermodynamic models, it is mandatory to collect many operating points of experimental data, which means several tests for each point. A long and onerous effort then follows to determine the reliability of the models [65].

Two specific analyses were carried out, thermodynamic one (section 5.1) on two micro gas turbine, Capstone C30 and Turbec T100, and one-dimensional other (section 5.2) on Capstone C30; for each case are reported a summary of the methodology application, the model used in calculation, the table with decision variables, the charts related to objective functions and the preferred design parameters.

5.1. Micro gas turbine thermodynamic analysis

The two plants analyzed have the same layout, which comprises a compressor, a recuperator, a combustion chamber and a turbine, as shown in Figure 33.

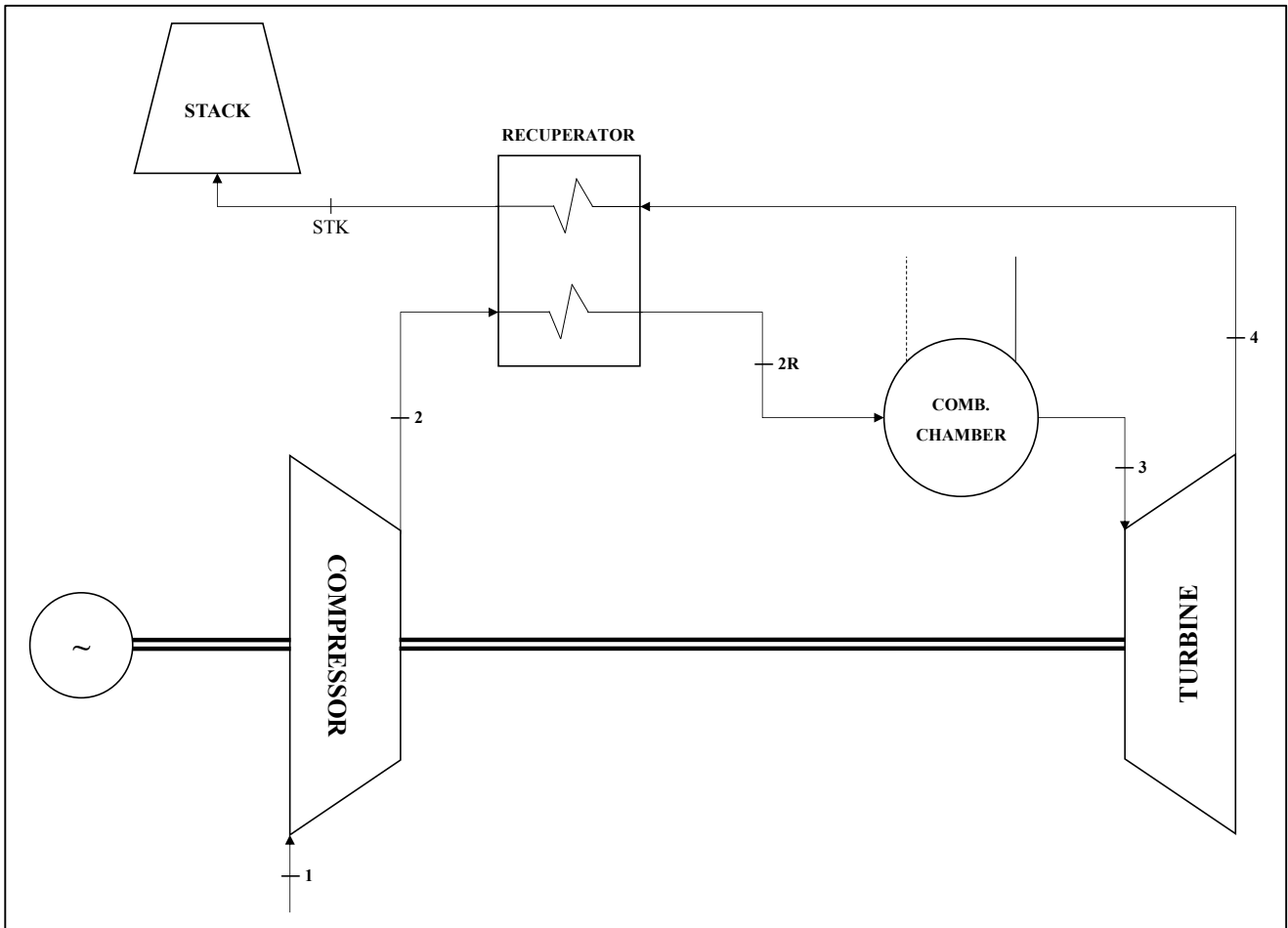


Figure 33: Micro gas turbine layout

The thermodynamic cycle starts with the incoming air flow to the compressor (1). The air exits the compressor (2) with a higher pressure as a function of the polytropic efficiency, given by:

$$\eta_{P,C} = \frac{\frac{m}{m-1}RT_1 \left[1 - \beta^{\frac{m-1}{m}} \right]}{c_p T_1 \left[1 - \beta^{\frac{m-1}{m}} \right]} \quad (5.1)$$

The compressed air flows through the recuperator, a countercurrent heat exchanger, where it is heated by the exhaust gases coming out from the turbine (4), following the known heat transfer law:

$$Q_{HX} = UAT_{ML} \quad (5.2)$$

Thus, the heated air enters (2R) the combustion chamber where it burns when mixed with the incoming fuel. The exhaust gases (3) expand in the turbine with an expansion polytropic efficiency of:

$$\eta_{P,T} = \frac{c_p T_3 \left[1 - \left(\frac{1}{\beta} \right)^{\frac{m-1}{m}} \right]}{\frac{m}{m-1} RT_3 \left[1 - \left(\frac{1}{\beta} \right)^{\frac{m-1}{m}} \right]} \quad (5.3)$$

The methodology was applied using different ranges for all the decision variables, except for the fuel, since both turbines are supplied by natural gas, whose composition is reported in Table 7.

Table 7: Fuel composition [66]

| FUEL COMPOSITION | | |
|------------------|-----------|-------|
| | RANGE | UNITS |
| Methane | 87.0–96.0 | %vol |
| Ethane | 1.8–5.1 | %vol |
| Propane | 0.1–1.5 | %vol |
| Butane | 0.02–0.6 | %vol |
| Carbon dioxide | 0.1–1.0 | %vol |
| Nitrogenous | 1.3–5.6 | %vol |
| Oxygen | 0.01–0.1 | %vol |

In Figure 34, the maximum theoretical isentropic and polytropic efficiencies of radial turbomachinery [67] are plotted as a function of the specific speed:

$$N_s = \frac{\omega \sqrt{\dot{V}}}{(gH_{IS})^{3/4}} \quad (5.4)$$

The variation of the specific speed in the operating interval for both radial machines is reported in Figure 34, with the blue area for the turbine range and with the red area for the compressor range.

Comparing the efficiency values of these areas, we demonstrated the validity of the assumed efficiencies constraint:

$$\eta_{P,C} \leq \eta_{IS,T} \quad (5.5)$$

In other words, the constraint (5.5) means that, for the same technologic level, turbine isentropic efficiency is always greater than or equal to compressor polytropic efficiency. The assumption is confirmed also by experimental data reported in the technical literature [68]. This correlation is used as a constraint in the optimization process for both the micro gas turbine plants (Table 9 and Table 12).

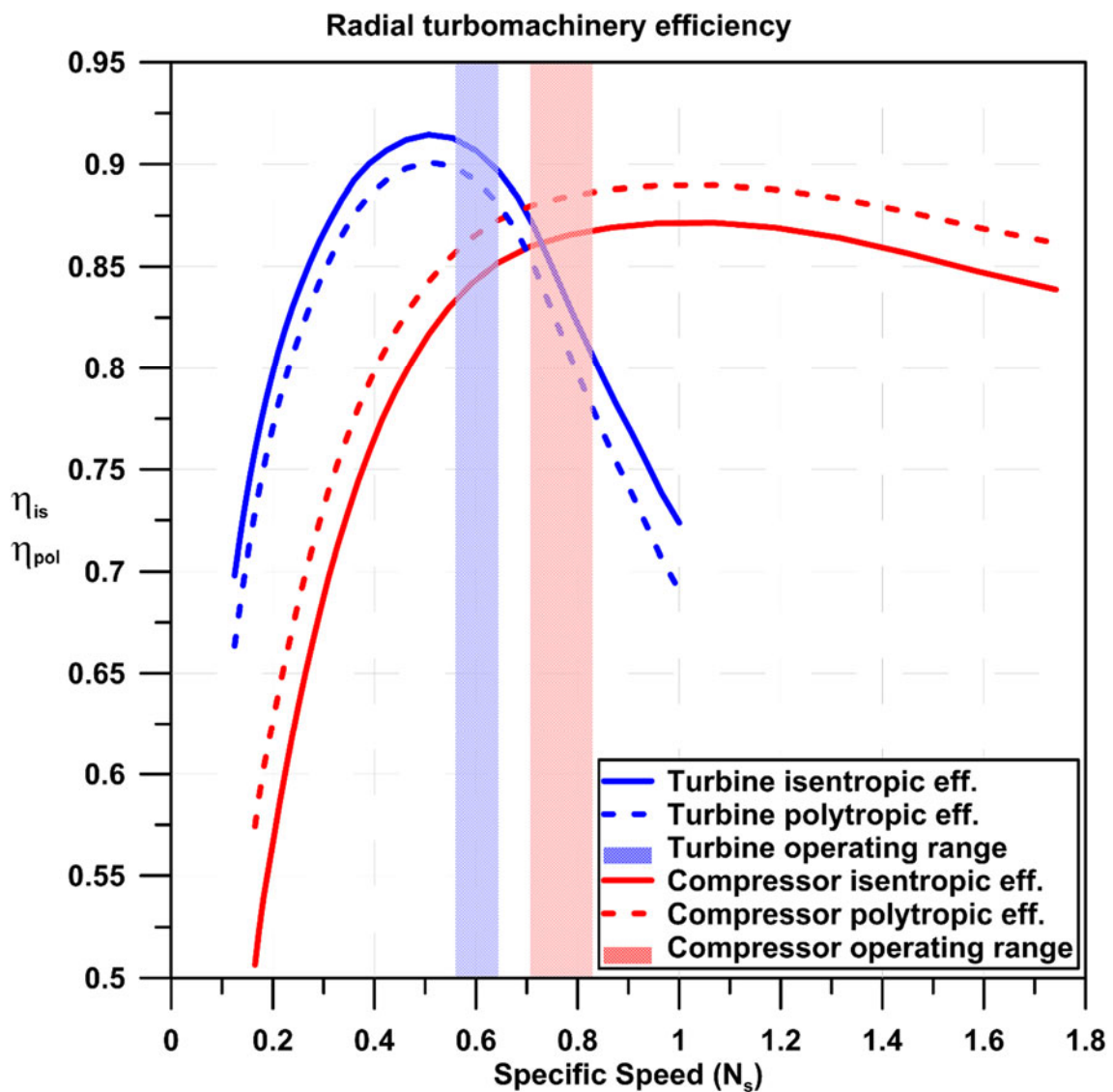


Figure 34: Radial turbomachinery efficiency [67]

As stated above, the two studied micro gas turbines are Capstone C30 (Figure 35 and section 5.1.1) and Turbec T100 (Figure 36 and section 5.1.2). The so called “thermodynamic micro gas turbine model” (Figure 35 and Figure 36) is referred to the thermodynamic analyses above described in this paragraph. Decision variables (Figure 35 and Figure 36) are the same thermodynamic and mechanical parameters for both turbines except for their range, as listed in Table 9 for C30 and in Table 12 for T100. Concerning the objective functions, both methodology applications are aimed to minimize the difference between calculated and experimental value for chosen parameters: net electric power (P_E), overall efficiency (η_G) and turbine inlet temperature (T_3) are objectives for the two plants. Furthermore, the C30 has one more objective, namely, the thermal power supplied by fuel with reference to its higher heating value ($\dot{m}_c \cdot \text{HHV}$), whereas the T100 plant has two more objectives, the turbine outlet temperature (T_4) and the combustion chamber pressure (p_{CC}). It must be emphasized that the decision variables and the optimization objectives are not always the same but that they depend on the assembled data.

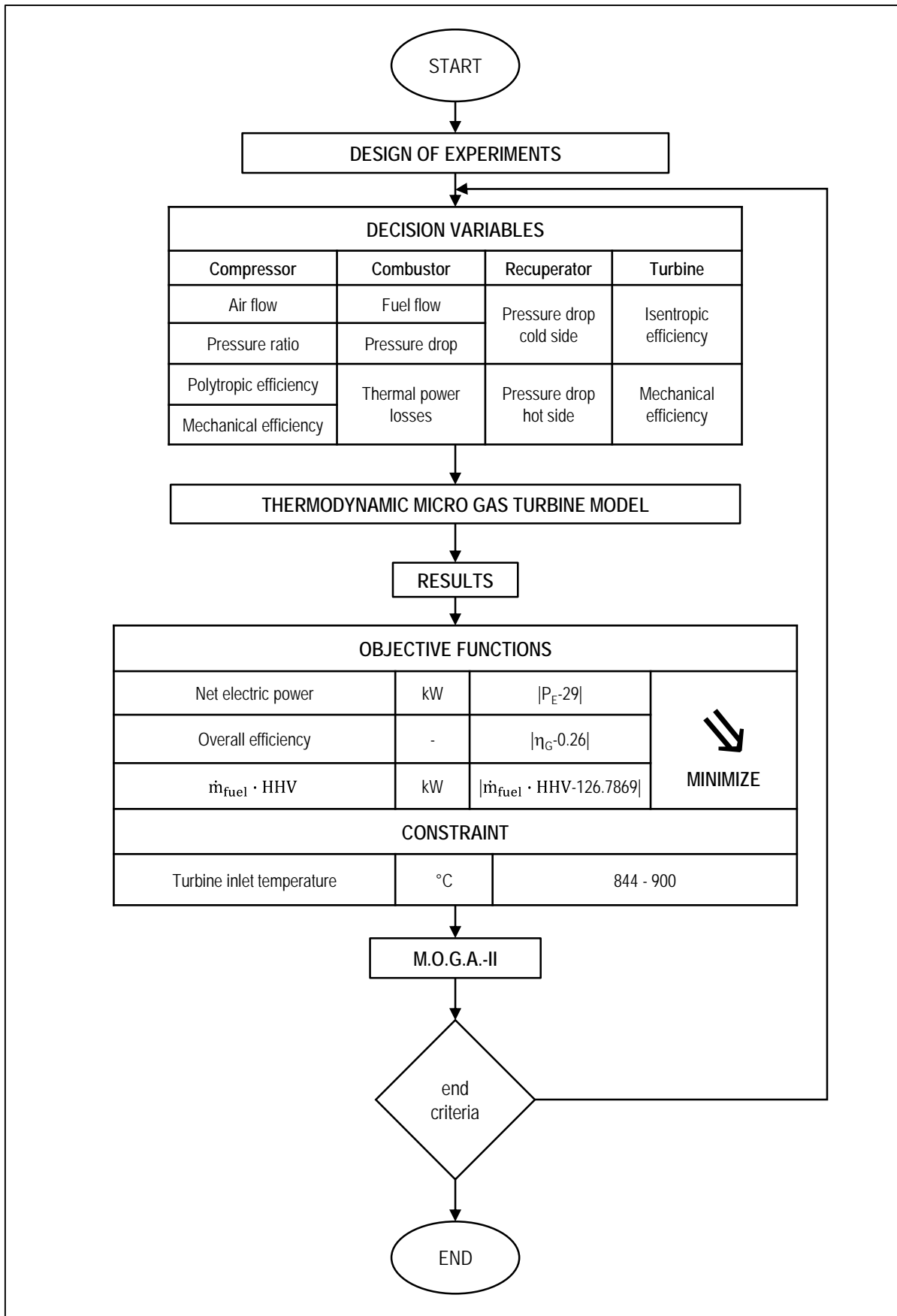


Figure 35: Methodology application on Capstone C30 thermodynamic analysis model

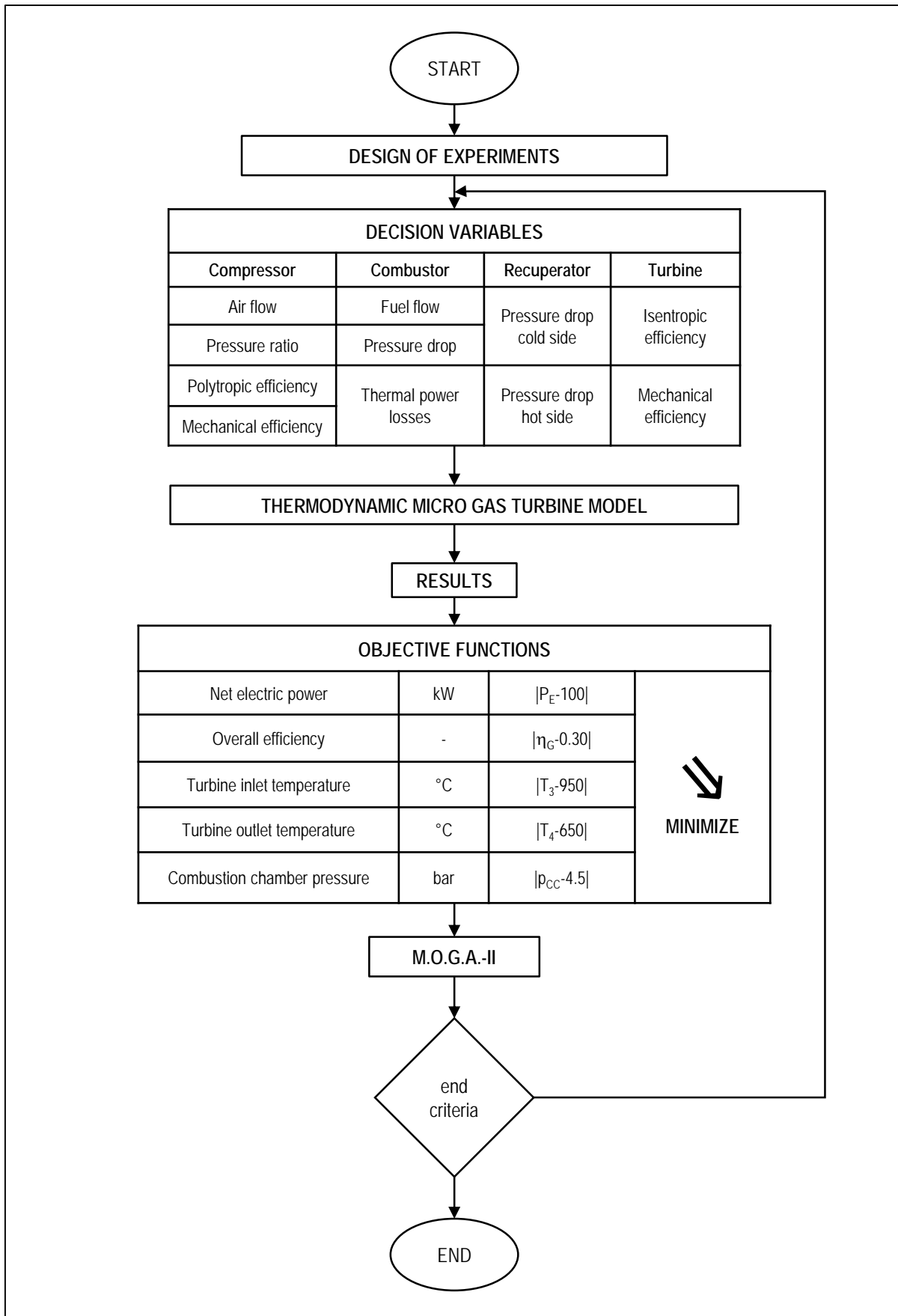


Figure 36: Methodology application on Turbec T100 thermodynamic analysis model

5.1.1. Experimental validation: Capstone C30

Much experimental data regarding the Capstone C30 turbine is available [57],[69]-[71], but Table 8 shows that they are not mutually concordant; two of these ([69],[70]) are explicitly realized in ISO conditions. The input variable ranges and the optimization objectives and constraints for Capstone C30 are listed in Table 9.

Table 8: Capstone C30 reference data

| CAPSTONE C30: REFERENCE DATA | | | | | | | |
|------------------------------|-------------|-------|------|--|----------|-------|------|
| | VALUE | UNITS | REF | | VALUE | UNITS | REF |
| Net electric power | 29 ± 1 | kW | [69] | $\dot{m}_{\text{fuel}} \cdot \text{HHV}$ | 126.7869 | kW | [69] |
| Overall efficiency | 0.26 ± 0.02 | — | [69] | Turbine inlet temperature | 844 | °C | [71] |
| Gas flow | 0.31 | kg/s | [69] | Turbine inlet temperature | 871 | °C | [57] |
| Pressure ratio | 3.6 | — | [71] | Turbine inlet temperature | 900 | °C | [70] |
| Pressure ratio | 3.2 | — | [70] | | | | |

Table 9: Methodology setting for Capstone C30 thermodynamic analysis

| CAPSTONE C30: METHODOLOGY SETTING | | |
|--|-----------------|-------|
| DECISION VARIABLE | RANGE | UNITS |
| COMPRESSOR | | |
| Air flow | 0.30719–0.30754 | kg/s |
| Pressure ratio at compressor | 3.1–3.7 | — |
| Polytropic efficiency | 0.77–0.886 | — |
| Mechanical efficiency | 0.85–0.98 | — |
| COMBUSTOR | | |
| Fuel flow | 0.00246–0.00281 | kg/s |
| Thermal power losses | 0.0001–2.5 | kW |
| Pressure drop | 0.0001–0.3 | bar |
| RECUPERATOR | | |
| Pressure drop, hot side | 0.001–0.4 | bar |
| Pressure drop, cold side | 0.001–0.4 | bar |
| TURBINE | | |
| Isentropic efficiency | 0.795–0.91 | — |
| Mechanical efficiency | 0.88–0.98 | — |
| OBJECTIVES | | |
| Net electric power | 29 | kW |
| Overall efficiency | 0.26 | — |
| $\dot{m}_{\text{fuel}} \cdot \text{HHV}$ | 126.7869 | kW |
| CONSTRAINT | | |
| Turbine inlet temperature | 844–900 | °C |

It must be noticed that the table lists the numerical values of input variables and objectives (with constraints being a particular objective) defined in Figure 35.

The two charts in Figure 37 show the methodology results concerning two objectives, namely net electric power and overall efficiency: the chart on the left shows most of the results on objective functions plane, while the right chart shows the absolute values of those parameters. On both diagrams the Pareto front is marked with blue circles, while a red circle indicates the so-called preferred design: since more than 25,000 designs were analyzed during the optimization, the author, as well as others did in [72], sorted the results using the Euclidean norm to evaluate the variation in all objectives and constraints with a single value:

$$\text{PreferredDesign} = \sqrt{\left(\frac{\Delta P_E}{P_{E,\text{exp}}}\right)^2 + \left(\frac{\Delta \eta_G}{\eta_{G,\text{exp}}}\right)^2 + \left(\frac{\Delta (\dot{m}_{\text{fuel}} \cdot \text{HHV})}{(\dot{m}_{\text{fuel}} \cdot \text{HHV})_{\text{exp}}}\right)^2} \quad (5.6)$$

The design characterized by the lowest Euclidean norm is indicated in Table 10.

Figure 38, as well as the two following, have the same layout of Figure 37, and it is focused on the thermal power supplied by fuel with reference to its higher heating value and net electric power; Figure 39 depicts the results on objectives plan ($\eta_G, \dot{m}_{\text{fuel}} \cdot \text{HHV}$), and finally Figure 40 shows the results in terms of net electric power and overall efficiency as a function of turbine inlet temperature.

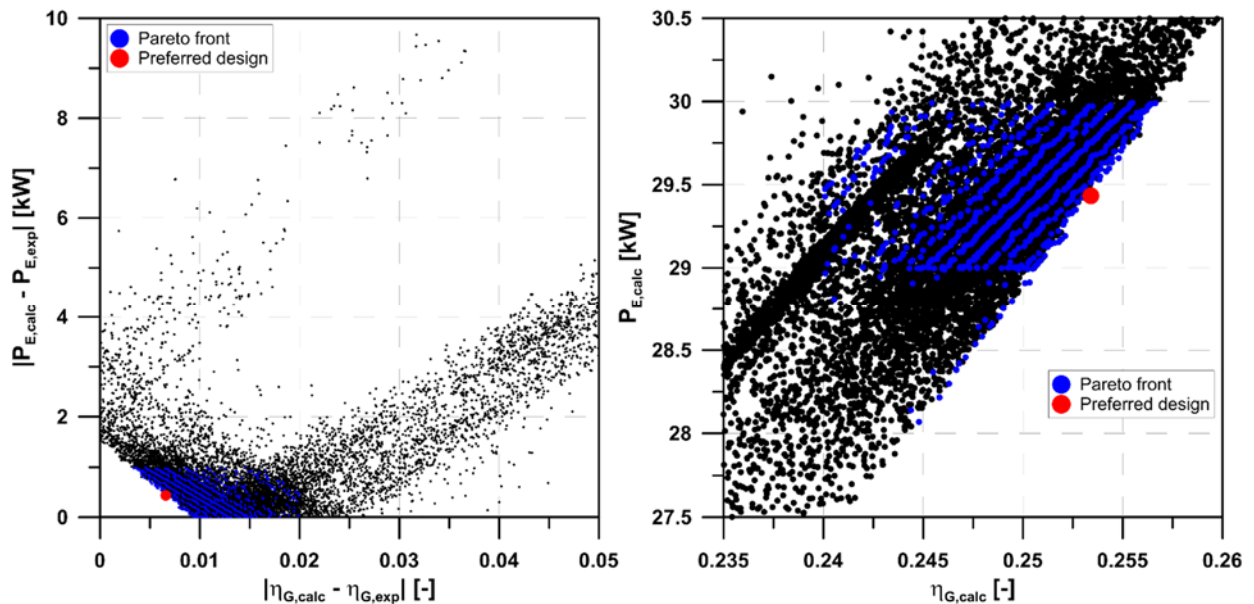


Figure 37: Capstone C30 thermodynamic analysis, multi-variable multi-objective results (η_G, P)

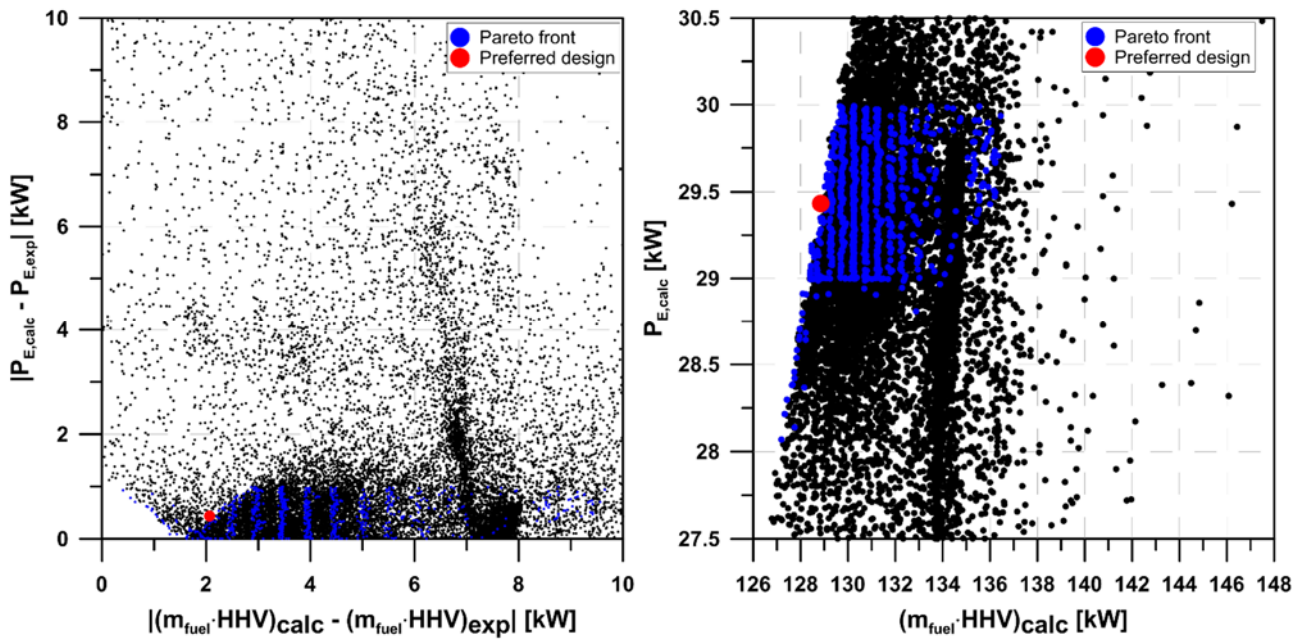


Figure 38: Capstone C30 thermodynamic analysis multi-variable multi-objective results ($\dot{m}_{fuel} \cdot HHV, P$)

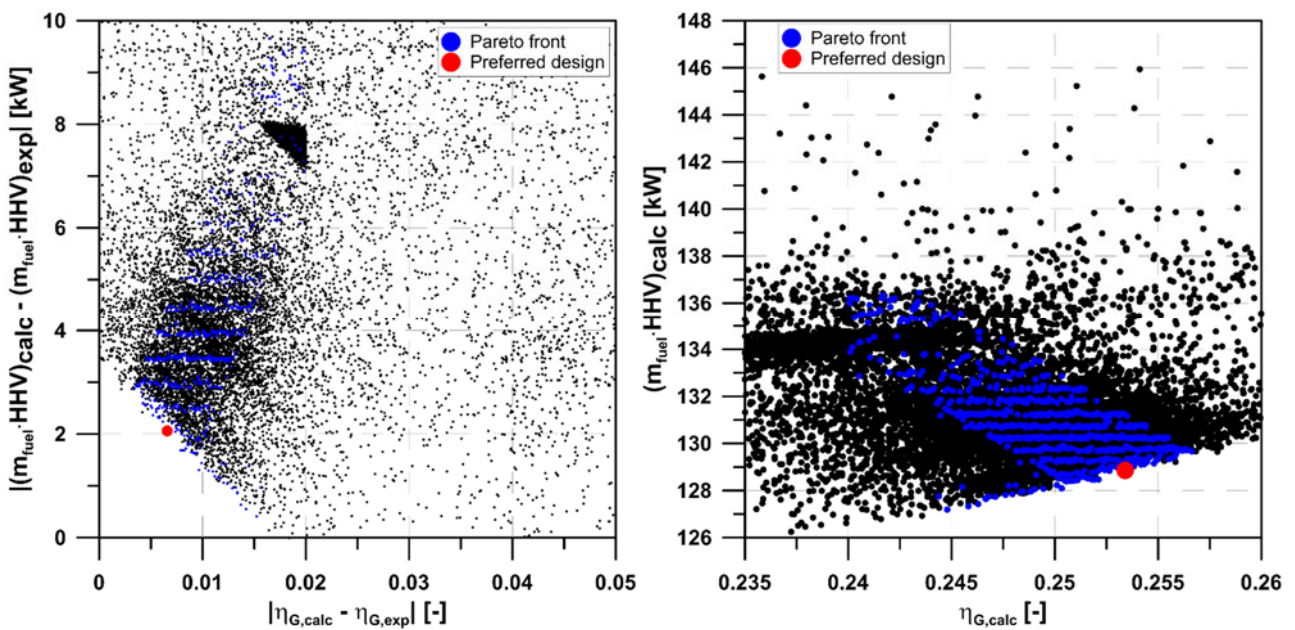


Figure 39: Capstone C30 thermodynamic analysis multi-variable multi-objective results ($\eta_G, \dot{m}_{fuel} \cdot HHV$)

On charts related to objective functions, there is a kind of triangle near to axes origin without circles: these lack of results means that there is not any set of decision variables able to achieve the target values of at least two objectives at same time. In other words, there is an incongruity in experimental data, thermodynamic model or both of them.

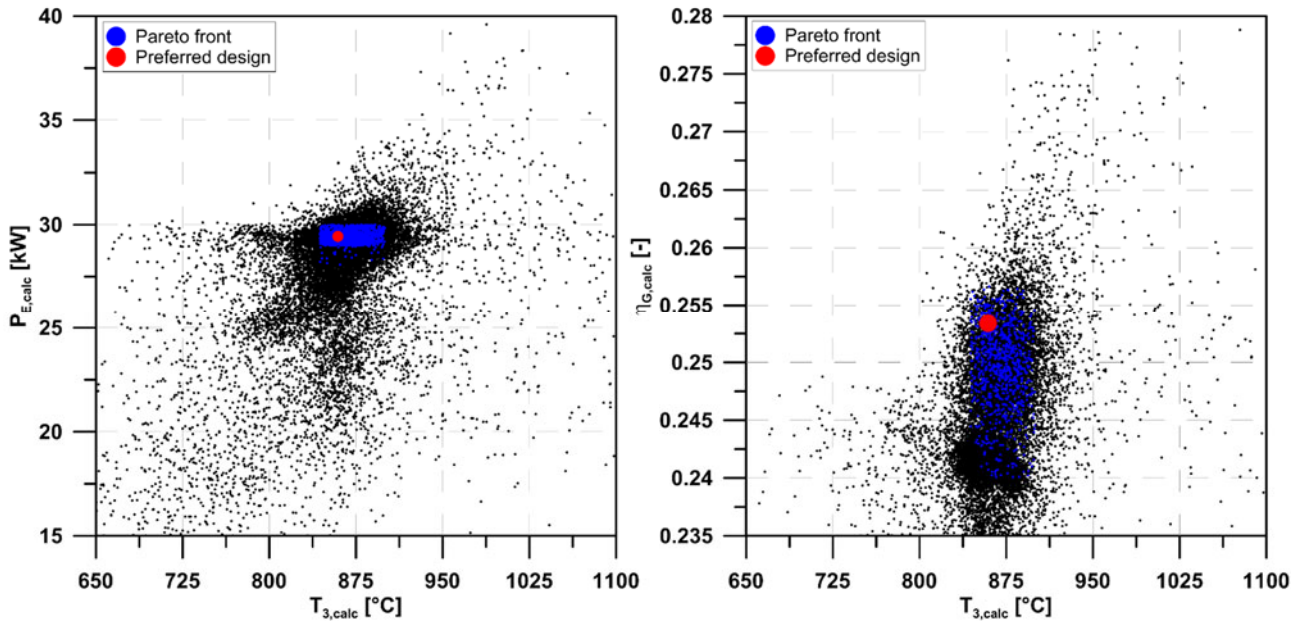


Figure 40: Capstone C30 thermodynamic analysis, multi-variable multi-objective results (T_3, P and T_3, η_G)

Table 10: Capstone C30 preferred design

| CAPSTONE C30: PREFERRED DESIGN | | |
|---------------------------------------|--------------|--------------|
| INPUT VARIABLES | RANGE | UNITS |
| COMPRESSOR | | |
| Air flow | 0.30745 | kg/s |
| Pressure ratio at compressor | 3.39 | — |
| Polytropic efficiency | 0.8265 | — |
| Mechanical efficiency | 0.98 | — |
| COMBUSTOR | | |
| Fuel flow | 0.00255 | kg/s |
| Thermal power losses | 0.0001 | kW |
| Pressure drop | 0.3 | bar |
| RECUPERATOR | | |
| Pressure drop, cold side | 178.6 | mbar |
| Pressure drop, hot side | 18.5 | mbar |
| TURBINE | | |
| Isentropic efficiency | 0.8555 | — |
| Mechanical efficiency | 0.9785 | — |
| OBJECTIVES | VALUE | UNITS |
| Net electric power | 29.433 | kW |
| Overall efficiency | 0.2534 | — |
| $\dot{m}_{fuel} \cdot HHV$ | 128.85 | kW |
| CONSTRAINT | VALUE | UNITS |
| Turbine inlet temperature | 859.42 | °C |

The preferred result reported in Table 10, besides the optimization objectives, is characterized by compressor and turbine efficiencies already found in the literature [73],[74], and it was compared with Capstone C30 performance maps found in [71] and [74]. In Figure 41, a red point that represents the design operating condition is shown on both compressor and turbine maps: the point fits with shaft speed, efficiency and pressure ratio for both the pieces of turbomachinery. This fitting shows, at least for this instance, the proposed methodology effectiveness, because the red point, resulting from the calculation, is congruent with the matching between compressor and turbine.

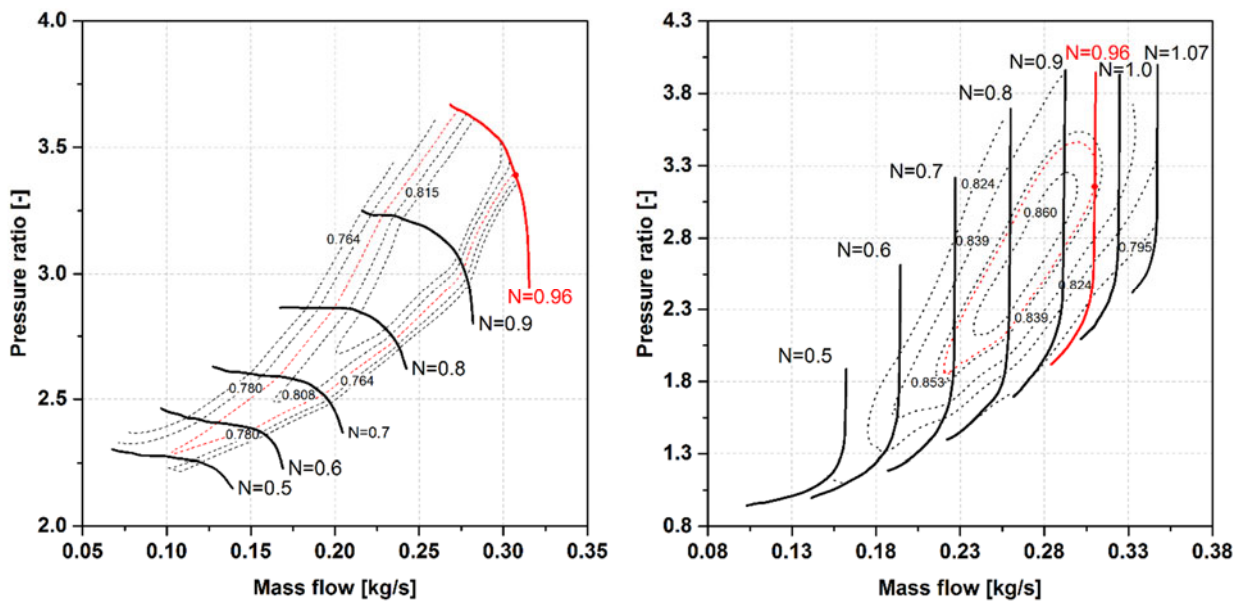


Figure 41: Capstone C30 compressor (left) and turbine (right) performance maps

5.1.2. Experimental validation: Turbec T100

Turbec T100 reference values are listed in Table 11.

Table 11: Turbec T100 reference data [75].

| TURBEC T100: REFERENCE DATA | | | | | |
|------------------------------------|----------|-------|----------------------------|-------|-------|
| | VALUE | UNITS | | VALUE | UNITS |
| Net electric power | 100 ± 3 | kW | Turbine inlet temperature | 950 | °C |
| Overall efficiency | 0.30 ± 1 | — | Turbine outlet temperature | 650 | °C |
| Pressure ratio at compressor | 4.5 | — | Gas flow | 0.80 | kg/s |

The decision variable ranges and the methodology objective functions for Turbec T100 are listed in Table 12.

Table 12: Methodology setting for Turbec T100 thermodynamic analysis

| TURBEC T100: METHODOLOGY SETTING | | |
|---|---------------|-------|
| INPUT VARIABLES | RANGE | UNITS |
| COMPRESSOR | | |
| Air flow | 0.7900–0.7935 | kg/s |
| Pressure ratio at compressor | 4.0–5.0 | — |
| Polytropic efficiency | 0.77–0.886 | — |
| Mechanical efficiency | 0.85–0.98 | — |
| COMBUSTOR | | |
| Fuel flow | 0.0065–0.0100 | kg/s |
| Thermal power losses | 0.01–6 | kW |
| Pressure drop | 0.01–0.2 | mbar |
| RECUPERATOR | | |
| Pressure drop, hot side | 0.001–0.2 | bar |
| Pressure drop, cold side | 0.001–0.2 | bar |
| TURBINE | | |
| Isentropic efficiency | 0.77–0.91 | — |
| Mechanical efficiency | 0.85–0.98 | — |
| OBJECTIVES | VALUE | UNITS |
| Net electric power | 100 | kW |
| Overall efficiency | 0.30 | — |
| Turbine inlet temperature | 950 | °C |
| Turbine outlet temperature | 650 | °C |
| Combustion chamber pressure | 4.5 | bar |

Figure 42–Figure 45 refer to methodology application results, and they have the same layout as the Capstone C30 charts. In particular, the results for electric power versus overall efficiency are shown in Figure 42, those for electric power versus turbine inlet temperature are shown in Figure 43, those

for electric power versus turbine outlet temperature are shown in Figure 44, and those for electric power versus combustion chamber pressure are shown in Figure 45.

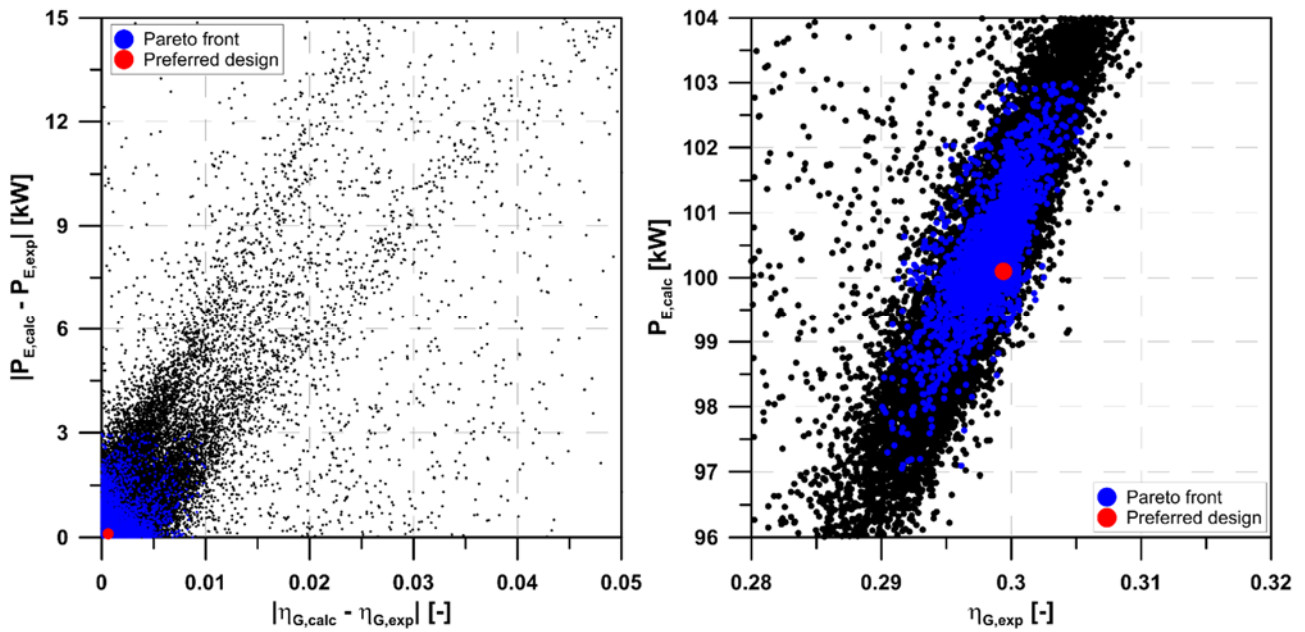


Figure 42: Turbec T100 thermodynamic analysis, multi-variable multi-objective results (η_G, P)

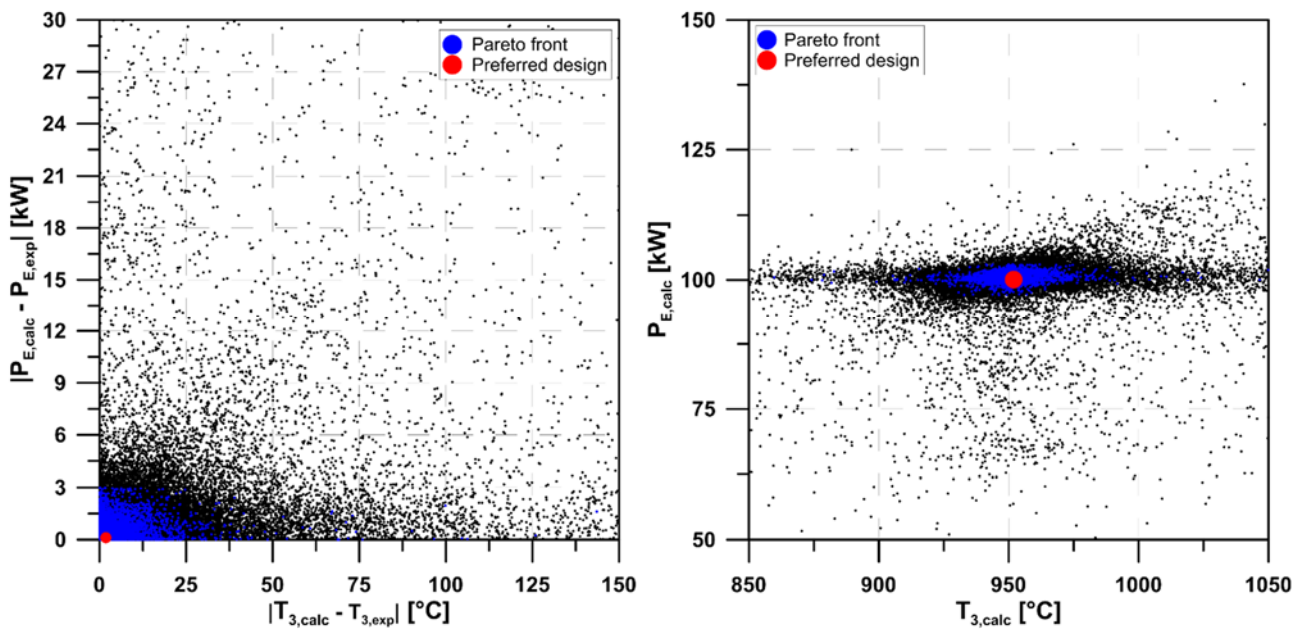


Figure 43: Turbec T100 thermodynamic analysis, multi-variable multi-objective results (T_3, P)

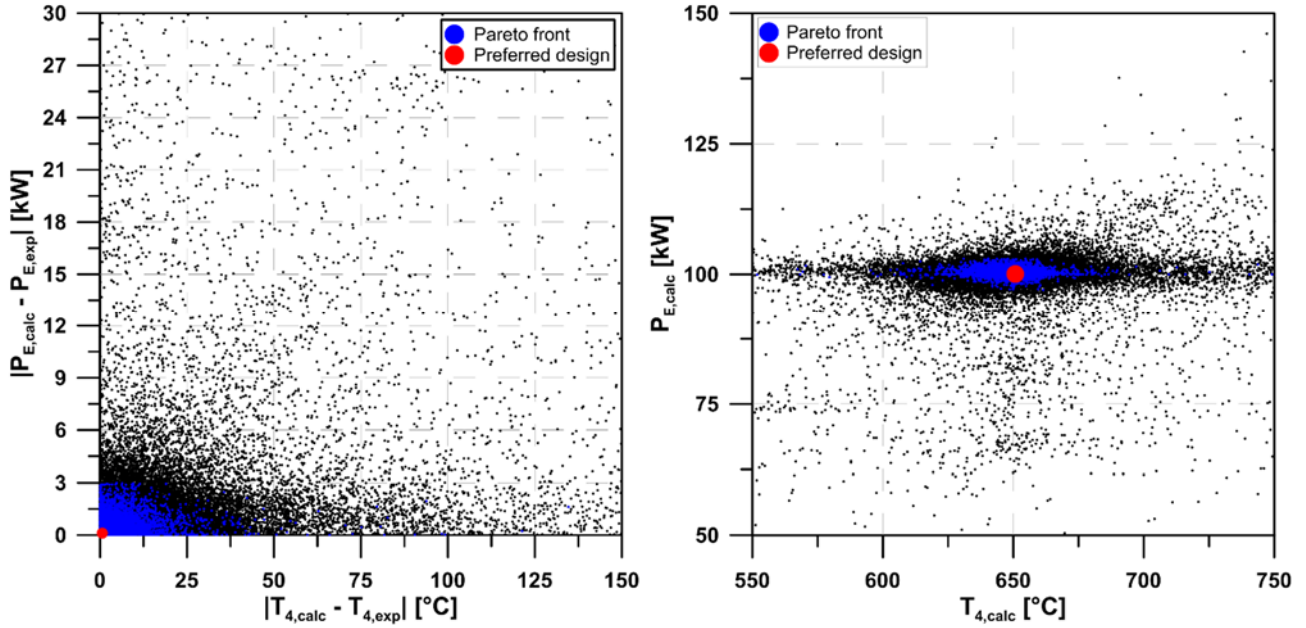


Figure 44: Turbec T100 thermodynamic analysis, multi-variable multi-objective results (T_4, P)

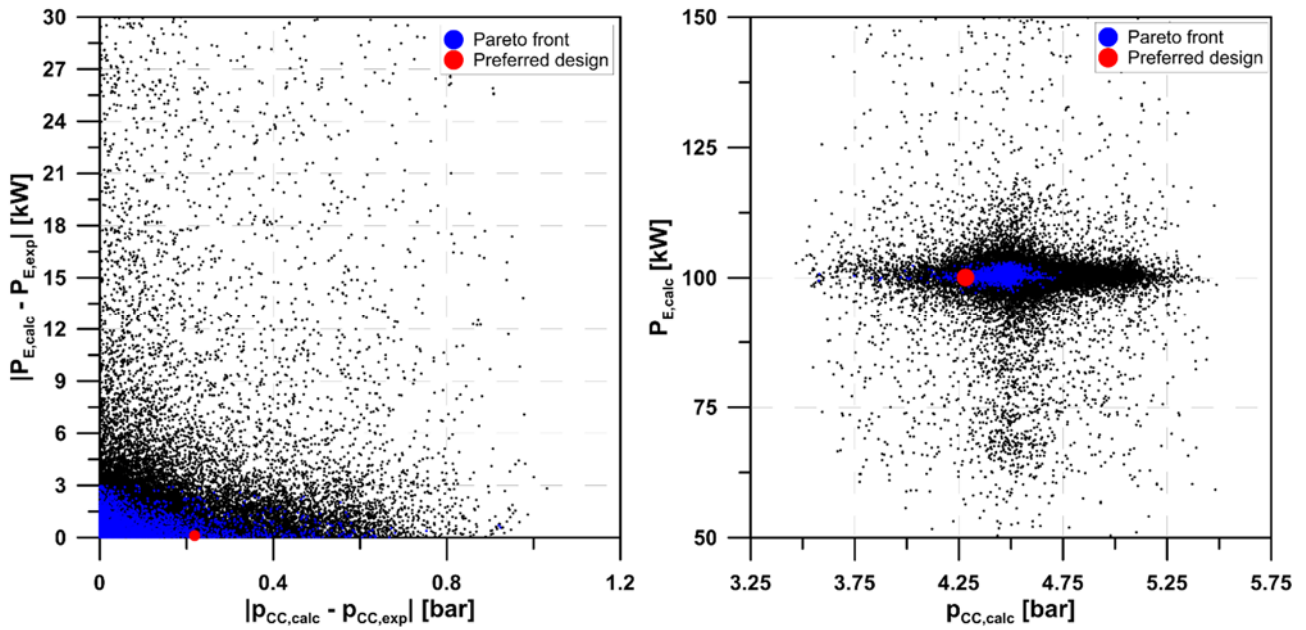


Figure 45: Turbec T100 thermodynamic analysis, multi-variable multi-objective results (p_{cc}, P)

Again, the nearly 25,000 designs obtained for the Turbec T100 are sorted by using the lowest Euclidean norm.

$$\text{PreferredDesign} = \sqrt{\left(\frac{\Delta P_E}{P_{E,\text{exp}}}\right)^2 + \left(\frac{\Delta \eta_G}{\eta_{G,\text{exp}}}\right)^2 + \left(\frac{\Delta T_3}{T_{3,\text{exp}}}\right)^2 + \left(\frac{\Delta T_4}{T_{4,\text{exp}}}\right)^2 + \left(\frac{\Delta p_{cc}}{p_{cc,\text{exp}}}\right)^2} \quad (5.7)$$

As for the Capstone C30, and the parameters for the preferred design are listed in Table 13.

Table 13: Turbec T100 preferred design

| TURBEC T100: PREFERRED DESIGN | | |
|--------------------------------------|--------------|--------------|
| INPUT VARIABLES | RANGE | UNITS |
| COMPRESSOR | | |
| Air flow | 0.7928 | kg/s |
| Pressure ratio at compressor | 4.65 | — |
| Polytropic efficiency | 0.812 | — |
| Mechanical efficiency | 0.963 | — |
| COMBUSTOR | | |
| Fuel flow | 0.0072 | kg/s |
| Thermal power losses | 0.6876 | kW |
| Pressure drop | 170.9 | mbar |
| RECUPERATOR | | |
| Pressure drop hot side | 259.3 | mbar |
| Pressure drop cold side | 93.5 | mbar |
| TURBINE | | |
| Isentropic efficiency | 0.873 | — |
| Mechanical efficiency | 0.98 | — |
| OBJECTIVES | VALUE | UNITS |
| Net electric power | 100.102 | kW |
| Overall efficiency | 0.2994 | — |
| Turbine inlet temperature | 951.87 | °C |
| Turbine outlet temperature | 650.71 | °C |
| Combustion chamber pressure | 4.28 | bar |

5.1.3. Discussion

The methodology led to different conclusions for the two analyzed micro gas turbines: the Capstone C30 case highlighted a larger uncertainty concerning input data, objectives and constraints, whereas the study of the Turbec T100 yielded more reliable results, being able to match almost all the data collected with the smallest variance. The only parameter with a high variance is the combustion chamber pressure, which is defined as “approximately 4.5 bar” in [75]. In Table 14, objectives and constraint for this methodology application on thermodynamic model are listed for both micro gas turbine plants: the T100 preferred design achieves results with a maximum variance of 0.263%, whereas the C30 reaches a maximum of 2.538%.

Table 14: Methodology application overview

| METHODOLOGY APPLICATION ON THERMODYNAMIC MODEL VALIDATION | | | |
|--|---------|-------|----------|
| CAPSTONE C30 | | | |
| OBJECTIVES | VALUE | UNITS | VARIANCE |
| Net electric power | 29.433 | kW | -1.493% |
| Overall efficiency | 0.2534 | — | -2.538% |
| $\dot{m}_{\text{fuel}} \cdot \text{HHV}$ | 128.85 | kW | +1.627% |
| CONSTRAINTS | VALUE | UNITS | |
| Turbine inlet temperature | 859.42 | °C | feasible |
| TURBEC T100 | | | |
| OBJECTIVES | VALUE | UNITS | VARIANCE |
| Net electric power | 100.102 | kW | +0.120% |
| Overall efficiency | 0.2994 | — | -0.200% |
| Turbine inlet temperature | 951.87 | °C | +0.198% |
| Turbine outlet temperature | 650.71 | °C | +0.263% |
| Combustion chamber pressure | 4.28 | bar | -4.889% |

5.2. Micro gas turbine one-dimensional analysis

The results of the thermodynamic analysis performed on Capstone C30 micro gas turbine, shown in past subsections of this chapter, led the work to a next step: one-dimensional analysis. In fact, the lack of solutions with target values of net electric power and overall efficiency was a suggestion to perform a more extended investigation. The model, described in this section, was carried out increasing input variables and objective functions compared to thermodynamic analysis, as shown in Figure 50.

The one-dimensional micro gas turbine scheme, reported in Figure 46, was developed including zero-dimensional (compressor, heat exchanger, combustion chamber, turbine) and one dimensional components for connection pipes and ducts. Most of pipes cross sections are circular, except two annular. The recuperator is modeled using a heat exchanger operating at steady state, and the heat transfer rate is a function of the two fluid properties, mass flow rates and temperatures.

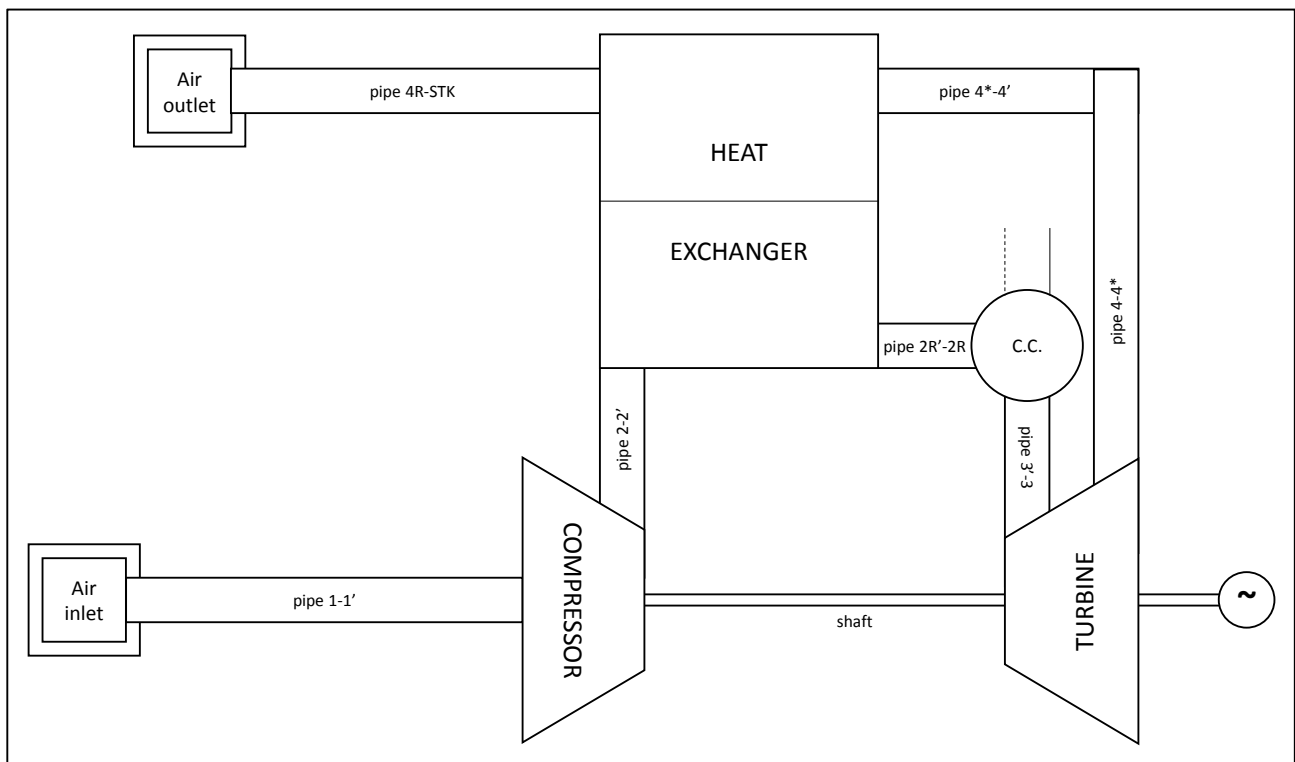


Figure 46: 1D Capstone C30 micro gas turbine model schematization

The model was implemented out using GT-SUITE environment by Gamma Technologies: the flow model involves the solution of Navier-Stokes equations, namely the conservation of continuity, momentum and energy equations; these equations are solved in one dimension, which means that all

quantities are averages across the flow direction. More details about numerical calculation can be found on [76].

The combustion chamber is modeled as a cylindrical pipe in which fuel, with same composition and properties of thermodynamic analysis (Table 7), is consumed to produce combustion products with no ignition delay; fuel mass flow rate is related to air flow rate through their ratio, that represent a decision variable. At each time step, the combustor resolves the mixture composition of 13 standard combustion species using equilibrium chemistry, which will properly determine the resulting gas temperature and heat release from fuel consumption. The modeled combustor is adiabatic, with 213 mm in diameter and 170 mm in length. Pressure losses is first evaluated from geometry, and it is scaled by a multiplier factor, that is a decision variable.

The shaft is simulated by a turbocharger shaft, with a moment of inertia of $0.005 \text{ kg}\cdot\text{m}^2$ that takes in account the inertia of both compressor and turbine rotors. Unlike the thermodynamic analysis, in which compressor and turbine had their mechanical efficiency, in this case the overall efficiency of mechanical transmission is accounted by a unique parameter that is included in decision variables. A resisting torque, depicted in Figure 47, is applied on shaft in order to replicate the electric generator behavior.

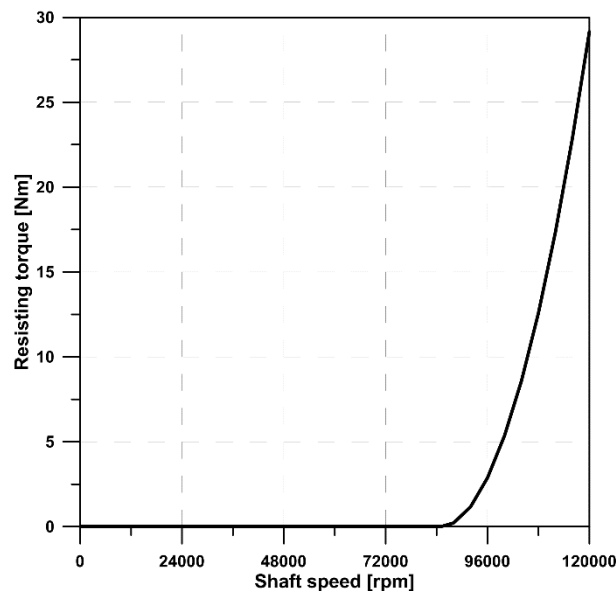


Figure 47: Capstone C30 1D model, electric generator

Pipes, turbomachinery and recuperator will be described in next subsections.

5.2.1. Pipes

In one-dimensional model shown in Figure 46 there are 7 pipes: all of them are adiabatic, and have pressure losses depending on friction along the walls, except one from combustion chamber to turbine and one from ambient to compressor. Pipes walls are smooth, and flow losses are calculated automatically via Fanning friction factor as a function of Reynolds number, as equation (5.x) shows for turbulent regime:

$$C_f = \frac{0.08}{Re^{0.25}} \quad (5.8)$$

Geometry has been estimated from literature [77], and the related pressure drops are scaled by friction multiplier coefficients, included in decision variables: Table 15 summarizes pipes dimensions as well as they are schematized in one-dimensional model.

Table 15: Capstone C30 1D model, pipes features [mm]

| CAPSTONE C30 1D MODEL: PIPES FEATURES | | | | | | | |
|--|-------------|-------------------|-------------|--------------|-------------|-------------|--------|
| ROUND PIPES | | | | | | | |
| CODE | FROM | TO | INLET DIAM. | OUTLET DIAM. | LENGTH | | |
| 2-2' | Compressor | Recuperator | 156.2 | 176.4 | 28 | | |
| 2R'-2R | Recuperator | Combustor | 176.4 | 176.4 | 206.7 | | |
| 3'-3 | Combustor | Turbine | 213.31 | 213.31 | 36.7 | | |
| 4-4* | Turbine | Recuperator (1/2) | 55 | 223.1 | 1000 | | |
| 4R-STK | Recuperator | Stack (ambient) | 223.1 | 200 | 206.7 | | |
| ANNULAR PIPES | | | | | | | |
| CODE | FROM | TO | INLET | | OUTLET | | LENGTH |
| | | | INNER DIAM. | OUTER DIAM. | INNER DIAM. | OUTER DIAM. | |
| 1-1' | Ambient | Compressor | 130 | 250 | 130 | 250 | 300 |
| 4*-4' | Turbine | Recuperator (2/2) | 267 | 457 | 267 | 457 | 206.7 |

5.2.2. Turbomachinery

Both compressor and turbine behavior is described through their own performance maps (Figure 41). The maps can be summarized as a series of performance data points, each of which describes the operating condition by speed, pressure ratio, mass flow rate, and thermodynamic efficiency. The maps are configured so that if the speed and either the mass flow or pressure ratio are known, the efficiency and either the mass flow rate or pressure ratio (whichever is not known) can be found in the map.

5.2.3. Recuperator

In order to model Capstone C30 recuperator, it was fundamental to collect more specifications. It is a plate type Primary Surface Recuperator (PSR) heat exchanger, with annular geometry, made by alternate flat plates called “parting sheets” and fin corrugations, brazed together as a block [78]. The fluid streams flow along the corrugated strip fins, where each new edge starts a new boundary layer which is very thin, thus high heat-transfer coefficients are obtained. The goal is to obtain high heat-transfer coefficients without correspondingly increased pressure-loss penalties [79].

This gas-to-gas recuperator uses all primary surfaces that are envisioned from the cost reduction point of view, since the manufacturing can be automated. With improved and relatively less expensive well-established manufacturing technology, thin foil of metals can be formed in any desired shape as recuperator surface, and the recuperator core can be made in any shape and size. The Capstone C30 annular recuperator has an involute form and 169 air cells, and each air cell is fabricated by welding individual fin-folded 347 stainless steel having 0.100 mm initial thickness [80]; the specification about dimensions, weight and detailed geometry were found on [77]-[82]. Table 16 summarizes the recuperator geometry.

Table 16: Capstone C30 1D analysis, recuperator features

| CAPSTONE C30 1D MODEL: RECUPERATOR FEATURES | | | |
|--|-------------------------------|----------------------|---------------------|
| COLD FLUID CONNECTION DIAM. | HOT FLUID CONNECTION DIAM. | COLD FLUID VOLUME | HOT FLUID VOLUME |
| [mm] | [mm] | [dm ³] | [dm ³] |
| 60 | 176.4 | 7.623 | 7.623 |

To find the heat transfer coefficients, it was adopted a conventional approach suggested in [83], which is specifically suited for heat exchangers having complicated geometries, that is:

$$Nu = A \cdot Re^B \cdot Pr^C \left(\frac{\mu_f}{\mu_w} \right)^D \quad (5.9)$$

where

$$Re = \frac{\rho \cdot c \cdot L}{\mu} = \frac{\rho \cdot c \cdot D_{eq}}{\mu} = \frac{c \cdot D_{eq}}{\nu} \quad (5.10)$$

$$Pr = \frac{\nu}{\alpha} \quad (5.11)$$

A, B, C, D are generic coefficients. For single phase interaction, the equation (5.12) changes into:

$$Nu = 0.2536 \cdot Re^{0.65} \cdot Pr^{0.4} \quad (5.12)$$

In Figure 48, the annular recuperator as it was modelled in one dimensional computational model is shown: the two axes are the stream mass flow rate and the color contours represent the heat transfer rate per unit of temperature.

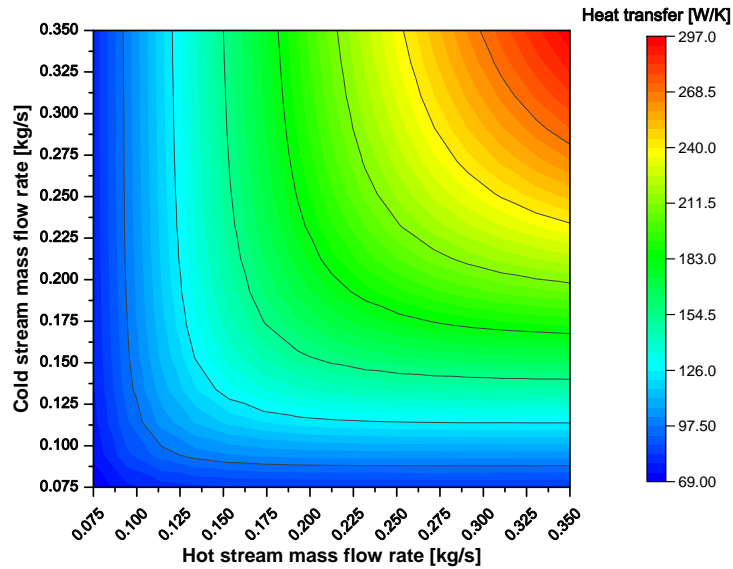


Figure 48: Capstone C30 annular recuperator model

Regarding the static pressure drops through both sides of recuperator, it is described by the following equation:

$$\Delta p = b \cdot \dot{m}^2 \tag{5.13}$$

where b [$1/(m \cdot kg)$] is a constant included within decision variables, and \dot{m} [kg/s] is the mass flow rate of fluids; Figure 49 depicts the pressure losses for cold and hot streams as a functions of mass flow rate.

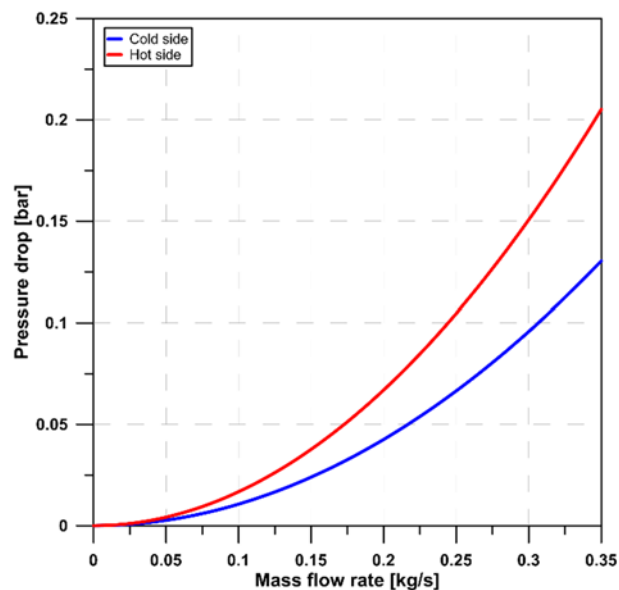


Figure 49: Pressure drops in recuperator

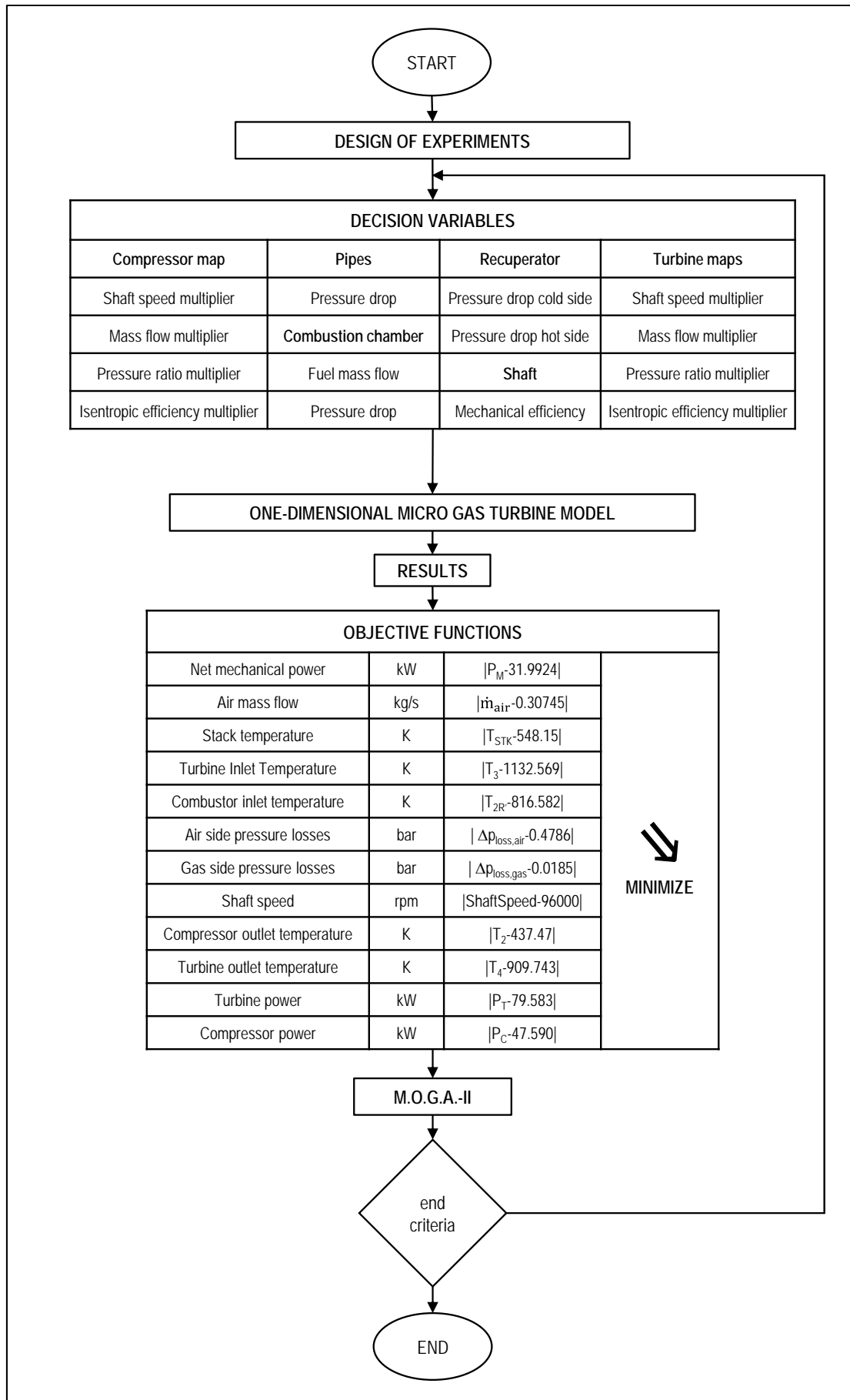


Figure 50: Methodology application on Capstone C30 1D thermodynamic model

5.2.4. Experimental validation: Capstone C30

As reference data for one-dimensional application it was taken in account the preferred design of thermodynamic analysis (Table 10).

Table 17: Methodology setting for Capstone C30 one-dimensional analysis

| CAPSTONE C30: METHODOLOGY SETTING (1D ANALYSIS) | | |
|--|----------------------------|--------|
| DECISION VARIABLES | RANGE | UNITS |
| COMPRESSOR MAP | | |
| Shaft speed multiplier | 0.83 - 1.20 | — |
| Mass flow multiplier | 0.83 - 1.20 | — |
| Pressure ratio multiplier | 0.83 - 1.20 | — |
| Isentropic efficiency multiplier | 0.83 - 1.20 | — |
| SHAFT | | |
| Friction mechanical efficiency | 0.800 - 0.999 | — |
| COMBUSTOR | | |
| Friction multiplier | 0.01 - 10.0 | — |
| Air/Fuel mass flow ratio | 90 - 150 | — |
| RECUPERATOR | | |
| Pressure drop air side | $(0.01 - 3) \cdot 10^{-5}$ | 1/m·kg |
| Pressure drop gas side | $(0.01 - 3) \cdot 10^{-5}$ | 1/m·kg |
| TURBINE MAPS | | |
| Shaft speed multiplier | 0.83 - 1.20 | — |
| Mass flow multiplier | 0.83 - 1.20 | — |
| Pressure ratio multiplier | 0.83 - 1.20 | — |
| Isentropic efficiency multiplier | 0.83 - 1.20 | — |
| PIPES - FRICTION MULTIPLIER | | |
| Pipe 2-2' | 0.1 - 10.0 | — |
| Pipe 2R'-2R | 0.1 - 10.0 | — |
| Pipe 4-4* | 0.01 - 10.00 | — |
| Pipe 4*-4' | 0.1 - 10.0 | — |
| Pipe 4R-STK | 0.1 - 10.0 | — |
| OBJECTIVES | VALUE | UNITS |
| Net mechanical power | 34.569 | kW |
| Air flow | 0.30745 | kg/s |
| Stack temperature | 548.15 | K |
| Turbine Inlet Temperature | 1132.569 | K |
| Combustor inlet temperature | 816.582 | K |
| Air side pressure losses | 0.4786 | bar |
| Gas side pressure losses | 0.0185 | bar |
| Shaft speed | 96000 | rpm |
| Compressor outlet temperature | 437.469 | K |
| Turbine outlet temperature | 909.743 | K |
| Turbine power | 81.207 | kW |
| Compressor power | 46.638 | kW |

In order to define the preferred design, Euclidean norm criterion was used (5.14), and the results are listed in Table 18.

$$\text{PreferredDesign} = \sqrt{\left(\frac{\Delta P_M}{P_{M,exp}}\right)^2 + \left(\frac{\Delta \dot{m}_{air}}{\dot{m}_{air}}\right)^2 + \left(\frac{\Delta T_{STK}}{T_{STK}}\right)^2 + \left(\frac{\Delta T_3}{T_{3,exp}}\right)^2 + \left(\frac{\Delta T_{2R}}{T_{2R,exp}}\right)^2 + \left(\frac{\Delta(p_{loss,air})}{(p_{loss,air})_{exp}}\right)^2 + \left(\frac{\Delta(p_{loss,gas})}{(p_{loss,gas})_{exp}}\right)^2 + \left(\frac{\Delta \text{ShaftSpeed}}{\text{ShaftSpeed}_{exp}}\right)^2 + \left(\frac{\Delta T_2}{T_{2,exp}}\right)^2 + \left(\frac{\Delta T_4}{T_{4,exp}}\right)^2 + \left(\frac{\Delta P_T}{P_{T,exp}}\right)^2 + \left(\frac{\Delta P_C}{P_{C,exp}}\right)^2} \quad (5.14)$$

Next figures show the result related to one-dimensional application of the methodology: each figure is made by two charts, one depicts the objective functions and one depicts the absolute values of the same parameters including the thermodynamic one used as a reference; black points represent the whole results, blue points depicts the Pareto front, which comprises almost 50% of the whole designs, red circle shows the preferred one and black cross is the target used in objective functions.

Both Figure 51 and Figure 52 have net mechanical power on y-axis while on x-axis there are compressor power and turbine power, respectively: the power absorbed by compressor is slightly bigger than the one resulting from thermodynamic analysis (+1.355%), as well as the turbine generated power (+0.291%), while the net mechanical power is modestly smaller (-0.553%).

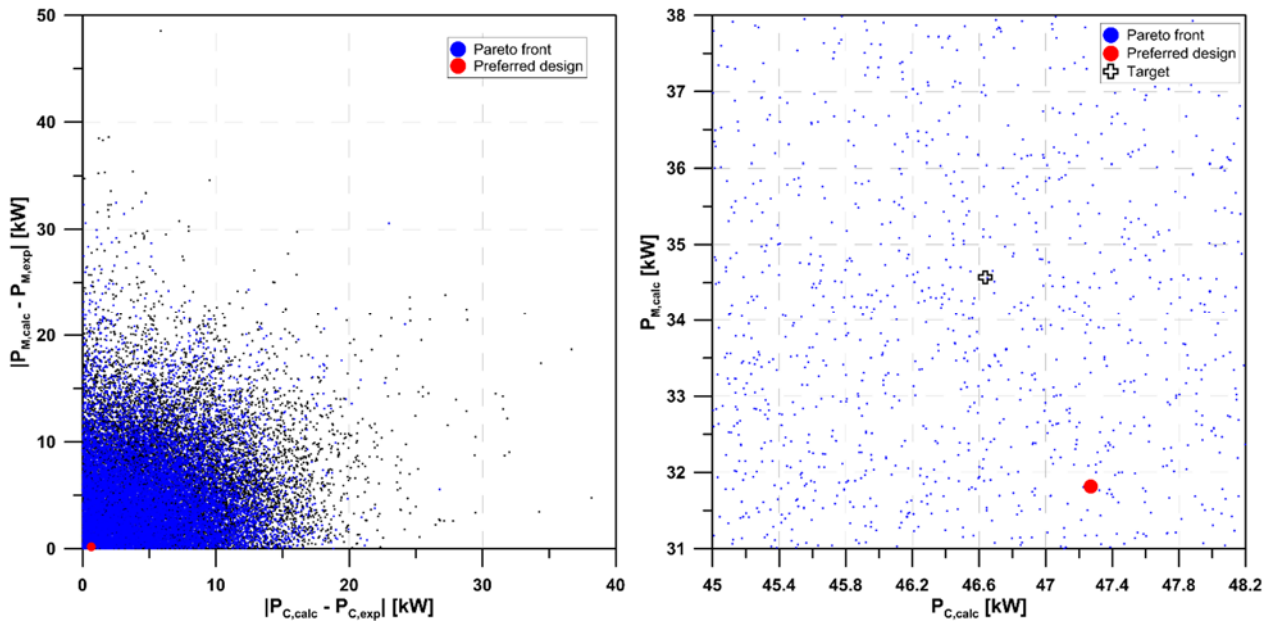


Figure 51: Capstone C30 1D analysis, multi-variable multi-objective results (Pc, P)

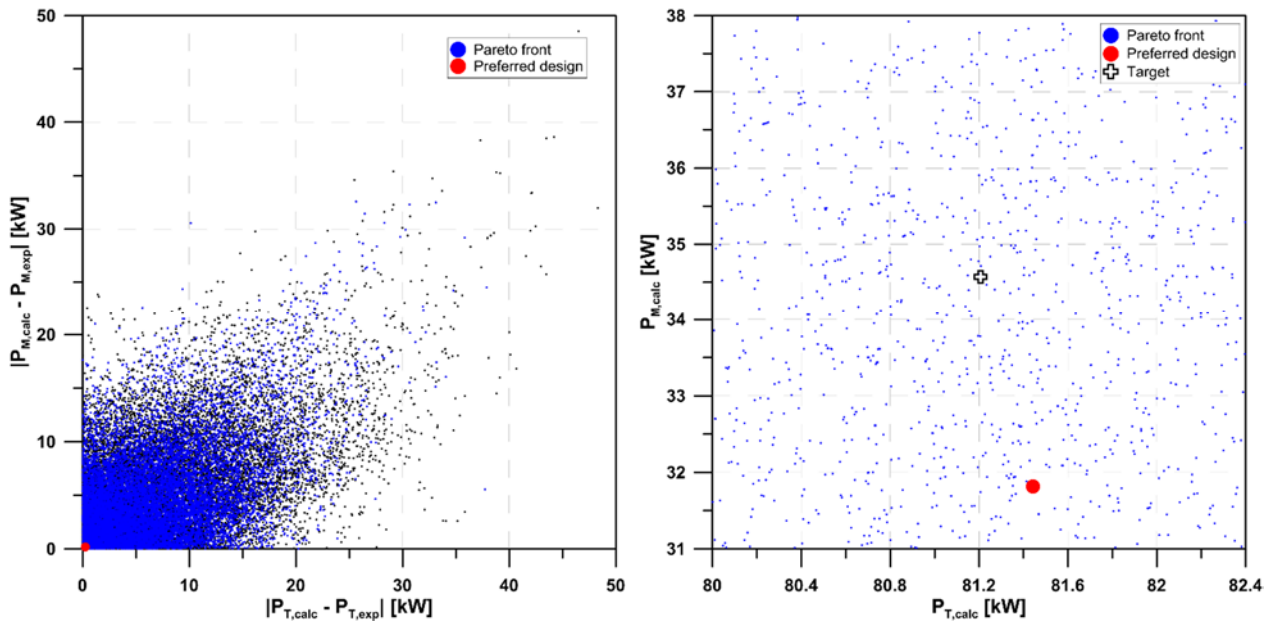


Figure 52: Capstone C30 1D analysis, multi-variable multi-objective results (P_T, P)

Figure 53 shows the results related to compressor input power and overall turbine output power: on the objective functions chart (left), the result marked by red circle shows a difference smaller than 1 kW for both turbomachinery, as clearly noticeable on right chart.

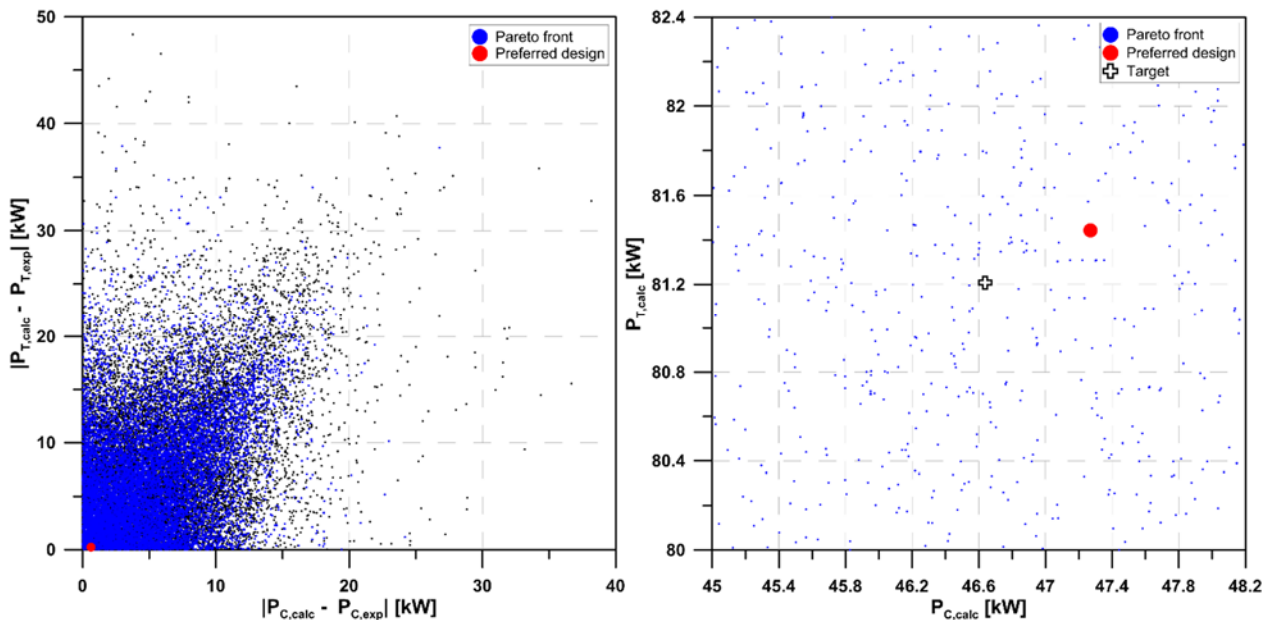


Figure 53: Capstone C30 1D analysis, multi-variable multi-objective results (P_C, P_T)

Air mass flow rate and shaft speed are shown in Figure 54: their values are below 2% of variance, meaning a +1.145% in air flow rate and a -1.657% in shaft speed.

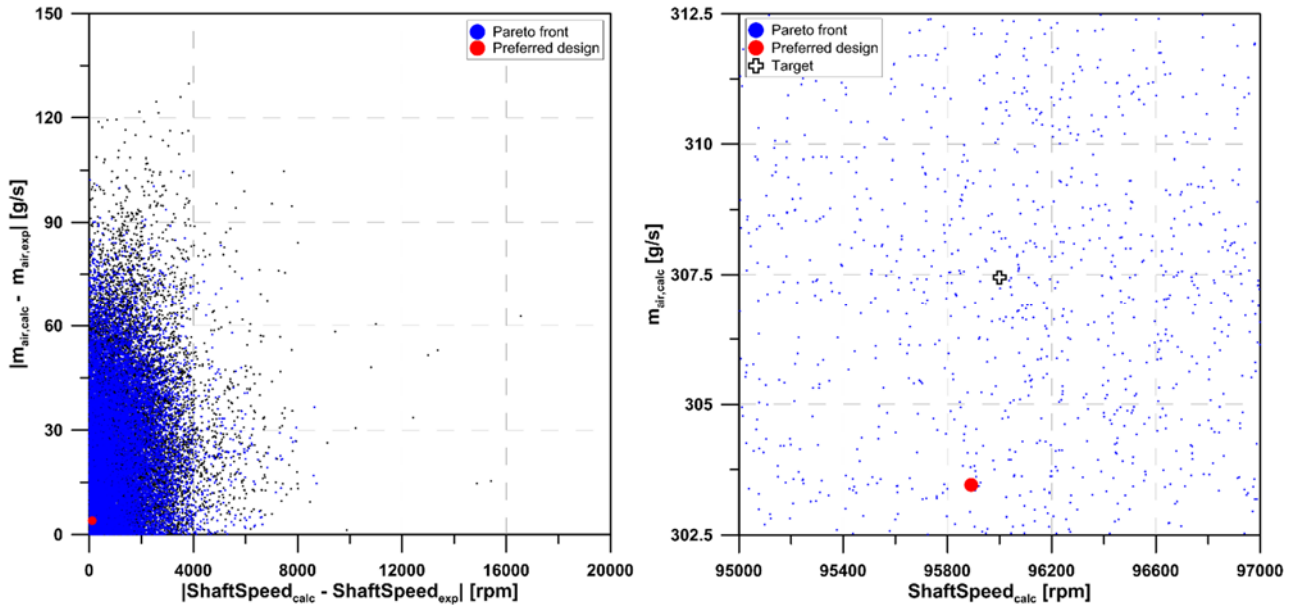


Figure 54: Capstone C30 1D analysis, multi-variable multi-objective results (shaft speed, mass air flow)

Objective functions and related calculated results concerning pressure drops in micro gas turbine plant are reported in Figure 55: these parameters have the larger variance in the whole calculation, probably because in thermodynamic analysis, pressure drops were concentrated just in recuperator and combustor, while in one-dimensional simulation there are additional pressure losses in five pipes. In other words, the target values used in objectives calculation concern the pressure losses concentrated in recuperator cold side, combustion chamber and recuperator hot side found out in thermodynamic analysis while in one-dimensional model there are also five pipes characterized by pressure drops. Thus, the target values were compared with the sum of losses in the two gas turbine plant sides, as illustrated in equations 5.14 e 5.15:

$$\Delta p_{\text{loss,air}} = \Delta p_{\text{pipe } 2-2'} + \Delta p_{\text{rec,cold}} + \Delta p_{\text{pipe } 2R'-2R} + \Delta p_{\text{combustor}} \quad (5.14)$$

$$\Delta p_{\text{loss,gas}} = \Delta p_{\text{pipe } 4-4*} + \Delta p_{\text{pipe } 4*-4'} + \Delta p_{\text{rec,hot}} + \Delta p_{\text{pipe } 4R-STK} \quad (5.15)$$

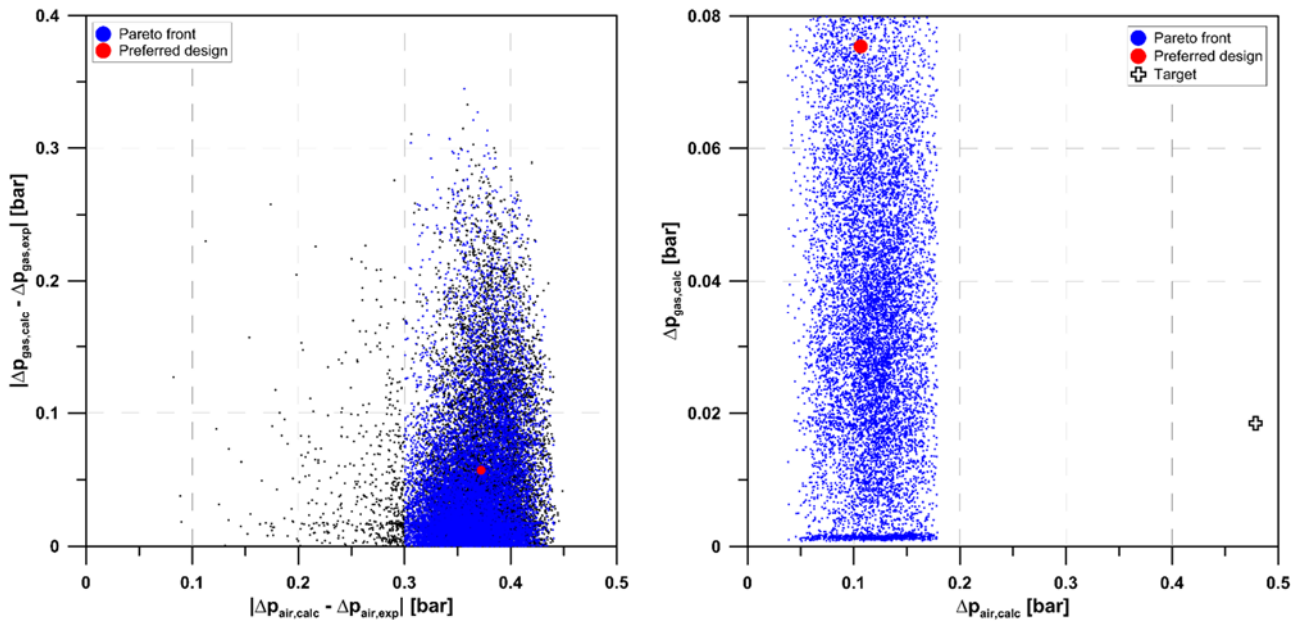


Figure 55: Capstone C30 1D analysis, multi-variable multi-objective results ($\Delta p_{loss,air}, \Delta p_{loss,gas}$)

From Figure 56 to Figure 61, the temperatures along the micro gas turbine plant are shown: smaller difference from thermodynamic reference is related to compressor outlet temperature (T_2) and exhausted gas in stack pipe (T_{stk}), respectively +3.981 K (+0.910%) and +7.500 K (+1.368%), reported in Figure 58. The three other temperatures have larger variance, between 16.893 and 26.161 K, which correspond to 1.857-2.310% percent range.

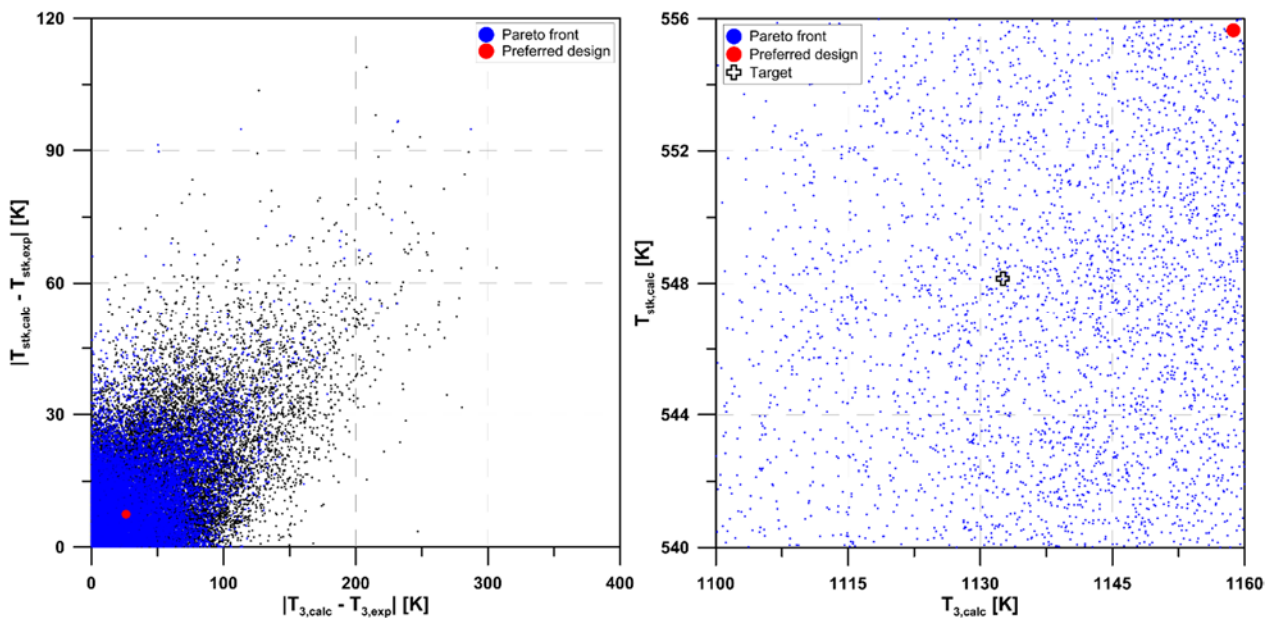


Figure 56: Capstone C30 1D analysis, multi-variable multi-objective results (T_3, T_{stk})

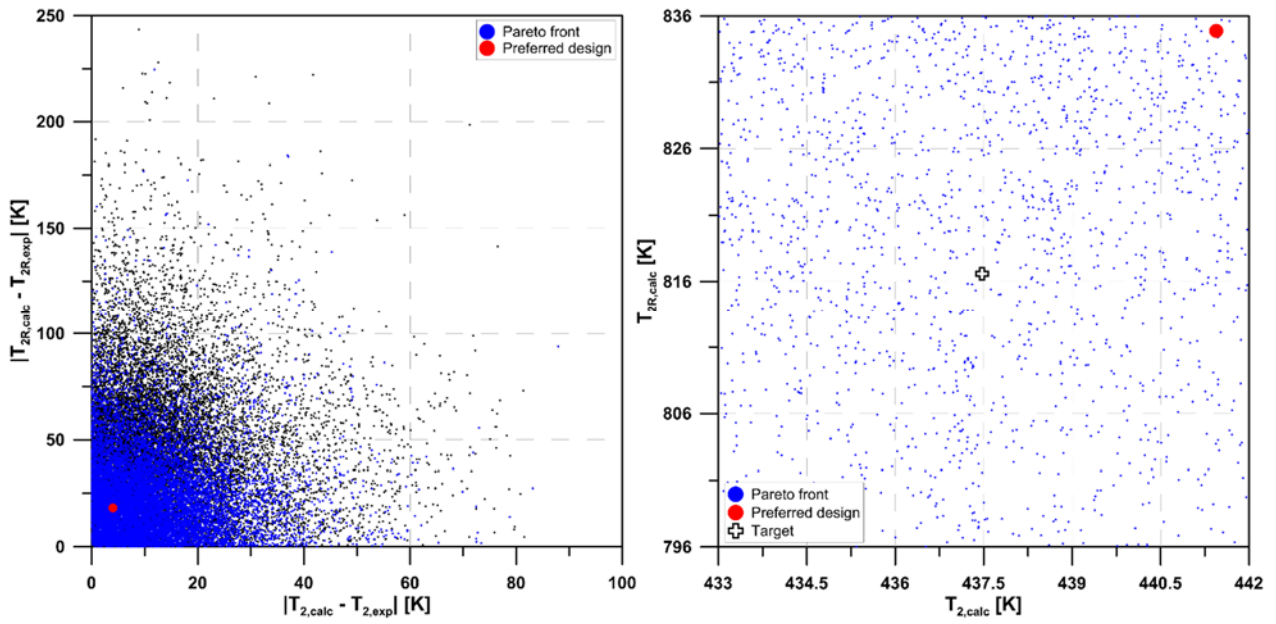


Figure 57: Capstone C30 1D analysis, multi-variable multi-objective results (T_2 , T_{2R})

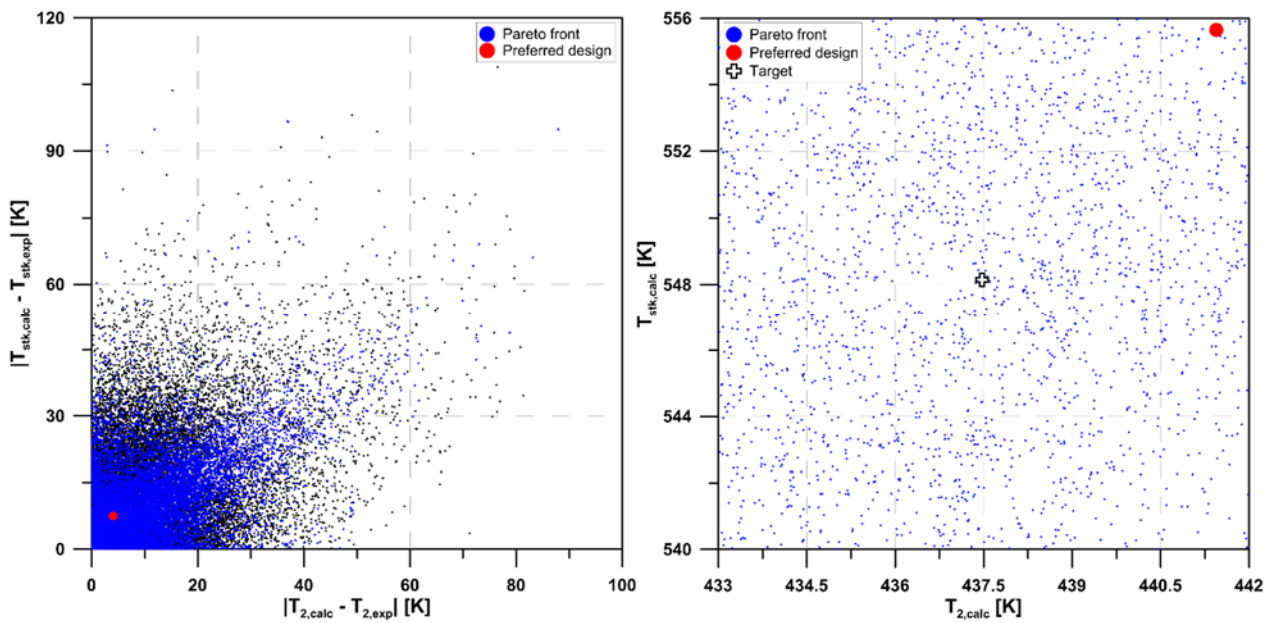


Figure 58: Capstone C30 1D analysis, multi-variable multi-objective results (T_2 , T_{stk})

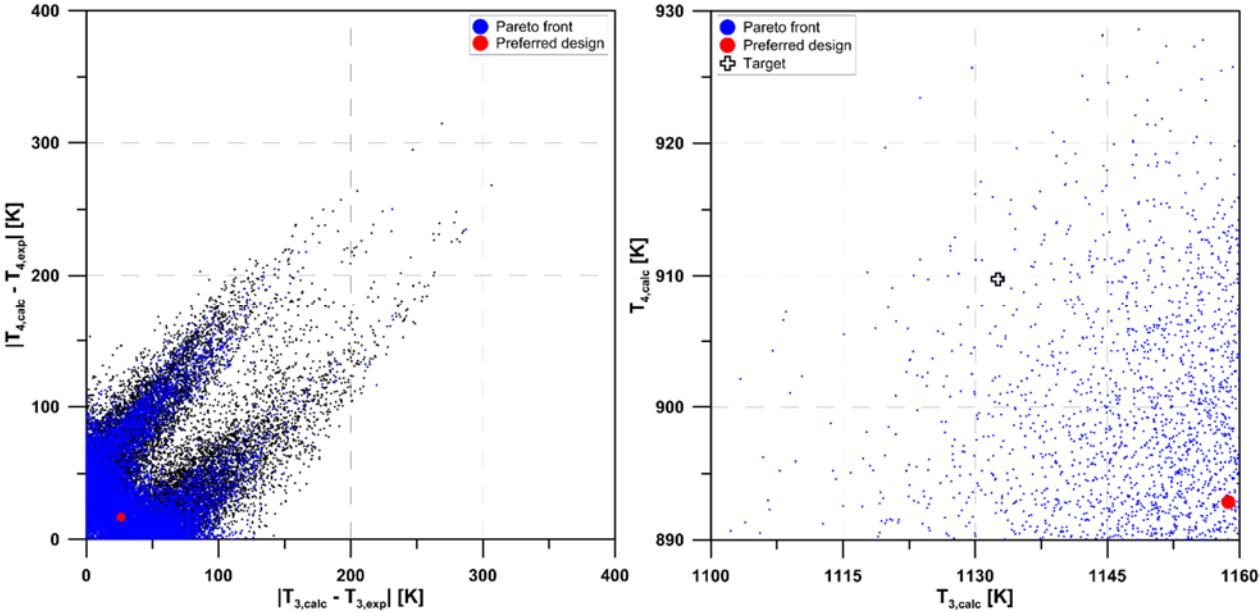


Figure 59: Capstone C30 1D analysis, multi-variable multi-objective results (T_3 , T_4)

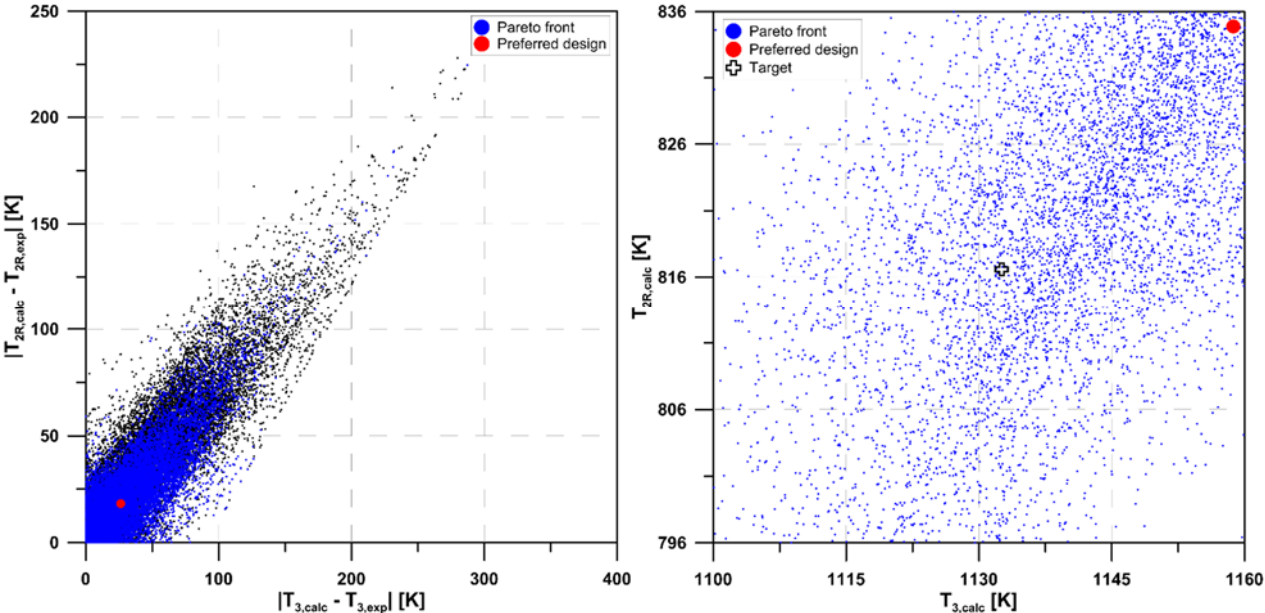


Figure 60: Capstone C30 1D analysis, multi-variable multi-objective results (T_3 , T_{2R})

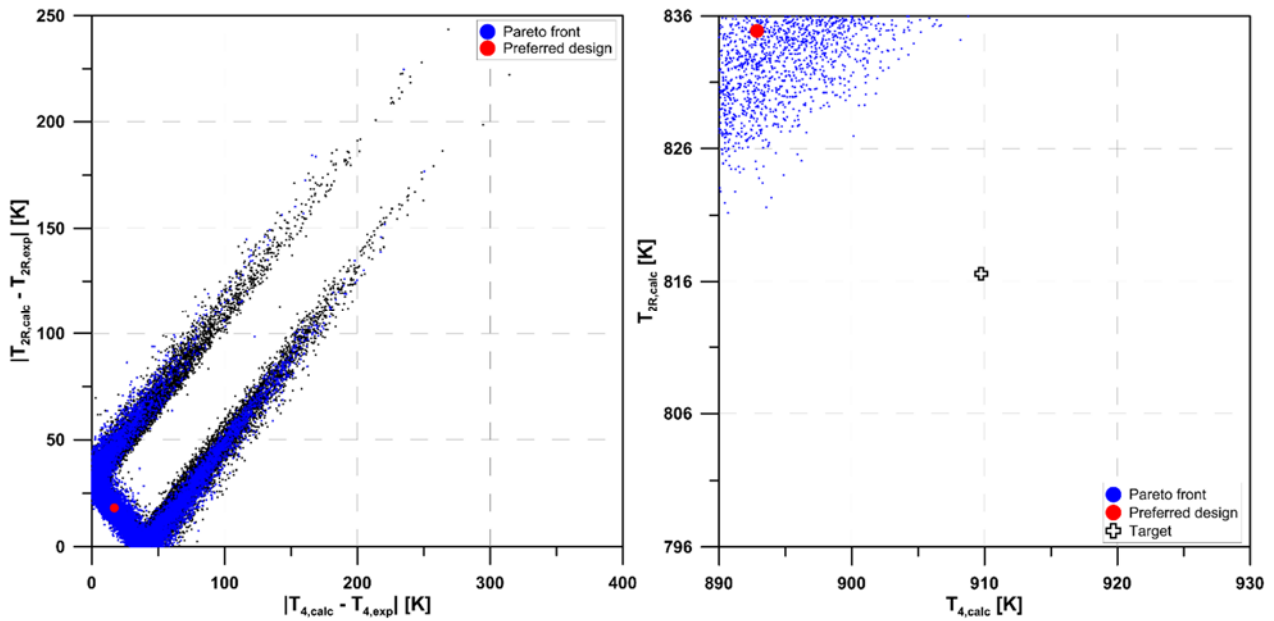


Figure 61: Capstone C30 1D analysis, multi-variable multi-objective results (T_4 , T_{2R})

In Figure 61 there is the same kind of triangle without results close to axes origin, as already discussed for Capstone C30 thermodynamic analysis (5.1.1): again, this lack of design able to achieve target values for both temperatures, clearly appreciable in right chart, highlights an incongruity in experimental data and/or mathematical model.

Table 18: Capstone C30 preferred design (1D analysis)

| CAPSTONE C30 PREFERRED DESIGN (1D ANALYSIS) | | | |
|--|------------------------|--------|-----------|
| DECISION VARIABLES | VALUE | UNITS | |
| COMPRESSOR MAP | | | |
| Shaft speed multiplier | 0.861 | — | |
| Mass flow multiplier | 1.167 | — | |
| Pressure ratio multiplier | 0.848 | — | |
| Isentropic efficiency multiplier | 0.956 | — | |
| SHAFT | | | |
| Friction mechanical efficiency | 0.931 | — | |
| COMBUSTOR | | | |
| Friction multiplier | 3.718 | — | |
| Air/Fuel mass flow ratio | 113.77 | — | |
| RECUPERATOR | | | |
| Pressure drop gas side | $0.7970 \cdot 10^{-5}$ | 1/m·kg | |
| Pressure drop air side | $0.4470 \cdot 10^{-5}$ | 1/m·kg | |
| TURBINE MAPS | | | |
| Shaft speed multiplier | 0.862 | — | |
| Mass flow multiplier | 1.107 | — | |
| Pressure ratio multiplier | 1.038 | — | |
| Isentropic efficiency multiplier | 0.953 | — | |
| PIPES - FRICTION MULTIPLIER | | | |
| Pipe 2-2' | 2.826 | — | |
| Pipe 2R'-2R | 2.758 | — | |
| Pipe 4-4* | 7.092 | — | |
| Pipe 4*-4' | 3.252 | — | |
| Pipe 4R-STK | 7.533 | — | |
| OBJECTIVES | VALUE | UNITS | VARIATION |
| Net mechanical power | 31.815 | kW | -0.553% |
| Air flow | 0.30346 | kg/s | -1.298% |
| Stack temperature | 555.65 | K | 1.368% |
| Turbine Inlet Temperature | 1158.73 | K | 2.310% |
| Combustor inlet temperature | 834.88 | K | 2.241% |
| Air side pressure losses | 0.1065 | bar | -77.748% |
| Gas side pressure losses | 0.0754 | bar | 307.568% |
| Shaft speed | 95891 | rpm | -0.114% |
| Compressor outlet temperature | 441.45 | K | 0.910% |
| Turbine outlet temperature | 892.85 | K | -1.857% |
| Turbine power | 81.443 | kW | 0.291% |
| Compressor power | 47.270 | kW | 1.355% |

5.2.5. Discussion

The results concerning the methodology application to one-dimensional micro gas turbine model highlighted some interesting aspects: first, number of generations is too small compared to number of decision variables and objectives, thus Pareto front is too large and it does not depict a limited number of optimal sets. Second, excluding pressure losses in whole plant, all the objectives have several designs closer to the axes origin, meaning that the adopted one-dimensional model is able to identify a larger number of reliable solutions compared to thermodynamic model. However, the methodology showed its effectiveness even in pressure losses analysis: the lack of results near the target values emphasizes a large incongruity related to the schematization of this aspect, and the need and the convenience to analyze more in detail both thermodynamic and one-dimensional models came out.

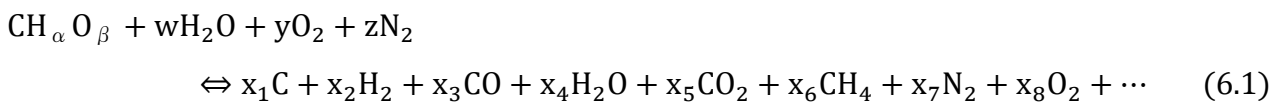
Thus, the more complex one-dimensional schematization of micro gas turbine plant represented a valid and useful tool aimed to investigate the unsteady behavior of energy conversion systems, even for basically steady plants.

6. Case experimental validation study: Pyro-gasification system

Energy production in 2015 was supplied with biofuels and waste by almost 15%, that represents more than the sum of nuclear (4.9%) and hydro (2.4%) sources [84]. The leading role of power sector in global climate change is already highlighted in [3], with renewable component breaking its own records for deployment year after year. On IEA 2016 Outlook, is also analyzed the sustainability of biofuels source, ensuring the sustainability requirements satisfaction for the use of residues from existing activities: in fact, biofuels derive from biomass that includes waste, in addition to residues from agricultural, forest, wood process, and many other industrial and household scraps. Harvesting of food and fiber crops, which are by-products of modern agricultural processes, belong to primary residues, while secondary residues include food, fiber and material processing wastes; finally, demolition timber, sewage sludge, and municipal solid waste belong to tertiary residues. Since each material within these three categories contains a suitable energy amount that can be exploited, all of these can be used as biomass feedstocks.

However, they can not supply an internal combustion engine or a gas turbine, but theoretically they could be used as fuel in external combustion engine with unfavorable efficiency; another way to employ the energy contained within biomass is to convert it in biofuels. This conversion is achievable through several techniques to provide more useful energy carriers in form of solid fuels, liquid fuels, gaseous fuels (synthesis gas, biogas, hydrogen) or direct heat [85].

The two thermochemical conversion processes studied in this chapter are pyrolysis and gasification: the gasification process entails the partial combustion of a carbon based material to produce a combustible gaseous fuel rich in carbon monoxide and hydrogen. The gasification occurs in a gasifier, which is mostly an incinerator operating under reducing conditions. Even if the reaction kinetics of the gasification process are quite complex and still the subject of considerable debate [86], the general gasification reaction of a $\text{CH}_\alpha\text{O}_\beta$ molecule can be described by following eq. (6.1) [5]:



Heat to keep up with the process is obtained from exothermic reactions, while the combustible elements of the low-energy gas are generated by endothermic reactions. When a gasifier is operated at atmospheric pressure with air as the oxidant, the end products of the gasification process are a low-energy gas because of the diluting effect of the nitrogen in the input air: biogas from gasification usually has a lower heating value in the range of the 5.2 to 6.0 MJ/m³ [86]. Finally, even if gasification

process entails energy and environmental benefits, incinerators (which gasify and burn in one chamber) are favored over gasifiers.

Pyrolysis is a process of thermochemical decomposition of organic materials into gaseous, liquid, and solid fractions via thermal cracking and condensation reactions: basically, the organic molecules break into chain with a lower molecular weight upon heating in a total absence of an oxidizing agent. In contrast to the exothermic combustion process, pyrolysis is extremely endothermic. The resulting fractions from thermochemical decomposition are solid, liquid and gaseous: solid fraction consisting of pure carbon (char) and inert components; liquid fraction containing tar, and many other organic species; gaseous fraction consisting mainly of hydrogen, methane, carbon monoxide and carbon dioxide. The distribution of the three fractions depends on the temperature at which the pyrolysis is performed. Under conditions of maximum gasification, the energy content of the resulting gas is about 26.1 MJ/kg, while the energy content of pyrolytic oils has been estimated to be about 23.2 MJ/kg [86].

The proposed methodology was applied to a pyro-gasification plant named RM-09 (*Recupero Metalli*, metals recovery), in order to perform experimental data and thermodynamic model validation: based on certified analysis of component volume fraction in produced gaseous biofuel, the evolutionary algorithm carried out a large numbers of calculation aimed to find the set of decision variables that minimize the variance of syngas composition.

6.1. RM-09 system model

RM is a pyro-gasification plant designed to recovery metals from a variety of waste; the studied case was focused on RM supplied by pulp paper source. The plant comprises:

- biomass supply, where waste is delivered to the process;
- combustor, that produces the hot and inert gas needed by thermochemical process;
- rotary pyro-gasifier reactor, where the two dissociation processes occur;
- metals and inert dumping;
- combustion of gaseous and liquid biofuel;
- reactor heating / exhaust gas bypass;
- exhaust gas treatment.

Concerning the thermochemical models, it includes three process blocks, combustor, pyrolyzer and gasifier (Figure 62): even if real plant has both pyrolyzer and gasifier joined in one component, it was necessary to split it in two blocks. In first block (pyrolyzer), the pulp paper, consisting mainly

of polyethylene, is broken into its basic ethylene molecules, while in second block (gasifier) the ethylene molecules are further decomposed into the basic products, such as CO, CO₂, H₂, CH₄.

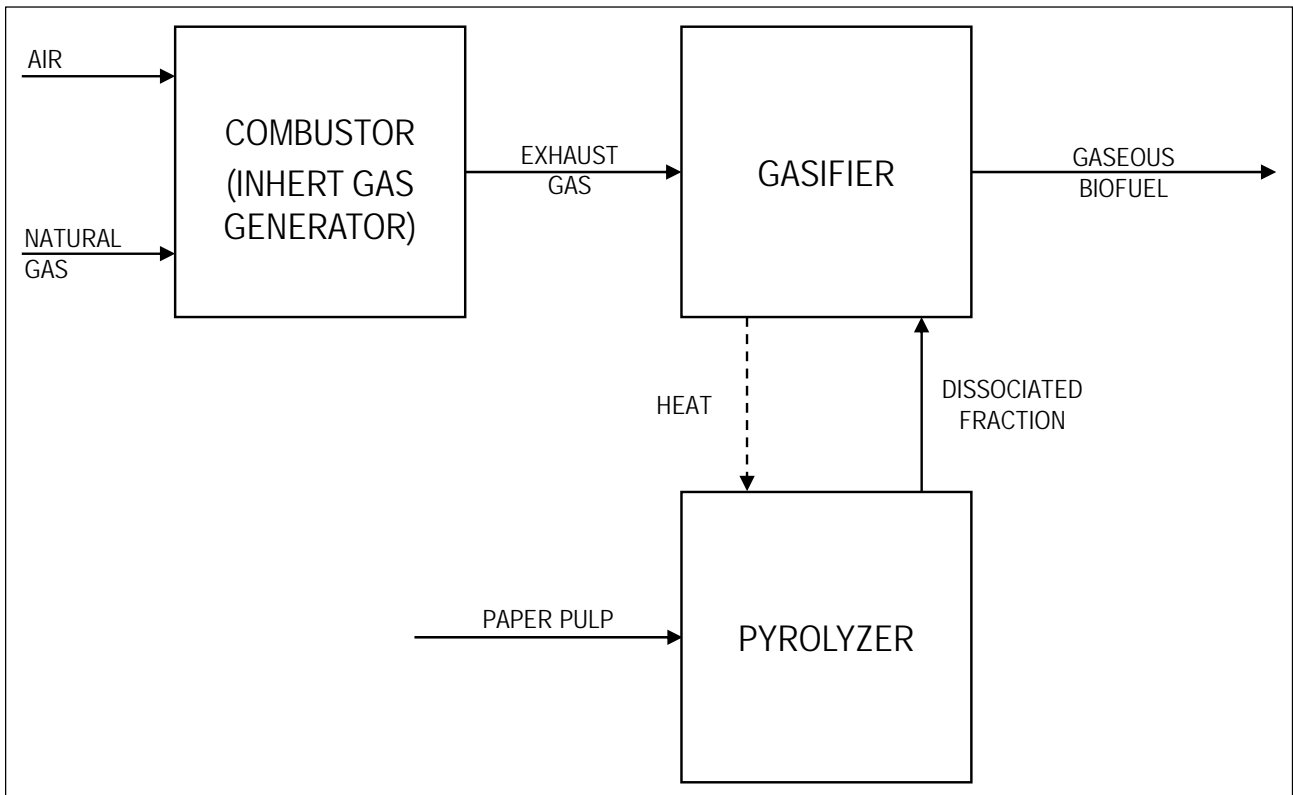


Figure 62: Pyro-gasification plant schematization

In combustor block, the two incoming flows represent two decision variables, fuel flow (methane, in this study) and air flow: they react producing exhaust gas, that is required by the whole plant process because it provides the heat needed by endothermic decomposition reactions. This block is modeled as a stoichiometric reactor, and the ratio air/fuel is set higher than stoichiometric, in order to burn the whole fuel. The fluctuating value of air flow administers the heat supplied to the process, since the temperature of burned gas is related to air/fuel ratio. The paper pulp feed, modeled according to its ultimate and proximate analysis (Table 19), joins the process entering in pyrolyzer block, schematized as a yield reactor: this reactor model is useful when reaction stoichiometry and kinetics are unknown and when yield distribution data are available: in this study, the yield distribution at pyrolyzer outlet represents a decision variable that will be optimized by the methodology in order to be consistent with produced gaseous biofuel.

Table 19: Pulp paper feedstock composition

| RM-09: PULP PAPER COMPOSITION | |
|--------------------------------------|-------------|
| ULTIMATE ANALYSIS | |
| SPECIES | %vol |
| Carbon | 85.81 |
| Hydrogen | 13.86 |
| Nitrogen | 0.12 |
| Sulphur | 0.06 |
| Ash | 0.15 |
| PROXIMATE ANALYSIS | |
| Moisture | 0.00 |
| Volatile matter | 99.85 |
| Fixed carbon | 0.00 |
| Ash | 0.15 |

Finally, gasifier block is modeled to calculate phase and chemical equilibrium by Gibbs free energy minimization: this is a recommended setting when temperature and pressure are known and reaction stoichiometry is unknown [87]. It must be noticed the heat stream between gasifier and pyrolyzer in Figure 62: it characterizes the sensible heat flux of exhaust gas that contribute to both process stage, and being inert, it can be shared by the two block through a heat flux.

Figure 63 depicts the methodology application to RM-09 pyro-gasification plant.

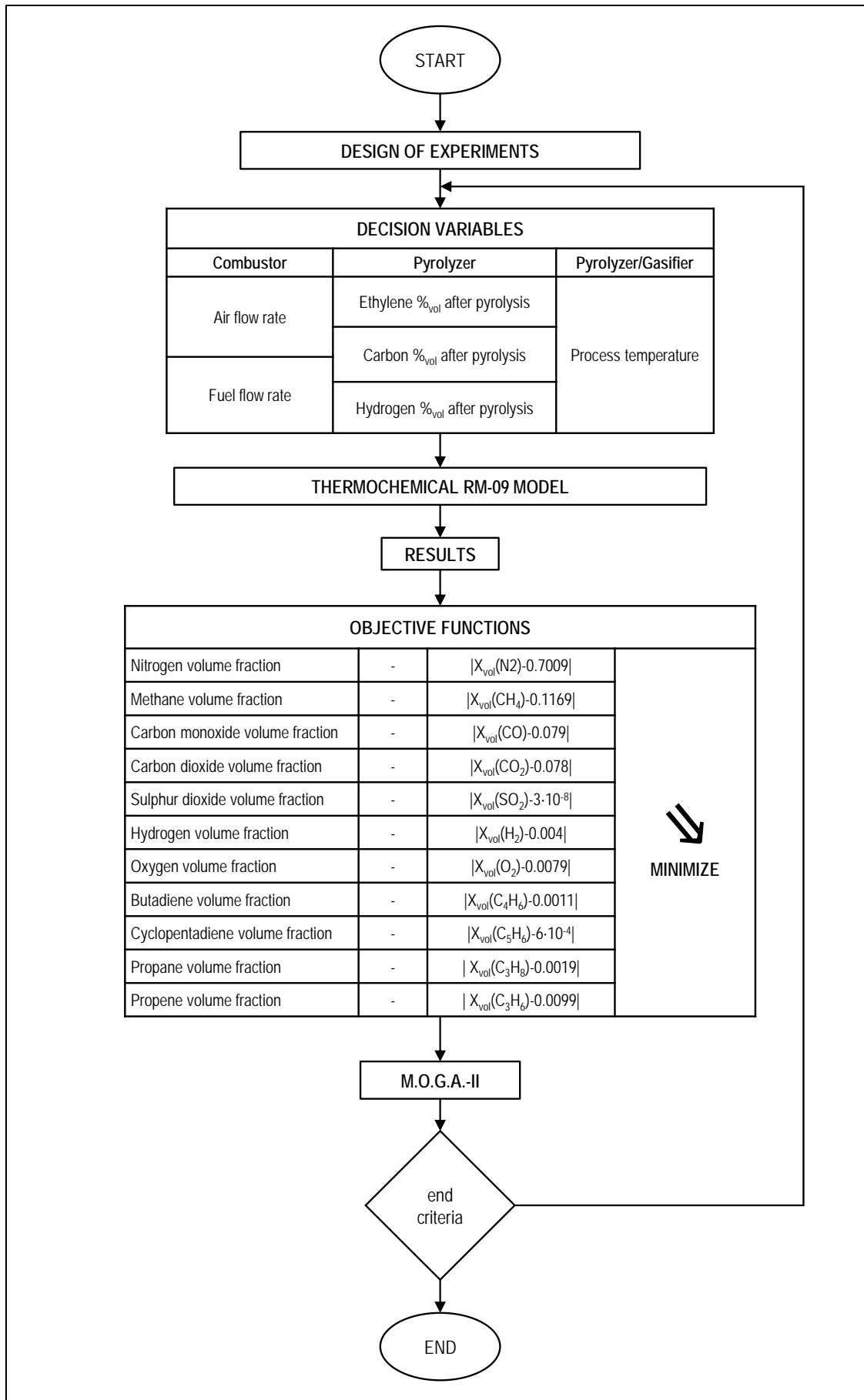


Figure 63: Methodology application on RM-09 pyro-gasifier

6.2. Experimental validation results

The range set for the decision variables and the objectives target values are listed in Table 20.

Table 20: Methodology setting for RM-09 thermochemical analysis

| RM-09: METHODOLOGY SETTING | | |
|-----------------------------------|-------------------|------------------|
| DECISION VARIABLES | RANGE | UNITS |
| COMBUSTOR | | |
| Air mass flow rate | 0.08333 - 2.77778 | kg/s |
| Fuel mass flow rate | 0.00278 - 0.16667 | kg/s |
| PYROLYZER | | |
| Ethylene after pyrolysis | 70 - 100 | % _{vol} |
| Carbon after pyrolysis | 0 - 30 | % _{vol} |
| Hydrogen after pyrolysis | 0 - 10 | % _{vol} |
| PYROLYZER / GASIFIER | | |
| Process temperature | 573.15 - 1273.15 | K |
| OBJECTIVES | VALUE | UNITS |
| Nitrogen volume fraction | 70.09 | % _{vol} |
| Methane volume fraction | 11.69 | % _{vol} |
| Carbon monoxide volume fraction | 7.9 | % _{vol} |
| Carbon dioxide volume fraction | 7.8 | % _{vol} |
| Sulphur dioxide volume fraction | 0.000003 | % _{vol} |
| Hydrogen volume fraction | 0.4 | % _{vol} |
| Oxygen volume fraction | 0.79 | % _{vol} |
| Butadiene volume fraction | 0.11 | % _{vol} |
| Cyclopentadiene volume fraction | 00.059997 | % _{vol} |
| Propane volume fraction | 0.19 | % _{vol} |
| Propene volume fraction | 0.99 | % _{vol} |

The following figures show the results of methodology application on some of the objective plans; designs belonging to Pareto front are marked by blue circle, and the preferred design is represented by a red circle. The two charts in Figure 64 show the methodology results for the objectives planes (CO,CO₂) and (CH₄,N₂): the first one is depicted on the left and that kind of triangle without designs close to the axes origin highlights the same uncertainty already seen in previous cases, meaning that there are too high measurement chain errors and it could not be pointed out a set of reliable results. The right chart on same figure, on the other hand, shows a better congruence between experimental data and thermochemical model, due to the results close to plane origin; however, for both charts, the preferred design is not close to target values as expected.

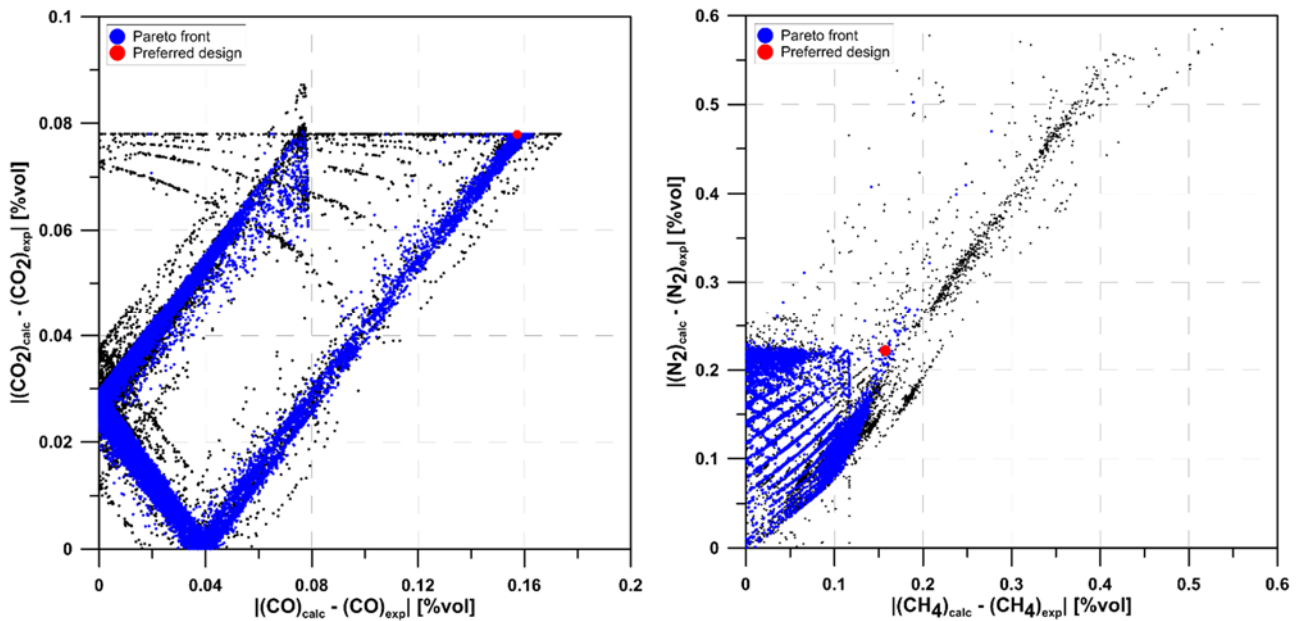


Figure 64: RM-09 thermochemical analysis, multi-variable multi-objective results (syngas volume concentration of CO,CO₂, and CH₄,N₂).

Figure 65 depicts the objective functions concerning planes (C₃H₆,C₃H₈) and (SO₂,H₂): again, in both these plans, there are not many results close to axes origin, and the preferred design for left chart does not indicate the best solution related to the two objectives.

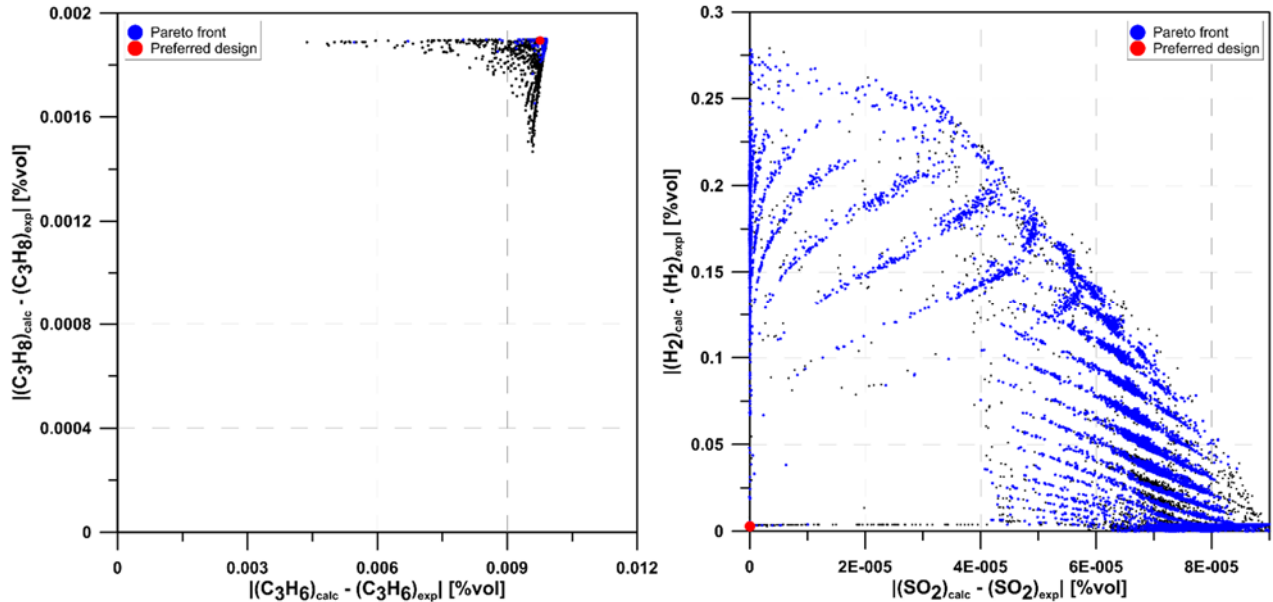


Figure 65: RM-09 thermochemical analysis, multi-variable multi-objective results (syngas volume concentration of C₃H₆,C₃H₈ and SO₂,H₂).

In Figure 66 the results are reported on objectives planes (CO,O₂) and (CH₄,C₃H₈): the left chart shows many Pareto optimal results near the axes origin, while it does not happen for right chart, and for both objectives couples, the preferred design is far from the desirable values.

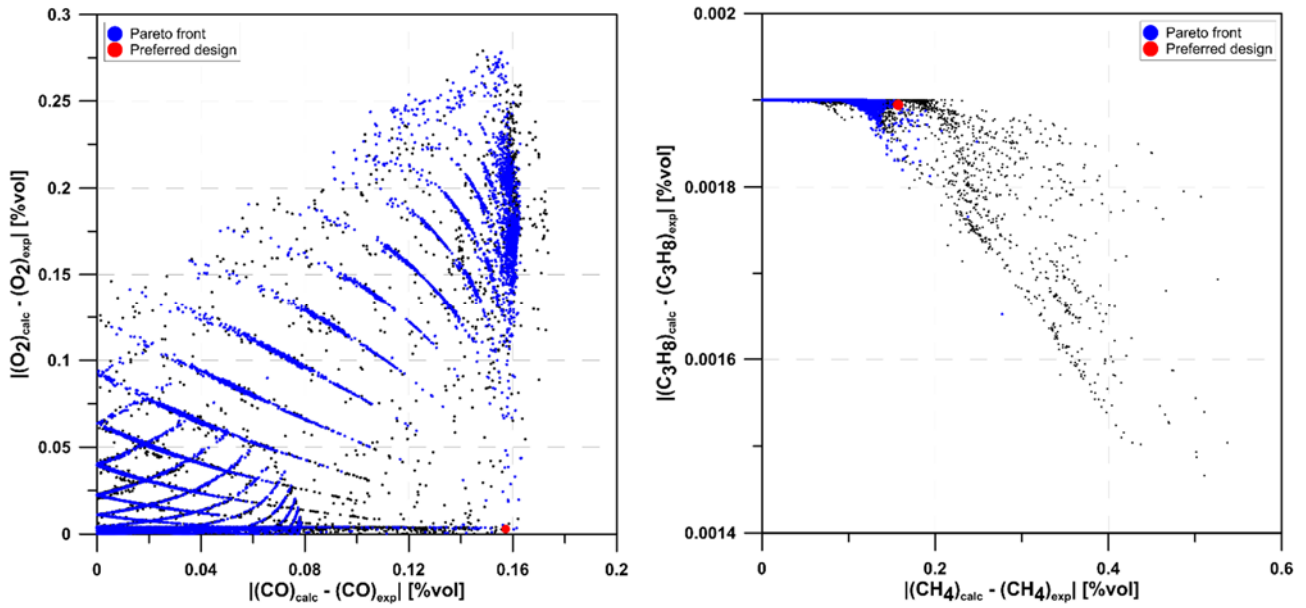


Figure 66: RM-09 thermochemical analysis, multi-variable multi-objective results (syngas volume concentration of CO, O₂ and CH₄, C₃H₈)

Finally, in Figure 67 the methane volume concentration in biogas produced is shown as a function of ratio λ in combustor block, described in (6.2) as the comparison between air/fuel mass flow rate with the same ratio in stoichiometric conditions:

$$\lambda = \frac{\left(\frac{\dot{m}_{\text{air}}}{\dot{m}_{\text{fuel}}}\right)}{\left(\frac{\dot{m}_{\text{air}}}{\dot{m}_{\text{fuel}}}\right)_{\text{stoich}}} \quad (6.2)$$

as expected, lean mixture ($\lambda > 1$) led to lower concentration of CH₄ in syngas produced. Furthermore, the Pareto front follows the assigned constraint related to λ , which was defined feasible for value ranging between 1 and 1.48, and the preferred design is again far from the target value for CH₄ volume concentration.

The preferred design, determined by Euclidean norm criterion (6.2), and is listed in Table 21.

PreferredDesign =

$$= \sqrt{\left(\frac{\Delta X_{\text{vol}} \text{N}_2}{(X_{\text{vol}} \text{N}_2)_{\text{exp}}}\right)^2 + \left(\frac{\Delta X_{\text{vol}} \text{CH}_4}{(X_{\text{vol}} \text{CH}_4)_{\text{exp}}}\right)^2 + \left(\frac{\Delta X_{\text{vol}} \text{CO}}{(X_{\text{vol}} \text{CO})_{\text{exp}}}\right)^2 + \left(\frac{\Delta X_{\text{vol}} \text{CO}_2}{(X_{\text{vol}} \text{CO}_2)_{\text{exp}}}\right)^2 + \left(\frac{\Delta X_{\text{vol}} \text{SO}_2}{(X_{\text{vol}} \text{SO}_2)_{\text{exp}}}\right)^2 + \left(\frac{\Delta X_{\text{vol}} \text{H}_2}{(X_{\text{vol}} \text{H}_2)_{\text{exp}}}\right)^2 + \left(\frac{\Delta X_{\text{vol}} \text{O}_2}{(X_{\text{vol}} \text{O}_2)_{\text{exp}}}\right)^2 + \left(\frac{\Delta X_{\text{vol}} \text{C}_4\text{H}_6}{(X_{\text{vol}} \text{C}_4\text{H}_6)_{\text{exp}}}\right)^2 + \left(\frac{\Delta X_{\text{vol}} \text{C}_5\text{H}_6}{(X_{\text{vol}} \text{C}_5\text{H}_6)_{\text{exp}}}\right)^2 + \left(\frac{\Delta X_{\text{vol}} \text{C}_3\text{H}_8}{(X_{\text{vol}} \text{C}_3\text{H}_8)_{\text{exp}}}\right)^2 + \left(\frac{\Delta X_{\text{vol}} \text{C}_3\text{H}_6}{(X_{\text{vol}} \text{C}_3\text{H}_6)_{\text{exp}}}\right)^2} \quad (6.2)$$

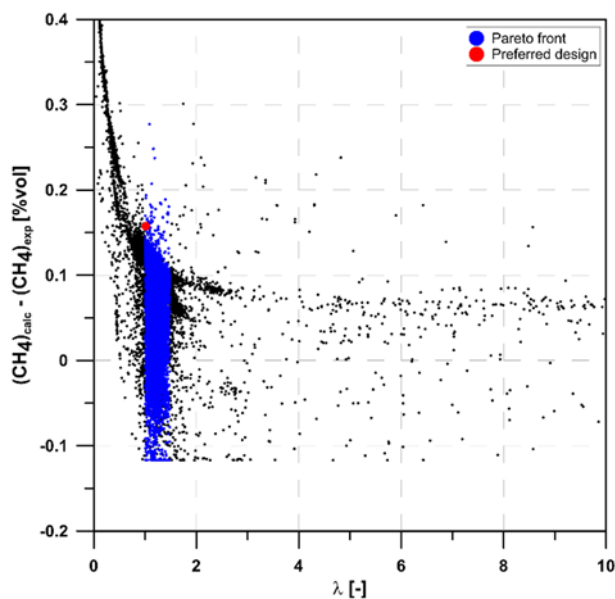
Figure 67: RM-09 thermochemical analysis, multi-variable multi-objective results (air/fuel ratio vs CH₄ in syngas)

Table 21: RM-09 preferred design

| RM-09: PREFERRED DESIGN | | | |
|---------------------------------|-----------------------|------------------|-----------|
| DECISION VARIABLES | VALUE | UNITS | |
| COMBUSTOR | | | |
| Air mass flow rate | 0.748 | kg/s | |
| Fuel mass flow rate | 0.043 | kg/s | |
| PYROLYZER | | | |
| Ethylene after pyrolysis | 0.8250 | % _{vol} | |
| Carbon after pyrolysis | 0.1521 | % _{vol} | |
| Hydrogen after pyrolysis | 0.0195 | % _{vol} | |
| PYROLYZER / GASIFIER | | | |
| Process temperature | 853.15 | K | |
| OBJECTIVES | VALUE | UNITS | VARIATION |
| Nitrogen volume fraction | 0.2219 | % _{vol} | -68.34% |
| Methane volume fraction | 0.1573 | % _{vol} | 34.56% |
| Carbon monoxide volume fraction | 0.1572 | % _{vol} | 98.99% |
| Carbon dioxide volume fraction | 0.0779 | % _{vol} | -0.15% |
| Sulphur dioxide volume fraction | $9.75 \cdot 10^{-9}$ | % _{vol} | -67.49% |
| Hydrogen volume fraction | 0.0028 | % _{vol} | -29.14% |
| Oxygen volume fraction | 0.0079 | % _{vol} | 0.00% |
| Butadiene volume fraction | 0.0011 | % _{vol} | 0.00% |
| Cyclopentadiene volume fraction | $8.836 \cdot 10^{-4}$ | % _{vol} | 47.27% |
| Propane volume fraction | 0.0019 | % _{vol} | -0.29% |
| Propene volume fraction | 0.0098 | % _{vol} | -1.46% |

6.3. Discussion

In this studied case, the methodology was applied on a biomass plant, where pyrolysis and gasification occur. The objective functions, based on the experimental volume concentrations of chemical species in resulting biogas, were oriented to minimize the variance between calculated and experimental concentration. The significant triangle without solutions close to origin axes, as in previous case, implies some incongruences in mathematical system schematization and/or experimental data: in order to improve the simulation reliability, additional test must be performed, since in available data there was not a certified composition of biomass feedstock. Moreover, the lowest Euclidean norm criteria, used to determine the preferred design, did not provide a solution close to target values for most of the objectives: this could be related to the objectives units, since they already are non-dimensional, implying a non-general effectiveness for this criteria. In other words, other criteria must be used in order to find a suitable one in case of non-dimensional objectives.

7. Conclusions and outlook

The research carried out in this doctorate thesis was focused on the development of a multi-variable multi-objective methodology applied to energy conversion systems, in order to examine their energy performances and to validate mathematical models and experimental data reliability. In particular, the target of the study was to find out high efficiency energy systems, supplied by fossil and renewable sources, that were able to maximize primary energy saving exploitation.

The methodology followed this logical thread: on the Design of Experiments step, several sets of decision variables are combined by mathematical methods, and they represent the first sets to be used as input in calculation. Thus, the different energy conversion systems models realized for each studied case started to perform energetic analysis using the DoE sets as input, and the generated results vector for each input are appropriately manipulated and ranked by genetic evolutionary algorithm through objective functions; these objective functions varied depending on the peculiar application: for energy systems design cases, the objective functions were aimed to maximize total primary energy saving and minimize investment simple pay back, while the application to model validation was aimed to minimize relative difference between calculated and experimental parameters. After all the DoE sets were evaluated, the genetic algorithm generates new decision variables sets to be used as input in energy conversion system models, in order to find out solutions aimed to achieve the specified objective functions.

The methodology was applied on the two kind of investigation shown in previous chapters, and the main results achieved in this work are:

- The opportunity to perform detailed study on energy conversion systems through the analysis of the complex interaction between system and user in order to satisfy its energy demand;
- The feasibility of executing the validation of mathematical energy models and experimental data aimed to verify their both reliability.

Concerning the study on system-user interaction, the methodology carried out in this thesis work provides a useful and flexible tool that can be focused on several innovative aspects within field of the energy systems. The models of combined heat and power energy systems were realized, taking into account both fossil and renewable sources, in order to analyze the interaction between energy supplied and energy demand of particular users; the three studied users, in turn, were modeled with hourly discretization, after an accurate monitoring of final energy consumption. The analysis performed and described in chapter 3 included an uncommon and effective approach to identify the most stable plant configurations through a multi-objective robust design optimization.

Future improvements of the proposed methodology will address part load efficiency integration needed to obtain optimal operation strategies for the energy system. Finally, the possibility to enhance the mathematical models of energy systems with regard to solar photovoltaic and other renewable technologies should be implemented, also enabling the use of energy storage technologies.

The second application of the proposed methodology regarded the validation of energy systems mathematical model and the examination of experimental data congruence. Thermodynamic and one-dimensional analyses were carried out, showing how the methodology was able to verify experimental data congruity and highlighting the less reliable parameters: for instance, the combustion chamber pressure for the Turbec T100 has a variance that is one order of magnitude greater than that of other parameters. The Capstone C30 has the overall efficiency as the least reliable parameter, but the other ones have similar variances. Moreover, the methodology was able to define one optimal set of thermodynamic input data, using the Euclidean norm to evaluate the preferred solution: this useful mathematical tool ranks the obtained designs by the minimum variance of the overall objectives, determining the preferred design. Consequently, the preferred solution for each case has most reliable thermodynamic input parameters and the related results are very close to the objectives set. Furthermore, the methodology, when coupled with experimental tests, could decrease the needed measurement campaigns. The methodology effectiveness was proved by plotting the preferred experimental design onto turbomachinery performance maps, examining the congruent matching of the design operating conditions.

In addition, the methodology was applied again on Capstone C30 to validate one-dimensional model of the micro gas turbine: in this case, the objective functions evaluated the difference between calculated parameters and thermodynamic preferred design ones. The choice to perform an unsteady state investigation on a basically steady plant like a micro gas turbine was suggested by two factors: first, the plant can be supplied by renewable sources, and most of them are not regular, so is useful to expand the analysis on plant working conditions. Second, since every user energy demand is intrinsically fluctuating, the knowledge of micro gas turbine behavior in unsteady state is useful to analyze how the plant can efficiently follow these fluctuations. The calculation time was very long and, even if the model and the decision variables range need to be refined, the methodology allowed to achieve promising results, encouraging the research in this field.

Concerning the methodology application case of biomass plant validation, a thermochemical model was carried out to replicate the pyrolysis and gasification processes of pulp paper that occur in biomass conversion plant. Calculated composition of produced biogas was compared to data from experimental tests and the objective functions were aimed to minimize this variance. Eleven

composition objectives were set in methodology, and five of them have variance under 1.5% in preferred design, while the other six have larger difference between calculated and experimental values, probably due to inaccurate analysis of feedstock biomass.

In closing, the methodology, through its applications, showed to be a relevant tool with significant potential regarding conversion energy systems analysis: in particular, energy plants which satisfy user demands with maximizing primary energy usage can be designed. Moreover, both thermodynamic and one-dimensional models of energy systems can be validated, performing, at same time, a validation on experimental data.

The outlook of this work is to improve energy system modeling and to implement models of integrated and hybrid energy systems, fueled by both fossil and renewable sources (micro gas turbine, internal combustion engine, solar photovoltaic, ORC, etc.), to achieve a high efficiency conversion of primary energy along with a larger exploitation of renewables.

The author, with this thesis, hopes to give his contribution about world energy issue².

² *L'autore ce crede, ma nun s'ò credere.*

References

- [1] United Nations Framework Convention on Climate Change. FCCC/CP/2015/L.9/Rev.1 “Adoption of the Paris Agreement”. Conference of the Parties, Twenty-first session. Paris 2015.
- [2] International Energy Agency. World Energy Outlook 2014.
- [3] International Energy Agency. World Energy Outlook 2016.
- [4] Tuck CO, Perez E, Horwath IT, Sheldon RA, Poliakoff M. Valorization of biomass: deriving more value from waste. *Science* 2012;337:695-699.
<http://dx.doi.org/10.1126/science.1218930>.
- [5] Orecchini F, Naso V. Energy systems in the era of energy vectors. Springer 2012.
- [6] Gimelli A, Muccillo M. The key role of advanced mathematical methods for the optimal design of polygeneration systems. 12th SDEWES 2017.
- [7] Serra LM, Lozano MA, Ramos J, Ensinas AV, Nebra SA. Polygeneration and efficient use of natural resources. *Energy* 2009;34(5):575–86.
- [8] Calise, F., Rafal Damian Figaj, Massarotti, N., Mauro, A., Vanoli, L., Polygeneration system based on PEMFC, CPVT and electrolyzer: Dynamic simulation and energetic and economic analysis, *Applied Energy*, Volume 192, 15 April 2017, Pages 530–542.
<https://doi.org/10.1016/j.apenergy.2016.08.018>.
- [9] Calise, F., Cipollina, A., Dentice d’Accadia, M., Piacentino, A., A novel renewable polygeneration system for a small Mediterranean volcanic island for the combined production of energy and water: Dynamic simulation and economic assessment, *Applied Energy* 135 (2014) 675–693, <http://dx.doi.org/10.1016/j.apenergy.2014.03.064>.
- [10] Zhihang Guo, Qinhui Wang, Mengxiang Fang, Zhongyang Luo, Kefa Cen, Thermodynamic and economic analysis of polygeneration system integrating atmospheric pressure coal pyrolysis technology with circulating fluidized bed power plant, *Applied Energy* 113 (2014) 1301–1314, <http://dx.doi.org/10.1016/j.apenergy.2013.08.086>.
- [11] Annamaria Buonomano, Francesco Calise, Gabriele Ferruzzi, Laura Vanoli, A novel renewable polygeneration system for hospital buildings: Design, simulation and thermo-economic optimization, *Applied Thermal Engineering* 67 (2014) 43-60,
<http://dx.doi.org/10.1016/j.applthermaleng.2014.03.008>.
- [12] Stefano Bracco, Federico Delfino, Fabio Pampararo, Michela Robba, Mansueto Rossi, A dynamic optimization-based architecture for polygeneration microgrids with tri-generation, renewables, storage systems and electrical vehicles, *Energy Conversion and Management* 96 (2015) 511–520, <http://dx.doi.org/10.1016/j.enconman.2015.03.013>.

- [13] El-Emam, R. S., Dincer, I., Assessment and Evolutionary Based Multi-Objective Optimization of a Novel Renewable-Based Polygeneration Energy System, ASME. *J. Energy Resour. Technol.* 2016;139(1):012003-012003-13. doi:10.1115/1.4033625.
- [14] Calise, F., d'Accadia, M. D., Libertini, L., Quiriti, E., Vicidomini, M., A novel tool for thermoeconomic analysis and optimization of trigeneration systems: A case study for a hospital building in Italy, *Energy*, Volume 126, 1 May 2017, Pages 64–87. <https://doi.org/10.1016/j.energy.2017.03.010>.
- [15] d'Accadia, M. D., Sasso, M., Sibilio, S., Vanoli, L., Micro-combined heat and power in residential and light commercial applications, *Applied Thermal Engineering* 2003(10);23:1247-1259.
- [16] Erik Merkel, Russell McKenna, Wolf Fichtner, Optimisation of the capacity and the dispatch of decentralised micro-CHP systems: A case study for the UK, *Applied Energy* 140 (2015) 120–134, <http://dx.doi.org/10.1016/j.apenergy.2014.11.036>.
- [17] Monteiro, E., Moreira, N. A., Ferreira, S., Planning of micro-combined heat and power systems in the Portuguese scenario, *Applied Energy* 2009;86:290–298.
- [18] Carlson, A., Berry, J., Experiences with Combined Heat and Power during the August 14, 2003 Northeast Blackout. *Power-Gen* 2004.
- [19] Pepermans G, Driesen J, Haeseldonckx D, D'haeseleer W, Belmans R. Distributed generation: definition, benefits and issues. *Energy Policy* 2005;33(6):787–798. <http://dx.doi.org/10.1016/j.enpol.2003.10.004>
- [20] Colmenar-Santos A, Reino-Rio C, Borge-Diez D, Collado-Fernández E. Distributed generation: A review of factors that can contribute most to achieve a scenario of DG units embedded in the new distribution networks. *Renewable and Sustainable Energy Reviews* 2016;59:1130-1148. <http://dx.doi.org/10.1016/j.rser.2016.01.023>
- [21] Montoya-Bueno S, Muñoz-Hernández JI, Contreras J. Uncertainty management of renewable distributed generation. <http://dx.doi.org/10.1016/j.jclepro.2016.02.135>.
- [22] Resolution 3/08, Italian Regulatory Authority for Electricity and Gas.
- [23] Gimelli A, Muccillo M. Optimization Criteria for Cogeneration Systems: Multi-Objective Approach and Application in a Hospital Facility. *Applied Energy* 2013;104:910-923. <http://dx.doi.org/10.1016/j.apenergy.2012.11.076>
- [24] Branke J, Kalyanmoy D, Miettinen K, Slowinski R. *Multiobjective Optimization – Interactive and Evolutionary Approaches*. Springer, 2008.
- [25] Coello Coello CA, Lamont GB, Van Veldhuizen DA. *Evolutionary Algorithms for Solving Multi-Objective Problems*. Springer, 2007.

- [26] Cavazzuti M. Optimization Methods - From Theory to Design Scientific and Technological Aspects in Mechanics. Springer, 2013.
- [27] Johnson ME, Moore LM, Ylvisaker D. Minimax and maximin distance designs. *Journal of Statistical Planning and Inference* 1990;26:131-148. [http://dx.doi.org/10.1016/0378-3758\(90\)90122-B](http://dx.doi.org/10.1016/0378-3758(90)90122-B).
- [28] Poles S, Rigoni E, Robič T, MOGA-II Performance on noisy optimization problems. *International Conference on Bioinspired Optimization Methods and their Application* 2004.
- [29] Poloni C, Pediroda V. GA coupled with computationally expensive simulations: tools to improve efficiency, in: *Genetic Algorithms and Evolution Strategies in Engineering and Computer Science*. John Wiley & Sons, 1997.
- [30] Muccillo M, Gimelli A, Sannino R. Multi-objective optimization and sensitivity analysis of a cogeneration system for a hospital facility. *Energy Procedia* 2015;81:585-596. <http://doi:10.1016/j.egypro.2015.12.043>.
- [31] Sannino R. Thermal characterization of CHP-User Needs interaction and optimized choice of the Internal Combustion Engines in the CHP plants. *Energy Procedia* 2015;82:929-935. <http://doi:10.1016/j.egypro.2015.11.841>.
- [32] Gimelli A, Sannino R. A multi-variable multi-objective methodology for experimental data and thermodynamic analysis validation: an application to micro gas turbines. *Applied Thermal Engineering*, *under final review*.
- [33] Sayyaadi H. Multi-objective approach in thermoenviromomic optimization of a benchmark cogeneration system. *Applied Energy* 2009;86(6):867-879. <http://dx.doi.org/10.1016/j.apenergy.2008.08.017>.
- [34] Wang JJ, Jing YY, Zhang CF. Optimization of capacity and operation for CCHP system by genetic algorithm. *Applied Energy* 2010;87(4):1325-1335. <http://dx.doi.org/10.1016/j.apenergy.2009.08.005>.
- [35] Toffolo A, Lazzaretto A. Evolutionary algorithms for multi-objective energetic and economic optimization in thermal system design. *Energy* 2002;27:549–567.
- [36] Kyung Tae Yun, Heejin Cho, Rogelio Luck, Pedro J Mago. Modeling of reciprocating internal combustion engines for power generation and heat recovery. *Applied Energy* 2013;102:327–335.
- [37] Muccillo M, Gimelli A. Experimental Development, 1D CFD Simulation and Energetic Analysis of a 15 kW Micro-CHP Unit based on Reciprocating Internal Combustion Engine. *Applied Thermal Engineering* 2014;71(2):760-770. <http://dx.doi.org/10.1016/j.applthermaleng.2013.11.025>.

- [38] Ghadimi P, Kara S, Kornfeld B, The optimal selection of on-site CHP systems through integrated sizing and operational strategy. *Appl Energy* 2014;126:38–46. <http://dx.doi.org/10.1016/j.apenergy.2014.03.085>.
- [39] Mehleri ED, Sarimveis H, Markatos NC, Papageorgiou LG, A mathematical programming approach for optimal design of distributed energy systems at the neighbourhood level. *Energy* 2012;44:96–104. <http://dx.doi.org/10.1016/j.energy.2012.02.009>.
- [40] Wang H, Yin W, Abdollahi E, Lahdelma R, Jiao W, Modelling and optimization of CHP based district heating system with renewable energy production and energy storage. *Appl Energy* 2015;159:401–21. <http://dx.doi.org/10.1016/j.apenergy.2015.09.020>.
- [41] Zhang D, Evangelisti S, Lettieri P, Papageorgiou LG, Optimal design of CHP based microgrids: multiobjective optimisation and life cycle assessment. *Energy* 2015;85:181–93. <http://dx.doi.org/10.1016/j.energy.2015.03.036>.
- [42] Dagoberto Cedillos Alvarado, Salvador Acha, Nilay Shah, Christos N. Markides, A Technology Selection and Operation (TSO) optimisation model for distributed energy systems: Mathematical formulation and case study. *Applied Energy*, Volume 180, 15 October 2016, Pages 491–503. <http://dx.doi.org/10.1016/j.apenergy.2016.08.013>.
- [43] Akbari K, Nasiri MM, Jolai F, Ghaderi SF, Optimal investment and unit sizing of distributed energy systems under uncertainty: a robust optimization approach. *Energy Build* 2014;85:275–86. <http://dx.doi.org/10.1016/j.enbuild.2014.09.009>.
- [44] Doltsinis I, Kang Z. Robust design of structures using optimization methods. *Computer Methods in Applied Mechanics and Engineering* 2004;193: 2221–2237. <http://dx.doi.org/10.1016/j.cma.2003.12.055>.
- [45] Sandgren E, Cameron TM. “Robust design optimization of structures through consideration of variation”. *Computers and Structures* 2002;80:1605–1613.
- [46] Zang C, Friswell MI, Mottershead JE. A review of robust optimal design and its application in dynamics. *Computers and Structures* 2005;83:315–326.
- [47] Yokoyama R, Ito K. Optimal design of energy supply systems based on relative robustness criterion. *Energy Conversion and Management* 2002;43:499-514.
- [48] Piacentino A, Cardona F. EABOT – Energetic analysis as a basis for robust optimization of trigeneration systems by linear programming. *Energy Conversion and Management* 2008; 49:3006–3016.
- [49] Torchio MF. Comparison of district heating CHP and distributed generation CHP with energy, environmental and economic criteria for Northern Italy. *Energy Conversion and Management* 2015;92:114–128. <http://dx.doi.org/10.1016/j.enconman.2014.12.052>.

- [50] Jenbacher CHP internal combustion engine data catalogue.
- [51] Poloni C, Giurgevich A, Onesti L, Pediroda V. Hybridization of a multi-objective genetic algorithm, a neural network and a classical optimizer for a complex design problem in fluid dynamics. *Comput. Methods Appl. Mech. Engrg.* 2000;186:403-420.
- [52] Carvalho M, Lozano MA, Serra LM. Multicriteria synthesis of trigeneration systems considering economic and environmental aspects. *Applied Energy* 2012;91:245–254.
- [53] International Energy Agency. Key world energy statistics 2017.
- [54] Bunse K, Vodicka M, Schönsleben P, Brühlhart M, Ernst FO. Integrating energy efficiency performance in production management e gap analysis between industrial needs and scientific literature. *Journal of Cleaner Production* 2011;19:667-679.
- [55] International Energy Agency. Energy efficiency 2017.
- [56] ClimateWorks Australia. Could boosting energy productivity improve your investment performance? A guide for investors. 2016.
- [57] Nascimento MR, Rodrigues LO, et al. Micro Gas Turbine Engine: A Review, in: *Progress in Gas Turbine Performance*. InTech, 2013, 107-141. <http://dx.doi.org/10.5772/54444>.
- [58] Huicochea A, River W, Gutiérrez-Urueta G, Bruno JC, Coronas A. Thermodynamic analysis of a trigeneration system consisting of a micro gas turbine and a double effect absorption chiller. *Applied Thermal Engineering* 2011;31:3347-3353. <http://dx.doi.org/10.1016/j.applthermaleng.2011.06.016>.
- [59] Tuccillo, R. Performance and Transient Behaviour of MGT Based Energy Systems. In *Micro Gas Turbines* (pp. 6-1 – 6-56). Educational Notes RTO-EN-AVT-131, Paper 6. 2005. Neuilly-sur-Seine, France: RTO. Available from: <http://www.rto.nato.int/abstracts.asp>.
- [60] Bozza F., Tuccillo R., Transient operation analysis of a cogenerating micro-gas turbine. *Proceedings of the 7th Biennial Conference on Engineering Systems Design and Analysis, ESDA 2004, Volume 1, 2004, Pages 51-63. ISBN: 0791841731;978-079184173-0.*
- [61] Verstraete D, Bowkett C. Impact of heat transfer on the performance of micro gas turbines. *Applied Energy* 2015;138:445-449. <http://dx.doi.org/10.1016/j.apenergy.2014.10.075>.
- [62] Majoumerd MM, Somehsaraei HN, Assadi M, Breuhaus P. Micro gas turbine configurations with carbon capture - Performance assessment using a validated thermodynamic model. *Applied Thermal Engineering* 2014; 73:172-184. <http://dx.doi.org/10.1016/j.applthermaleng.2014.07.043>.
- [63] Somehsaraei HN, Majoumerd MM, Breuhaus P, Assadi M. Performance analysis of a biogas-fueled micro gas turbine using a validated thermodynamic model. *Applied Thermal Engineering* 2014;66:181-190. <http://dx.doi.org/10.1016/j.applthermaleng.2014.02.010>.

- [64] R. Sargent, Verification and validation of simulation models, Proceedings of the 2010 Winter Simulation Conference 166-183. <http://dx.doi.org/10.1109/WSC.2010.5679166>.
- [65] Di Cairano S, Yanakiev D, Bemporad A, Kolmanovsky IV, Hrovat D. Model Predictive Idle Speed Control: Design, Analysis, and Experimental Evaluation. IEEE Transactions on Control Systems Technology 2012; 20:84-97. <http://dx.doi.org/10.1109/TCST.2011.2112361>.
- [66] Demirbas A. Methane Gas Hydrate. Springer, 2010.
- [67] Balje OE. Turbomachines – A Guide to Design, Selection and Theory. John Wiley & Sons, 1981.
- [68] Della Volpe Macchine.
- [69] Capstone C30 product datasheet.
- [70] Liu A, Weng Y. Effects of Lower Heat Value Fuel on the Operations of Micro-Gas Turbine, Energy and Power Engineering 2009;1:28-37. <http://dx.doi.org/10.4236/epe.2009.11005>.
- [71] Bakalis DP, Stamatis AG. Incorporating available micro gas turbines and fuel cell: Matching considerations and performance evaluation. Applied Energy 2013;103:607-617. <http://dx.doi.org/10.1016/j.apenergy.2012.10.026>.
- [72] Wang J, Yan Z, Wang M, Li M, Dai Y. Multi-objective optimization of an organic Rankine cycle (ORC) for low grade waste heat recovery using evolutionary algorithm. Energy Conversion and Management 2013;71:146-158. <http://dx.doi.org/10.1016/j.enconman.2013.03.028>.
- [73] Akbari P, Müller N. Performance improvement of small gas turbines through use of wave rotor topping cycles. Proceedings of ASME Turbo Expo 2003 Power for Land, Sea, and Air, 2003. <http://dx.doi.org/10.1115/GT2003-38772>.
- [74] Li Y, Weng Y. Performance study of a solid oxide fuel cell and gas turbine hybrid system designed for methane operating with non-designed fuels, Journal of Power Sources 2011;196:3824-3835. <http://dx.doi.org/10.1016/j.jpowsour.2011.01.011>.
- [75] Turbec T100 microturbine system. Technical description. Version 3, 2009. http://www.ansaldoenergia.com/easyUp/file/ansaldo_ae-t100_natural_gas.pdf.
- [76] GT-SUITE. Flow Theory Manual. Version 2016.
- [77] Wright SA, Vernon ME, Pickard P. Small Scale Closed Brayton Cycle Dynamic Response Experiment Results. Sandia Report SAND2006-3485, 2006.
- [78] Kuppam T. Heat exchanger design handbook. Marcel Dekker, 2000.
- [79] Smith EM. Advances in Thermal Design of Heat Exchangers. John Wiley & Sons, 2005.
- [80] Shah RK. Compact Heat Exchangers for Microturbines. RTO-EN-AVT-131, paper 2.

References

- [81] Treece B, Vessa P, McKeirnan R. Microturbine recuperator manufacturing and operating experience. Asme Turbo Expo 2002.
- [82] Turbine with exhaust vortex disrupter and annular recuperator. United States Patent US6634176B2.
- [83] Buonopane RA, Troupe RA, Morgan JC. Heat transfer design methods for plate heat exchangers. Chemical Engineering Progress 1963;59:57–61.
- [84] International Energy Agency. Key World Energy Statistics, 2016.
- [85] International Energy Agency. Bioenergy Project Development & Biomass Supply, 2007.
- [86] Perry RH, Green DW. Perry's chemical engineer's handbook 7th edition. McGraw-Hill, 1997.
- [87] Nikoo MB, Nader M. Simulation of biomass gasification in fluidized bed reactor using Aspen Plus. Biomass and bioenergy 2008;32:1245-1254.
<http://dx.doi.org/10.1016/j.biombioe.2008.02.020>.